AB INITIO STATISTICAL MECHANICS OF STRUCTURAL PHASE TRANSITIONS

by

KARIN M.RABE

A.B. Princeton University

(1982)

SUBMITTED IN PARTIAL FULFILLMENT OF
THE REQUIREMENTS OF THE DEGREE OF

DOCTOR OF PHILOSOPHY
IN PHYSICS

at the
MASSACHUSETTS INSTITUTE OF TECHNOLOGY
September 1987

Signature of Author_____
Department of Physics
September 1987

Certified by_____
John D.Joannopoulos
Thesis Supervisor

Accepted by_____
George F.Koster
Chairman, Departmental Committee

AB INITIO STATISTICAL MECHANICS OF STRUCTURAL PHASE TRANSITIONS

by

KARIN M. RABE

Submitted to the Department of Physics
in September 1987
in Partial Fulfillment of the Requirements of the
Degree of Doctor of Philosophy
in Physics

ABSTRACT

Modern theories of critical phenomena have been developed to a very high degree of sophistication. However, the application of these methods to the study of phase transitions in real materials, rather than model systems, is still generally conducted on a phenomenological level. Unfortunately, there are a number of issues that cannot be resolved on this basis.

Progress in the tractability and accuracy of *ab initio* total energy methods has made possible the '*ab initio* statistical mechanical' approach to structural phase transitions which is formulated in this thesis. In this approach, a realistic microscopic model for the material is developed where the parameters, rather than being deduced from experiment, are obtained directly from *ab initio* total energy calculations. The model Hamiltonian is constructed so that the free energy functional appearing in the statistical mechanical theory can be straightforwardly derived. Once the problem is cast in this form, techniques such as momentum space renormalization group can be applied to obtain information about the transition temperature and critical properties.

The 670K rocksalt-rhombohedral structural phase transition in the IV-VI narrow gap semiconductor GeTe is chosen as the prototype for the implementation of this approach. First, the use of *ab initio* pseudopotential total energy calculations to study the structural properties of GeTe, as well as the the other group IV tellurides SnTe and PbTe, is discussed in detail. Methodological issues such as the use of fully relativistic pseudopotentials and convergence in various calculational parameters are examined. The calculated lattice constants, bulk moduli and cohesive energies of the high-temperature rocksalt form are obtained. The character of the bonding in these materials is investigated through the examination of band structures and valence charge densities, and the effects of the rhombohedral distortion corresponding to the low temperature phase are studied. Calculated structural properties are seen to compare favorably with available experimental data, showing that the method provides an accurate description.

The results of these total energy calculations form the foundation for an *ab initio* statistical

mechanics study of GeTe. Starting from an anharmonic lattice Hamiltonian, a model Hamiltonian which includes coupling of the order parameter to long-wavelength strain is constructed. The parameters appearing in the model are fitted to the calculated total energies of a set of appropriately chosen crystal configurations. A Hubbard-Stratonovich transformation yields an n=3 model with cubic anisotropy and strain coupling. This is analyzed using a momentum space renormalization group approach. Values for the transition temperature and critical properties are obtained which are seen to compare favorably with available experiments, and insight is gained into the microscopic origin of the behavior at the transition. This provides an encouraging prospect for future *ab initio* statistical mechanical studies of the finite temperature properties of solids.

Thesis Supervisor: Dr. J.D.Joannopouios
Title: Professor of Physics

TABLE OF CONTENTS

I. INTRODUCTION

The central object in equilibrium statistical mechanics, the partition function, is in principle obtained by summing over the microscopic configurations of a system with weights obtained from the energy of the configuration. For a real material, both the energy calculation and the summation can be very difficult, and the need for such a direct construction of the partition function is circumvented by approaches using simplified Hamiltonians, such as the Ising model, or by using Landau-Ginzburg-Wilson free energy functionals as a starting point. In either case, there appear a few parameters which for applications to real systems are determined phenomenologically, without explicit connection to the microscopic physics of the system. However, even when a reasonably microscopic model Hamiltonian could be found, the accuracy to which the configuration energies need to be known was, before recent developments, beyond the scope of the available calculational techniques and computing capabilities.

In the last few years, the understanding of the structural properties of real materials has improved considerably as a result of the development of ab-initio total energy techniques which rely on density functional theory. The rest of this introduction will be devoted to a brief discussion of these techniques, followed by a description of the basic concepts of structural phase transitions, the current state of the application of modern statistical mechanics techniques to these systems, and finally, an overview of the research in this thesis, in which we formulate a synthesis between a microscopic chemical understanding of the solid obtained from ab-initio methods and the analysis of the transition through modern techniques of critical phenomena, and discuss its realization for a particular case.

(A) AB-INITIO CALCULATIONS OF THE STRUCTURAL PROPERTIES OF SOLIDS

A crystal is a collection of electrons in a field generated by a periodic array of atomic nuclei (point charges +Ze). The calculation of the properties of a crystal is a complicated quantum-mechanical many-body problem of which a complete solution is impossible. However, if we are willing to settle for finding the total energy and electronic charge density of the ground state (with specified ionic positions), the problem can be solved, at least approximately, and the resulting information is directly useful in extracting predictions about the measurable properties of solids.

The theoretical framework of these calculations comes in two parts. The complicated many-body nature arising from the electron- electron interactions is reduced to an equivalent one-body problem through density functional theory (DFT)[1,2]. Also, the problems of dealing with a strong electron-nuclei interaction are eliminated to a large extent by explicitly eliminating the low lying electronic 'core' states, which do not contribute to the solid-state properties, from the problem by using the pseudopotential approximation[3]. As we shall see, both components of this approach preserve the *ab initio* nature of the results in that still no input is necessary beyond the positions and charges of the nuclei.

The central result of density functional theory is the Hohenberg-Kohn theorem: *the total ground state energy of an interacting electron system in an external potential v(r) can be expressed as a universal functional of the charge density ρ(r).* It is usual to decompose the functional as follows:

$$E[\rho(r)] = \int dr\, v(r)\rho(r) + (1/2)\int dr\, \rho(r)\rho(r')/|r-r'| + G[\rho(r)]$$

where the third term contains the quantum-mechanical kinetic energy and the exchange and correlation energies of the interacting electrons.

The proof of this theorem is based on the quantum-mechanical variational principle, and thus has the additional feature that E[ρ(r)] is a functional which attains its minimum for the 'correct' ρ(r) corresponding to the given v(r). Thus an equation relating v(r) and ρ(r) can be

obtained by setting $\delta E/\delta\rho$ to zero, subject to the constraint that $N=\int dr\rho(r)$. By far the most convenient represention of $\rho(r)$, which has the added benefit of treating the kinetic energy quantum-mechanically, is

$\rho(r) = \Sigma\psi_n^*(r)\psi_n(r)$

where the $\psi_n(r)$ are the wavefunctions of the non-interacting electron gas system which has the charge density $\rho(r)$ in its ground state. Then the variation $\delta E/\delta\psi_n$ gives rise to the following system of Schrodinger-like equations, called the Kohn-Sham equations[5]:

$$[(-1/2)\nabla^2 + v_{eff}(r)]\psi_n(r) = \varepsilon_n\psi_n(r)$$

which is precisely that of a system of non-interacting electrons in an effective one body potential given by

$$v_{eff}(r) = v(r) + \int dr'\rho(r')/|r-r'| + \delta E_{xc}[\rho]/\delta\rho(r),$$

where we have written $G = T_{nonint} + E_{xc}$.

In principle, the density functional method could yield the total energy and charge density exactly. In practice, however, the explicit functional dependence of E_{xc} on $\rho(r)$ is unknown and thus an approximate form must be used. The most widely used form is the local density approximation (LDA)[5] in which E_{xc} is written as $\int dr\, \varepsilon_{xc}(\rho(r))\rho(r)$ and the function ε_{xc} is obtained from knowledge of the properties of the homogeneous electron gas[6]. This form is very simple to calculate with and turns out be a surprisingly accurate representation of the true functional, as will further be discussed below.

Thus, through DFT, the problem has been reduced to a system of one-body Schrodinger equations which, because of the dependence of v_{eff} on $\rho(r)$, must be solved self-consistently. One could now proceed directly using the appropriate nuclear charges for the material of

interest to perform an all-electron total energy calculation. For the kinds of results we will be interested in, which involve small energy differences between similar crystal configurations, such an approach has some serious drawbacks. These arise from the fact that while the low lying 'core electrons' dominate the total energy and, through the requirements of orthogonality, force a very highly structured wavefunction for the valence electrons in the core region, they basically are unaffected by the solid state environment and thus do not enter into energy differences-- that is, they can be regarded as a 'frozen core.' Consequently, the total energies have to be calculated to high precision and the basis sets needed to achieve the proper description of the valence wavefunctions in the core region are large or complicated.

These problems are solved by the elimination of the explicit appearance of the core electrons through the pseudopotential approximation[3], in which the all-electron problem is mapped to that of the valence electrons moving in an effective external field in which the lowest lying levels reproduce the valence electron eigenvalues and the charge density in the interstitial region, outside the ion cores. The construction of this effective field can be effected in a number of ways, and indeed is somewhat arbitrary. The scheme which is currently most widely used[7] preserves the *ab initio* character of the all-electron calculations by superimposing ionic pseudopotentials which are constructed from *ab initio* calculations for the constituent atoms. More precisely, the ionic pseudopotential reproduces the valence eigenvalues and wavefunctions outside some chosen core radius obtained from an all-electron calculation for a given atomic reference configuration. To do this exactly in general requires a non-local (angular momentum dependent) ionic pseudopotential. The norm-conserving character of these ionic pseudopotentials is crucial for the self-consistent density functional calculations and in determining their transferability into different crystal environments[8,9].

The primary practical problems which limit the complexity of the systems that can be studied and the accuracy of the calculations are the size of the basis set in which the one-electron wavefunctions are expanded and the density of k-point sampling in the

computation of quantities, such as $\rho(r)$, which involve averaging over the Brillouin zone. While a variety of basis sets can be used, one advantage of using the pseudopotential approximation is that it is usually possible to use a plane wave basis. Despite the fact that it is generally larger than sets of basis functions tailored for a specific problem, there is a payoff in flexibility (different atomic arrangements are treated in an unbiased way) and simplicity (ease in computing matrix elements and charge densities). The effects of the limitations on basis set and k-point set size can be systematically investigated by raising the cutoffs and checking the convergence of the total energy differences of interest.

With this scheme and currently available computers, it is possible to compute ground-state total energies for a wide variety of materials and for quite complicated structures. From the location and curvatures of energy minima can be obtained predictions for structural properties such as the lattice constant, cohesive energy, bulk modulus, elastic constants and even phonon frequencies, surface reconstructions, and atomic relaxations at defects, at zero temperature and in temperature regimes where energy considerations are expected to dominate. Indeed, there is already a large body of work in which these predictions compare favorably with experimental observations[10]. In addition, examination of the valence charge density, the bandstructure and individual terms contributing to the total energy provides microscopic insight into the nature of bonding in the materials and the factors favoring structural changes.

The quantitative success obtained in these studies suggests that the approximations involved must be very good. In the case of the local density approximation, this is particularly surprising. Although the density functional scheme is exact in principle, here a functional derived from results for a homogeneous electron gas is being applied to systems which are highly inhomogeneous, including ionic and covalently bonded solids. The situation was at first made even more mysterious by the failure of attempts to improve the functional by including higher order terms in a gradient expansion[11]. However, some understanding of the success of the LDA has been achieved. In the case of systems with nearly constant density, the validity of

linear response gives an independent expression which is over a range of q approximated better by the LDA than by gradient corrections[12]. Also, the LDA satisfies exactly the sum rules required by charge neutrality[13]. Lastly, $v_{xc}(r)$ and $n(r)$ for certain systems obtained through constructions which include some many-body effects (within the GW approximation) are negligibly different from those in the LDA[14].

In contrast, the pseudopotential scheme is inherently approximate. The validity of the frozen core approximation, which is in fact an independent approximation buried in the pseudopotential, has been examined in detail[15]. The transferability of the pseudopotential is good by construction: the norm conservation ensures that the logarithmic derivative of the wavefunction with respect to energy is exactly reproduced outside the cutoff radius, and thus that the scattering properties of the ion are well reproduced in different crystal environments[8,9]. Remaining problems can be dealt with by changing the choice of atomic reference configuration, and in cases where the core and valence charge distributions overlap in space, the errors due to the linearization of the exchange-correlation potential can be eliminated by storing the charge distribution of the frozen core[16].

When performing these density functional calculations, it is very important not to lose sight of their intrinsic limitations. For example, although the ground state charge density is correctly given, the wavefunction is not a Slater determinant of the ψ_n used in the construction of the Kohn-Sham equations. Also, in general the one-electron eigenvalues ε_n have no physical significance despite their resemblance to the bands observed in experiments such as photoemission, and in particular, there is no theoretical basis for the idea that the difference of ε_n will yield the correct fundamental gap for a semiconductor like Si, and indeed it does not[14].

Since the construction of a DFT actually only depends on the existence of a variational principle, one can in fact imagine a DFT for excited states, but with a functional which is quantum number dependent and at present unknown. The situation for a density functional theory for systems at finite temperature is somewhat brighter[17], since one can use the existing

results on a homogeneous electron gas at low but finite temperature to construct an appropriate local density functional. However, since this scheme has seen very little practical use[18] it is difficult to judge the reliability of the finite-temperature LDA, particularly in strongly inhomogeneous semiconducting materials where the gap at T=0 is incorrectly given by DFT.

In the absence of a practical scheme for obtaining electronic contributions to the entropy, *ab initio* calculations for finite temperature properties are confined to situations where the lattice contribution to the entropy dominates, since this can be obtained within the Born-Oppenheimer approximation keeping the electrons at zero temperature. Thus, natural candidates for an ab-initio study can be found among systems which undergo structural phase transitions as a function of temperature, which will be discussed in the next section.

(B) STRUCTURAL PHASE TRANSITIONS

Phase transitions in solids can occur as a result of varying external parameters such as temperature, pressure, and magnetic field. They are characterized by a quantity called the order parameter, which distinguishes the disordered phase, in which it is zero, from the ordered phase, where it takes on non-zero values characterizing a broken symmetry[19]. The order parameter is an thermal expectation value of some combination of the microscopic degrees of freedom of the system. The transition can be classified according to the nature of the operators as an electronic transition, e.g. magnetic or superconducting, or as a structural transition, in which the ordering occurs in the ionic parameters. The latter can be considered to include ferroelectric transitions, in which the order parameter is the electrical polarization and thus involves both electronic and ionic operators.

In a structural transition, the crystal distortion is usually strongly coupled to other degrees of freedom in the system such as strain. This leads to the concept of secondary order parameter, which is a quantity which is not in itself critical but in which ordering is induced by the non-zero primary order parameter[20]. These considerations are important when looking at the structural changes between the high and low temperature phases, and also when examining the critical behavior of the system, especially the phase diagram and other nonuniversal quantities.

As discussed above, within a ground-state density-functional approach it is only structural transitions which are accessible, and moreover, only those systems where the transition is driven by lattice entropy rather than electronic entropy. This is clearly the case in a system where there is a gap for electronic excitations which is larger than the transition temperature. Other possibilities exist-- for example, charge density wave systems with a short coherence length[21]. In constrast, the martensitic transitions in the A-15 compounds Nb_3Sn and V_3Si are cases in which the electronic contributions to the entropy seem to dominate[22].

There is a further classification of the lattice-driven structural phase transitions which

reflects properties of the microscopic potential and has a corresponding phenomenological signature due to differences in the dynamics of the soft mode[23]. At one end of the spectrum are the order-disorder transitions, for which the high temperature phase is microscopically distorted, though the thermal averaged distortion is zero. This corresponds to a strongly anharmonic, deep double-well potential for local distortions, and a diffusive character for the soft mode which arises from the hopping between wells. In such a case, it is natural to use a discrete spin picture to model the system. At the other extreme of behavior are the displacive transitions, in which the distribution of atomic positions is a phonon-like single peak about the average position, which corresponds to a weakly anharmonic lattice potential and phonon-like excitations with a temperature dependent dispersion relation. In this picture, the transition occurs when the frequency of the phonon mode whose polarization vector corresponds to the atomic displacements of the transition decreases to zero.

Experimental studies of structural phase transitions focus on the detection of the occurrence of the transition and the measurement of various quantities as the external parameters are varied around the transition point. Static structural determinations are used to study the order parameter in the ordered and disordered phases. These methods include x-ray diffraction and elastic neutron scattering[24], which probe the order on long length scales, and LEED spectroscopy[25], which is useful for detecting symmetry changes on surfaces. EXAFS yields information about the local order and in particular, can distinguish between displacive and order-disorder transitions[26]. Dynamic structural determinations, such as inelastic neutron scattering[24], Raman scattering and infrared spectroscopy[23], probe the characteristics of the collective modes, in particular, their frequencies and linewidths. Lastly, measurements of thermodynamical and mechanical quantities such as the specific heat, response functions and elastic constants can be used further to characterize the transition.

Structural phase transitions have been found to occur in numerous and widely diverse systems. Surfaces provide many examples of transitions in two dimensions. Phase transitions

between different surface reconstructions occur for many clean metal and semiconductor surfaces, including Si(100), Si(111), W(001) and Mo(001)[27]. In addition, phase transitions can occur in the ordering of physisorbed and chemisorbed surface layers, either driven by adsorbate-adsorbate interactions or by modifications by the adsorbate of the interactions which drive the reconstructions of the substrate layer. Interesting examples of adsorbed layer systems include rare gas atoms on graphite, O and Se on Ni(111), and H on W(100) and Mo(100)[28].

There is also a rich variety of systems in three dimensions. These include transitions between different forms of polymorphic crystals, among which are silica[29], ice[29] and tin[30]. Ionic molecular crystals such as $LiKSO_4$ show interesting effects due to the coupling between the translational and rotational degrees of the components[31,32], and some, such as Rb_2ZnCl_4, possess incommensurate phases[33]. Another example of long-period ordering (which, however, may be a kinetic rather than an equilibrium phenomenon) is a polytypic material such as ZnS, which occurs in about 200 different forms all composed of structurally identical layers which appear in a variety of stacking orders[34]. Ferroelectrics are a group of materials which share certain characteristic properties because the ordering in local atomic rearrangements gives rise to local electrical polarization. Related systems are antiferroelectrics and ferroelastics, in which the electrical polarization is induced by a transtion in the strain degrees of freedom[23]. Another class of transitions which primarily involves local rearrangements of atoms are ordering transitions in metal and semiconductor alloys. In the latter, the fabrication of strained alloys in heterostructures permit the observation of additional types of ordered phases[35,36]. Martensitic transformations, on the other hand, do not involve atomic rearrangements within the unit cell but rather the development of long wavelength strains which change its shape. Examples include the A-15 compounds Nb_3Sn and V_3Si, mentioned earlier, and β-NaN_3[37].

(C) LANDAU THEORY, THE RENORMALIZATION GROUP AND STRUCTURAL PHASE TRANSITIONS

As described above, the phenomena of interest at a phase transition include the behavior of the order parameter, correlation functions and thermodynamic quantities such as the specific heat and susceptibility. Close to a second-order transition, in the so-called critical region, these quantities are observed to scale according to simple power laws specified by the critical exponents. The values of the exponents in general are independent of the details of the system, being related only to the nature of the order parameter, the spatial dimensionality and the symmetry.

A Landau theory of the phase transition is constructed based on these three pieces of information[19], as follows. The free energy is expanded as an analytic function of a symmetry breaking quantity, such as the charge density, whose observed value is obtained by minimizing this expression. From this can be deduced that in a second order transition, the order parameter transforms according to an irreducible representation of the symmetry group of the high-symmetry phase, and thus the permitted ordered phases can be obtained. Because of the assumption of analyticity, it turns out that the critical exponents are fixed at the so-called 'classical' values. A similar expansion in invariants, where now the order parameter is a function of position, yields a Landau- Ginzburg- Wilson Hamiltonian, in terms of which the free energy can be expressed as a functional integral. Evaluating the functional integral via the stationary phase approximation recovers the Landau theory.

The universality and possible nonclassicality of the critical exponents have a natural explanation in a renormalization group (RG) treatment of the phase transition, which is designed to incorporate the effects of fluctuations[38,39]. Given the basic information, a Hamiltonian is constructed. Then, by integration over a subset of the degrees of freedom of the system, a new partition function is obtained and cast in the same form as the old, but where the Hamiltonian has a new set of parameters which are expressed in terms of the old by recursion

relations. The recursion relations are used to generate flow diagrams in Hamiltonian parameter space.

The fixed points play a central role in determining the properties of the transitions that a system will undergo. To describe a second order transition, the fixed points are located, their stability studied, and critical exponents extracted. First-order transitions can be identified from the topology of the flows or the absence of stable fixed points. From this information a phase diagram can be constructed.

Nonuniversal aspects of critical behavior are also of interest. These depend on the actual values of coupling for a particular system, and can be also obtained within a RG analysis. The simplest is the location of a particular system in the phase diagram, and from that the value of the critical temperature. Crossover phenomena, where the system is governed by a certain fixed point in one part of the critical region, and then by another (or becomes first order) closer to criticality, can be studied. Lastly, the thermodynamic quantities can be obtained by evaluating the scaling functions via RG[40].

This approach, while very powerful in understanding the origin of universality and classifying critical phenomena, has some weaknesses with respect to the study of behavior of specific materials. First, the emphasis is on global topology of flows and properties of fixed points, rather than accurate interpretation of the behavior of a system with a given microscopic Hamiltonian not necessarily in an L-G-W form. Thus, ambiguities in phenomenologically identifying the critical behavior for a particular system cannot be resolved, and such an analysis cannot give insight into the chemical origin of the couplings, which is useful in the design of model systems for a specific behavior. The calculations of nonuniversal properties are more involved and less technically developed than issues of universal behavior. In particular, universality leads to a natural emphasis on relevant variables, while irrelevant variables can significantly modify nonuniversal properties before they renormalize to zero[41].

(D) OVERVIEW OF RESEARCH

The questions which are left open by the statistical mechanical approach are related to the determination of the relative sizes of the various interactions permitted by symmetry. In striving to understand the behavior of a specific material, we can address this problem by using as a starting point an appropriate microscopic Hamiltonian.

Because this in some sense is the most natural approach to the statistical mechanics of real systems, several attempts have been previously made to carry out such a program. Phase transitions on the Si and Ge(100) surfaces have been examined using a semi- empirical tight-binding total energy method[42]. Transitions in the fluorine-based perovskite $RbCaF_3$, using a Gordon-Kim total energy method, have been studied within the anharmonic crystal model[43]. These schemes suffered from the lack of accuracy of the total energy methods. Recent work on Zr [44] used an accurate ab initio total energy method, but the self-consistent phonon treatment of the model chosen did not permit the examination of critical behavior.

It is crucial to formulate the procedure so that the tractability and accuracy of the various steps are ensured. Clearly, the full microscopic Hamiltonian for the electrons and ions, though completely specified in terms of fundamental constants, is impossible to work with. A lattice Hamiltonian obtained through the use of the Born-Oppenheimer approximation, while certainly providing a correct description of the transition(s) of the system, requires far too complex a specification. However, for studying a particular transition, a model Hamiltonian with relatively few parameters can be obtained by identifying the degrees of freedom, called local modes, which are important for describing the transition. Then, a simple model Hamiltonian is developed by expanding in symmetry invariant combinations of the local mode variables, and keeping only those interactions which are significant based on an understanding of the chemistry of the system and information about the properties of the lattice potential, obtained either phenomenlogically or *ab initio*.

Up to this point, this procedure does not differ much from the analogous approach to the

Landau- Ginzburg- Wilson free energy functional. The key difference lies in that, for a specific material, the coefficients in the model Hamiltonian can be determined from first principles by doing total energy calculations for a small number of configurations and carefully establishing the relationship between crystal configuration and local mode configuration energies. The correct description of the calculated energies, as well as the low lying configurations whose energies were not calculated directly, results then from the physically correct nature of the model Hamiltonian.

Using this simple microscopic Hamiltonian, one then can derive a Landau- Ginzburg-Wilson free energy functional, either by a coarse graining procedure or a Hubbard Stratonovich transformation. With this step, the problem is cast into a form suitable for the application of powerful statistical mechanical techniques such as RG, and the extensive work done in this area can be exploited to obtain information about the specific material we are interested in.

In this thesis I describe the implementation of this approach for a particular structural phase transition-- the 670K rocksalt - rhombohedral transition in the IV-VI narrow gap semiconductor GeTe. This system is an appropriate choice for a prototype study because of its structural simplicity and because the pseudopotentials for Ge and Te are both highly transferable and well behaved. The use of ab initio pseudopotential total energy calculations to study the structural properties of the group IV tellurides is discussed in Chapter 2, which describes the calculations on SnTe and PbTe, and Chapter 3, which describes those for GeTe. For all three materials, the calculated lattice constants, bulk moduli and cohesive energies of the high-temperature rocksalt form are compared with experiment, showing that the method provides an accurate description. The character of the bonding in these materials is investigated through the examination of band structures and valence charge densities, and the effects of the rhombohedral distortion corresponding to the low temperature phase are studied. Chapter 2 also includes discussion of the use of fully relativistic pseudopotentials and the importance of relativistic effects in the structural properties and bandstructure of SnTe and PbTe. Chapter 3

focuses more specifically on the issues which are relevant to the calculations used in the construction of the model Hamiltonian for the GeTe transition. In particular, the calculational accuracy of the effects of distortions on the total energy is investigated. This chapter also includes a discussion of the problems which, because of the approximate nature of the total energy method, arise in this context-- the underestimates of the fundamental gap and the equilibrium volume. In Chapter 4, the ab initio statistical mechanics study of GeTe is described in detail. The model Hamiltonian is constructed using ab initio pseudopotential total energy calculations. A Hubbard-Stratonovich transformation yields an n=3 model with cubic anisotropy and strain coupling. This is analyzed using a momentum space RG approach and values for the transition temperature and critical properties are obtained which are seen to compare favorably with available experiments. Lastly, in Chapter 5, I discuss the prospects for further ab initio statistical mechanics studies, identifying some systems of interest and important questions which can be addressed by these techniques, and also discuss some theoretical issues which could lead to an increase of the scope of such studies.

REFERENCES

1. W.Kohn and P.Vashishta, in Theory of the Inhomogeneous Electron Gas, ed.by S.Lundqvist and N.H.March (Plenum, New York, 1980), p.79.

2. A.R.Williams and U.von Barth, in Theory of the Inhomogeneous Electron Gas, ed.by S.Lundqvist and N.H.March (Plenum, New York, 1980), p.189.

3. G.B.Bachelet, D.R.Hamann and M.Schluter, Phys.Rev.B26, 4199 (1982).

4. P.Hohenberg and W.Kohn, Phys.Rev.136, B864 (1964).

5. W.Kohn and L.J.Sham, Phys.Rev.140, A1133 (1965).

6. D.M.Ceperley, Phys.Rev.B 18, 3126 (1978); D.M.Ceperley and B.J.Alder, Phys.Rev.Lett.45, 566 (1980); J.Perdew and A.Zunger, Phys.Rev.B 23, 5048 (1981).

7. D.R.Hamann, M.Schluter and C.Chiang, Phys.Rev.Lett.43, 1494 (1979).

8. R.W.Shaw and W.A.Harrison, Phys.Rev.163, 604 (1967).

9. W.C.Topp and J.J.Hopfield, Phys.Rev.B7, 1295 (1974).

10. M.L.Cohen, Phys.Scr.T1, 5 (1982).

11. D.C.Langreth and J.P.Perdew, Solid State Commun,31, 567 (1979).

12. D.J.W.Geldart, M.Rasolt and R.Taylor, Solid State Commun.10, 279 (1972).

13. O.Gunnarsson and B.I.Lundqvist, Phys.Rev.B13, 4274 (1976).

14. R.W.Godby, M.Schluter and L.J.Sham, Phys.Rev.Lett.56, 2415 (1986), Phys.Rev.B35, 4170 (1987).

15. U.von Barth and C.D.Gelatt, Phys.Rev.B21, 2222 (1980).

16. S.G.Louie, S.Froyen and M.L.Cohen, Phys.Rev.B26, 1738 (1982).

17. N.D.Mermin, Phys.Rev.137, A1441 (1965).

18. A.Ghazali and P.Leroux Hugon, Phys.Rev.Lett.41, 1569 (1978).

19. E.M.Lifshitz and L.P.Pitaevskii, Statistical Physics, 3rd ed., Chapter 14.

20. W.Cochran, in Structural Phase Transitions and Soft Modes, ed.by E.J.Samuelsen, E.Andersen and J.Feder (Universitetsforlaget, Oslo, 1971), p.1.

21. W.L.McMillan, Phys.Rev.B16, 643 (1977).

22. R.N.Bhatt and W.L.McMillan, Phys.Rev.B14, 1007 (1976).

23. M.E.Lines and A.M.Glass, Principles and Applications of Ferroelectrics and Related Materials (Clarendon, Oxford, 1977).

24. B.C.Frazer, in Structural Phase Transitions and Soft Modes, ed.by E.J.Samuelsen, E.Andersen and J.Feder (Universitetsforlaget, Oslo, 1971), p.43.

25. M.A.Van Hove and S.Y.Tong, Surface Crystallography by LEED (Springer-Verlag, Berlin, 1979)

26. B.A.Bunker, in Extended Abstracts of 1986 U.S.Workshop on the Physics and Chemistry of Mercury Cadmium Telluride, Dallas, October 1986.

27. E.Tosatti, in Modern Trends in the Theory of Condensed Matter, ed.by A.Pekalski and J.Przystawa (Springer-Verlag, Berlin,1980), p.501.

28. Ordering in Two Dimensions, ed.by S.K.Sinha (North Holland, New York, 1980).

29. G.Behnke, H.Bilz and H.Buttner, Phys.Rev.Lett.56, 1276 (1986).

30. J.Ihm and M.L.Cohen, Phys.Rev.B23, 1576 (1981).

31. N.Choudhury, S.L.Chaplot and K.R.Rao, Phys.Rev.B 33, 8607 (1986).

32. M.Kurzynski and M.Halawa, Phys.Rev.B34, 4846 (1986).

33. V.Katkanant, P.J.Edwardson, J.R.Hardy and L.L.Boyer, Phys.Rev.Lett.57, 2033 (1986).

34. S.Mardix, Phys.Rev.B33, 8677 (1986).

35. J.L.Martins and A.Zunger, Phys.Rev.Lett.56, 1400 (1986).

36. P.B.Littlewood, Phys.Rev.B34, 1363 (1986).

37. D.Sahu, Phys.Rev.B34, 4735 (1986).

38. P.Pfeuty and G.Toulouse, Introduction to the Renormalization Group and to Critical Phenomena (J.Wiley, Chichester, 1977).

39. S.-K. Ma, Modern Theory of Critical Phenomena (Benjamin/ Cummings, Reading, 1976).

40. J.Rudnick and D.R.Nelson, Phys.Rev.B13, 2208 (1976).

41. T.Natterman, J.Phys.C 9, 3337 (1976).

42. J.Ihm, D.H.Lee, J.D.Joannopoulos and J.J.Xiong, Phys.Rev.Lett.51, 1872 (1983).

43. L.L.Boyer and J.R.Hardy, Phys.Rev.B24, 2577 (1981).

44. Y.-Y.Ye, Y.Chen, K.M.Ho, B.N.Harmon and P.A.Lindgard, Phys.Rev.Lett.58, 1769 (1987).

CHAPTER II:

AB INITIO RELATIVISTIC PSEUDOPOTENTIAL STUDY OF THE ZERO TEMPERATURE STRUCTURAL PROPERTIES OF SnTe AND PbTe

I. INTRODUCTION

Understanding of the physics of the IV-VI compounds (Ge, Sn, Pb)-(S, Se, Te) has greatly improved over recent years. The initial focus was on the band structures of compounds with rocksalt structure: PbS, PbSe, PbTe, and at high temperature, SnTe and GeTe. These are semiconductors, with a narrow gap of several tenths of an eV at the L point. The band edges are highly nonparabolic, and the ordering of the levels at L is composition sensitive and determines the temperature and pressure coefficients of the band gap. These features, which are important for calculating transport properties, have been studied extensively both experimentally and with a variety of band structure techniques including APW, OPW, KKR and EPM.[1] The IV-VI compounds and pseudobinary alloys are observed to crystallize in orthorhombic, rhombohedral and CsCl structures, as well as rocksalt, as a function of composition, pressure and temperature. The tendency of the telluride compounds towards a transition from the rocksalt structure to a rhombohedral structure (Fig. 1) with decreasing temperature is of particular experimental[2] and theoretical[3] interest. In addition to being the simplest possible structural type of ferroelectric transition, with two atoms per unit cell in both the high temperature and low temperature structures, it is associated with an easily identifiable soft mode (the TO k=0 phonon) and is second order. However, attempts at a fully quantitative understanding of this transition are hindered by experimental and theoretical difficulties inherent in the materials.

A variety of experimental techniques have been developed to study structural transitions and soft mode behavior in ferroelectrics.[4] The application of these techniques to PbTe, SnTe and GeTe is complicated by the free carriers arising from defects in the crystals. While the nature of various defects, especially in PbTe, is itself quite an active area

of study,[1] for the purposes of this discussion the important defects are Group IV or Te vacancies. The electronic states associated with these vacancies lie deep in the bands so the free carriers do not freeze out at any temperature.[5] The crystal properties are very sensitive to the presence of the defects. In SnTe, variations in T_c from <0K to 100K are well correlated with free carrier concentration.[6,7]

The change in crystal structure with temperature has been studied directly in SnTe and GeTe using X-ray diffraction[8,9] and elastic neutron scattering.[10] The distorted structures are described by a rhombohedral Bravais lattice of angle α (equal to 60^o in the fcc structure) and a basis with atoms at $a_o(0, 0, 0)$ and $a_o(.5-\tau, .5-\tau, .5-\tau)$. Thus τ parameterizes the sublattice displacement, i.e., the amplitude of the frozen-in optic phonon as shown in Fig. 1. τ and α appear to be continuous at the transition temperature, indicating a second order (or at most very weakly first order) transition.

The temperature dependence of the soft mode frequency has been measured using inelastic neutron scattering,[11,12,13] far infrared spectroscopy in PbTe[14,15] and, in the rhombohedral phase, Raman scattering.[6,16,17] The temperature dependence is observed to obey a Curie-Weiss law

$$\omega^2 \propto (T-T_c) \quad T>T_c$$

$$\omega^2 \propto (T_c-T) \quad T<T_c$$

with values $T_c>0$ for SnTe and GeTe and $T_c<0$ for PbTe. Thus in PbTe the tendency towards instability can be studied even though no actual transition takes place. Other relevant measurable quantities include an anomalous resistivity near the transition due to large thermal populations of the soft phonons,[18,19] and specific heat, which shows a mean field like jump near T_c.[20]

In the Cochran-Anderson soft mode theory of ferroelectricity,[21,22] the stability of the lattice is studied by looking at its normal modes. In a lattice which exhibits a structural transition, some modes near the zone center are imaginary in the harmonic approximation. The strongly temperature dependent renormalization of the phonon frequency by anharmonic terms stabilizes the lattice for $T>T_c$. Thus, within this theoretical framework the investigation naturally divides into two parts.

First, the mechanism which makes the symmetric structure unstable at zero temperature must be analyzed and a quantitative model developed which at least reproduces chemical trends. The large ε_o,Z* and mixed ionic/covalent nature of the bonding in the tellurides suggest that resonant p-bonding results in a large electron-phonon coupling which drives the instability. Several empirical pseudopotential models based on this idea have been developed.[24,25,26] One interesting result which emerges from the analysis of Littlewood[24] and Porod and Vogl[25] is that the lattice instability is not a consequence of the narrow bandgap, but results from a combination of crystal geometry and the balance between ionicity and covalency.

Second, finite temperature effects must be incorporated into the theory. This is done by finding a model Hamiltonian to describe the anharmonic processes which stabilize the structure at high enough temperatures. In an anharmonic lattice model, a Hamiltonian which includes the coupling of the soft mode to the rest of the phonons is solved in quasi-harmonic or self-consistent-phonon approximations.[27] A local mode model formulates the problem in real space, using as degrees of freedom the amplitudes of atomic displacements corresponding to the soft mode within each unit cell and solving in mean field theory.[28] These models reproduce qualitatively the temperature dependence of the soft mode, but have difficulties quantitatively.[29] A nonlinear shell model which includes

the nonlinear quartic polarizability of the chalcogenide ion[30,31] succeeds, with relatively few empirical parameters, in quantitatively reproducing the temperature dependence of the soft mode as well as certain anomalies in the phonon dispersion relations.

All theoretical descriptions of the electronic and structural properties of the IV-VI materials have relied on empirical input. Experimentally it is known that the properties of the materials depend strongly on defect concentrations and extrapolation to a pure system is not well understood. Thus, empirically derived theoretical parameters implicitly contain defect effects, usually in some complex way.

In this paper, we undertake the first ab initio theoretical investigation of the electronic and structural properties of SnTe and PbTe. We present results of relativistic pseudopotential total-energy calculations in the local density approximation (LDA) for rocksalt structures and rhombohedral structures with various values of the parameters τ and α. A nonrelativistic approach has previously been applied to study bulk crystals, phonons, defects and surfaces in metals,[32,33,34] semiconductors[35,36,37,38] and insulators[39,40,41,42] with considerable quantitative success.[43] With the inclusion of relativistic effects to $O\left(\left(\frac{e^2}{\hbar c}\right)^2\right)$ and the very high accuracy calculation possible because of the simplicity of the structure, we can expect similar success in SnTe and PbTe.

In Section II, we discuss the application of the relativistic pseudopotential total-energy method to this system. In Sections III and IV, we present and discuss the results in the rocksalt structure for lattice constant, bulk modulus, cohesive energy, pseudocharge density and band structures. In Section V, we look at results in distorted structures for stability against distortion, pseudocharge density and bandstructures. In Section VI we discuss the TO k=0 phonon in PbTe. Finally, in Section VII

we summarize our results and make some concluding remarks.

II. METHOD

The theory and practice of self-consistent pseudopotential total energy calculations have been thoroughly discussed elsewhere.[44,45] The total energy can be written in the following form:

$$E_{tot} = E_{kin} + E'_{ei} + E'_{H} + E_{xc} + E'_{ii} \quad (1)$$

where E_{kin} is the total kinetic energy of the electrons; E'_{ei} is the electron-ion interaction energy; E'_{H} is the Hartree energy; E_{xc} is the exchange correlation energy; and E'_{ii} is the ion-ion interaction energy. This expression is evaluated in the momentum space formalism.[46] The primes indicate that the separately divergent q=0 contributions are excluded. We use the relativistic nonlocal atomic pseudopotentials for Sn, Pb and Te given by Bachelet, Hamann & Schluter[47] (BHS) shown in Fig. 2. Exchange and correlation are included through the LDA using the CAPZ parametrization.[48] Eigenfunctions are expanded in the plane wave basis $\{|\vec{k} + \vec{G}>: (\vec{k} + \vec{G})^2 < E_1\}$. The effect of plane waves with $E_1 < (\vec{k} + \vec{G})^2 < E_2$ is included using Lowdin perturbation theory.[49] Brillouin zone averages are performed using the special k-point scheme of Monkhorst and Pack.[50] E'_{ii} is obtained using the method described in Ref. 35. Computations were done on an IBM 370/3033 in single precision for Section III and IV and in double precision for Sections V and VI.

The method used by BHS to construct atomic pseudopotentials which contain all relativistic effects to $O(\left(\frac{e^2}{\hbar c}\right)^2)$ was first introduced by Kleinman.[51,52] The point is that although all-electron calculations in a heavy atom must be done using the Dirac equation, the valence electron wavefunctions outside the core region can be well described by retaining only the major component of the Dirac wavefunction. The radial wavefunction

obeys an effective Schrodinger equation outside the core. By performing a normconserving pseudization on the all-electron Dirac atom, pseudopotentials $V_{\ell j}$ are obtained, where the nodeless solution of the Schrodinger equation specified by a given $V_{\ell j}$ matches the corresponding major component of the Dirac wavefunction outside the core region. Errors of $O(\left(\frac{e^2}{\hbar c}\right)^2)$ occur in the decoupling of the major and minor components and in the neglect of the contribution of the minor component to the charge density outside the core.

The use of these pseudopotentials in crystal calculations involves only a straightforward modification of the nonrelativistic scheme

$$\hat{V} = \sum_{\ell} |\ell\rangle V_{\ell} \langle\ell| \rightarrow \sum_{\ell j} |\ell j\rangle V_{\ell j} \langle \ell j| \qquad (2)$$

so that the number of nonlocal potentials increases and the size of the plane wave basis must be doubled ($|\vec{k}\rangle \rightarrow |\vec{k}\uparrow\rangle$, $|\vec{k}\downarrow\rangle$). In practice, these changes require a substantial increase in computational effort, both in setup of the Hamiltonian matrix and in diagonalization. However, all relativistic effects except spin-orbit splitting can be included by writing

$$\hat{V} = \sum_{\ell} |\ell\rangle (V^{\ell}_{\text{ion}} + V^{\ell}_{\text{so}} \vec{L}\cdot\vec{S}) \langle\ell| \qquad (3)$$

and neglecting V^{ℓ}_{so}, which restores the problem to its nonrelativistic size. For a semiconductor, inclusion of V_{so} in first order perturbation theory does not change the charge density, and if higher order corrections are unimportant the total energy is approximately unaffected. These scalar relativistic (SR) potentials are used for all calculations unless otherwise specified. We examine the effects of this approximation by comparing fully relativistic (FR) and SR results for some test cases. We also compare SR calculations to results in PbTe and SnTe obtained using atomic pseudopotentials (Fig. 2) constructed using nonrelativistic (NR) atomic calculations and the parameters of Table 1.

The accuracy of the computation of pseudocrystal total energy is mainly limited by 1) the representation of the wavefunctions in terms of a finite

basis set and ii) the approximation of Brillouin zone averages using a finite sample of k-points. The smallness of the unit cell makes possible a high level of convergence using available computation facilities (IBM 370/3033). Convergence is evaluated by looking at changes in energy differences between different structures, rather than at the absolute value of energy. For the calculations in the RS structure, good convergence in lattice constant and bulk modulus (typical errors in energy differences $\sim 10^{-4}$ Ryd) was achieved with $E_1 = 10.5$, $E_2 = 16.5$ Ryd ($\sim$250 plane waves in basis set) and 10 k-points (single precision). Calculations in distorted structures required better energy resolution ($\sim 2\text{-}3 \times 10^{-5}$ Ryd) and so larger k-point sets (usually 32 k-points but up to 60) were necessary. The results of total energy calculations are generally insensitive to the precise form of the local density functional[45] but we could not test this because only relativistic atomic potentials calculated with CAPZ were available.

A calculation of the total energy of the free pseudoatoms is required to determine the cohesive energy. The observed term values for the atomic ground state are ^3P_o for Sn and Pb and $^3P_2$ for Te. The total energies of the scalar relativistic pseudoatoms are calculated, a spin polarization correction is made and the spin-orbit energy lowering is obtained in first order perturbation theory in $\hat{V}_{so}$. We neglect the mixing of terms by the spin-orbit interaction, although in Pb the spin-orbit perturbation (0.892 eV) is even larger than the energy lowering from the spin polarization (0.669 eV), and in Sn and Te the spin orbit correction is only about a factor of three smaller than the spin polarization correction.

III. ROCKSALT STRUCTURE

SnTe above its transition temperature and PbTe are observed to crystallize

in the rocksalt structure, which can be described as an fcc Bravais lattice of conventional side a_o with a basis of a Pb or Sn atom at $a_o(0,0,0)$ and a Te atom at $a_o(.5,.5,.5)$. A given rocksalt structure is specified completely by a single parameter - the volume per atom $V = \frac{a_o^3}{8}$. To obtain the equilibrium lattice constants, bulk moduli and cohesive energies of SnTe and PbTe in the RS structure, total energies per atom are calculated at several values of V near V_{expt} and fitted to a cubic polynomial. Calculated points deviate from the fitted curve by $\lesssim 10^{-4}$ Ryd/atom. The results for NR and SR SnTe are shown graphically in Fig. 3. The minimum of the NR curve occurs at a lower value of V than that of the SR curve, and has noticeably higher curvature at the minimum, corresponding to a larger bulk modulus. The NR curve is shifted upwards in energy from the SR curve by about 0.2 Ryd/atom. In Fig. 4, the various terms contributing to the total energy of SR SnTe are plotted as a function of V. As the structure is expanded, E_{kin} decreases slightly, while E_{xc} and E'_H show a small increase. The dominant changes are the increase in the Ewald energy E'_{ii}, which depends only on the lattice structure and ionic charges and favors low atomic volumes and high coordination number, and the electron-ion interaction energy E'_{ei}, which decreases as charge moves from the interatomic regions to become more localized around individual ions.

The $E_{tot}(V)$ results for NR and SR PbTe are shown in Fig. 5. Here, the minima and curvatures of the NR and SR curves are very similar; however, the overall shift of the NR energies up from the SR energies is about 0.4 Ryd/atom, twice as large as the shift in SnTe. The contributions to $E_{tot}(V)$ of SR PbTe are plotted in Fig. 6. The same trends are evident as in SR SnTe, though there are quantitative differences responsible for the different V_o and B.

The physical parameters extracted from the fits are given in Table 2 for comparison with the corresponding experimental values. PbTe is observed

to remain rocksalt down to the lowest temperatures at which measurements have been made, with a value of $T_c \lesssim -100$ K extrapolated from the Curie-Weiss temperature dependence of the TO k = 0 phonon. The calculated SR lattice constant agrees with the observed room temperature value to within 2% and the calculated and observed bulk moduli agree to 5%. For SnTe, the comparison with experiment is less definitive than for PbTe, since pure samples do not crystallize in the rocksalt structure at low temperature. Thus we compare results calculated in the rocksalt structure with data taken at 300 K or at low temperature in samples in which the transition temperature is suppressed by the defect concentration. The calculated SR lattice constant agrees with the experimental value to $\sim$1%. The SR calculated bulk modulus is higher than any of the available experimental values but the variation in these is so large that the value of a more quantitative comparison is doubtful. We also include in the table results of FR calculations which help to support our claim in Section II that a scalar relativistic description is adequate for the calculation of total energy differences between different structures.

The calculated FR cohesive energy is off from experiment by 36% for PbTe and 20% for SnTe. Neglecting the spin-orbit interaction entirely gives nearly equal cohesive energies for SnTe and PbTe, while the experimental value for PbTe is 1eV/pair lower than for SnTe. Thus, part of the error can be attributed to the treatment of the spin-orbit interaction in the atomic calculations. Errors due to the use of the local density functional are also expected to be significant.

IV. ROCKSALT BANDSTRUCTURES AND CHARGE DENSITIES

In Fig. 7 we present the bandstructures of SnTe and PbTe calculated at V_o for NR, SR and FR potentials. The general features compare favorably

with previous calculations. Since we are primarily interested in calculating total energies, which involves averaging valence band properties over the Brillouin zone, we have not studied in detail features of the bandstructure such as level ordering and gap structure in the immediate neighborhood of L. A comparison of the SR and FR bandstructures shows that while the spin-orbit interaction certainly has a significant effect on the bandstructure, it mainly acts to lift the degeneracies within groups of scalar relativistic levels. The spin-orbit splitting of the upper valence band at Γ increases only 30%, from 0.88 eV to 1.2 eV, in going from SnTe to PbTe, suggesting these levels have mostly Te p character, where Te has an atomic spin-orbit splitting of 1.2 eV. The direct gap at L is 0.4 eV in both FR SnTe and FR PbTe.

A comparison of SR and NR bandstructures shows some differences in the level orderings, especially near L. In fact, NR SnTe is not even a semiconductor, but rather a semimetal. Another important effect is the relativistic enhancement of the s-p splitting due to the Darwin term, which is clearly manifested in the atomic eigenvalues. In the crystal, the splitting between the two lowest bands, which are s-like and the next three, which are p-like, is significantly larger in the SR case than in NR. The lowering in energy of the s levels is responsible for the large shift in E_{tot} for NR vs. SR potentials observed above. However, as we have seen, this increased splitting does not have a significant effect on the calculated equilibrium properties since only the p-levels are significant in bonding.

Total valence charge densities in the (100) plane for PbTe and SnTe are shown in Fig. 8. The results for PbTe can be directly compared with the EPM charge densities of Ref. 53. In the EPM calculation, the charge density smoothly increases from the interstitial region to reach its maximum at the atomic origin, with roughly the same peak value on the Pb atom as on the Te. In the current calculation, because of the repulsive nature of the pseudopotentials, the charge density is zero at the atomic origins, increasing

to a maximum on a shell around the atom, and then decreasing into the interstitial regions. The shell around the Pb atom is broad and is at nearly half the nearest neighbor distance, while the shell around the Te is much more sharply peaked and more tightly bound. The position of the peak in the charge density outside the core is consistent with the expected behavior of 5s and 6s electrons.

Next we examine the charge densities of PbTe band by band (Fig. 9). The band by band breakdown in SnTe is very similar and will not be shown. Band 1 is almost pure Te s, with the charge density reaching its maximum on a shell at about one-quarter the nearest neighbor distance. Band 2 is mostly Pb s, with some Te p. This Pb charge shell represents the more tightly bound portion of the total charge associated with the Pb, though it still has a larger radius than the Te s shell. Bands 3 and 4 are predominantly Te p as indicated by the lack of spherical symmetry in the charge distributions around the Te atoms. The charge around the Te atom in band 5 appears nearly spherically symmetric, but guided by the bandstructures, the angular decomposition of the wavefunctions in Ref. 53 and the occurrence of the peak at the radius of the other p bands rather than the s band, we conclude it to be also mainly Te p. Band 6, the lowest conduction band, is Pb p and Te s.

V. RHOMBOHEDRAL STRUCTURE

In this section, we discuss results of total energy calculations in the rhombohedral structure which can be obtained by a small distortion of the rocksalt structure (see Fig. 1). The rhombohedral Bravais lattice with symmetry axis along (111) is characterized by V and α, the angle between the primitive vectors (equal to 60^{o} in the fcc structure). The basis consists of a Pb or Sn atom at $a_o(0,0,0)$ and a Te atom at $a_o(.5-\tau,.5-\tau,.5-\tau)$. The

3-D structural parameter space is too large to be explored completely. A reasonable simplification is to fix V at the equilibrium volume obtained in the rocksalt calculations, which reduces the parameter space to D = 2, making calculations feasible.

In Fig. 10, we investigate the stability of the rocksalt structure against the τ distortion only, holding α fixed at 60°. It is important to note that while the energy lowering driving the instability in SnTe appears small (1.1×10^{-4} Ryd), it is quite definite and moreover is expected to be small, considering that $T_c \sim 100$ K. PbTe is stable against this distortion, though the phonon is soft. The plots of the contributions to $E_{tot}(\tau)$ in SnTe and PbTe are very similar (Fig. 1). The Ewald energy E'_{ii} and the electronic energies E_{kin} and E'_H favor the more symmetric structure, while the electron-ion energy E'_{ei} acts to drive the instability. These trends are consistent with the resonant p-bonding picture. The qualitative difference in the $E_{tot}(\tau)$ curves for SnTe and PbTe is the result of a subtle quantitative change in these competing contributions. The values of the contributions at $\tau = 0.000$ and $\tau = 0.015$ for SnTe and PbTe are given in Table 3.

In order to investigate the full 2-D parameter space, we extended our calculations to a mesh of (α,τ) values, plotting out $E_{tot}(\alpha,\tau)$ surfaces for PbTe and SnTe which are shown in Fig. 12. The τ distortion in SnTe is further stabilized by a change in α. The fit minimum is $\tau = .015$ and $\alpha = 59.5^{\circ}$ which is in very reasonable agreement with the observed values $\tau = 0.008$ and $\alpha = 59.878^{\circ}$ given that the relevant energy differences are an order of magnitude smaller than those required for the calculation of the lattice constant and bulk modulus. In particular, distortions in τ are energetically unfavorable at all values of α near 60°, while an estimate for the shear elastic constant C_{44} from the relation

$$\Delta E_{tot}(\Delta\alpha = \alpha - \frac{\pi}{3},\ \tau=0) = \frac{3}{8}VC_{44}(\Delta\alpha)^2 \qquad (4)$$

yields a value of 5 x 10" dynes/cm^2, consistent with the observed value of 1.5 x 10^{11} dynes/cm^2. [54] Close examination of the behavior in PbTe of $E_{tot}(\alpha, \tau=0.000)$ for α near 60° shows that the global minimum occurs right at $\alpha = 60°$, making the rocksalt structure an extremum as it must be by symmetry. Also, there is some indication of a local minimum about 10^{-4} Ry higher at $\alpha = 60.4°$, though good resolution of this feature is beyond the accuracy of the current calculation.

Our success in obtaining the correct chemical trend of the instability is supported by calculations of total energies of rhombohedrally distorted GeTe, which show the same kind of instability as in SnTe with an energy gain about an order of magnitude larger, which is reasonable since the observed T_c in GeTe is 670 K compared to 100 K in SnTe. Study of the changes in charge density of SnTe with distortion in τ (Fig. 13) shows a movement of charge into the shorter bond and a deformation of the charge associated with the Te ion. The FR bandstructure for rhombohedral SnTe is shown in Fig. 14. The new features resulting from the distortion are the splitting of the bands into spin polarized levels through the breaking of inversion symmetry arising from the τ distortion, and the division of the eight L points into the two inequivalent sets {(111), $(\bar{1}\bar{1}\bar{1})$} and {$(\bar{1}11)$, $(1\bar{1}1)$, $(11\bar{1})$, $(1\bar{1}\bar{1})$, $(\bar{1}1\bar{1})$, $(\bar{1}\bar{1}1)$} by the rhombohedral distortion in the (111) direction. We have not made a comparison of NR and SR potentials in the rhombohedral structure, but it would probably show a stabilization of the rocksalt structure through the relativistic s-p splitting enhancement, which makes s-p hydridization unfavorable. Tests show that the inclusion of spin-orbit splitting preserves the qualitative features of this discussion.

VI. TO PHONON IN PbTe

In PbTe, although the calculation shows the rocksalt structure is stable, the TO k = 0 phonon is unusually soft. Its frequency can be obtained from a frozen phonon calculation, which is particularly simple in this case since the atomic displacement vectors are already known and the

of $V_{eff}(\tau)$ yields a harmonic approximation to the phonon frequency, but V_{eff} is quite anharmonic and thus to compare to experiment we need the renormalized phonon frequency. In the self-consistent phonon approximation, with a polynomial fit

$$V_{eff}(\tau) = b_o + 3a_o^2 b_1 \tau^2 + 9a_o^4 b_2 \tau^4 + 27a_o^6 b_3 \tau^6 \tag{5}$$

$\bar{\omega}$ obeys

$$\frac{1}{2}M\bar{\omega}^2 = b_1 + \frac{3b_2\hbar}{M\bar{\omega}} \coth\left(\frac{\hbar\omega\beta}{2}\right) + \frac{45}{2}\frac{b_3\hbar^2}{(M\bar{\omega})^2}\left[\frac{3}{2} + \frac{1}{4}\left(\frac{1}{\sinh^2\left(\frac{\hbar\omega\beta}{2}\right)} + \coth^2\left(\frac{\hbar\bar{\omega}\beta}{2}\right)\right)\right] \tag{6}$$

where M is the reduced mass of the ions. We use this equation with T = 0 and include only a constant coupling to a single optical branch. Very large k-point sets (44 k-points) are required to obtain convergence of ω_{TO}. Our SR values for the bare and renormalized phonon frequencies are 31cm^{-1} and 35cm^{-1} respectively, to be compared with the experimental value of 26cm^{-1}.[15] The theoretical values are in reasonable agreement with experiment given that the frequencies are so low, i.e. that the relevant energy differences are so small. Among the effects we have left out are defects, which according to current models should raise the phonon frequency from its value in the perfect crystal.[2] Also, FR calculations with 19 k-points indicate that the inclusion of spin-orbit splitting tends to lower the frequency.

In a recent experiment,[15] the Gruneisen parameter was measured to be about twice as large (19.6) as predicted values of $\frac{dT_c}{dP}$ would imply. We have determined a value for the mode Gruneisen parameter $\gamma = \frac{B}{\omega_{TO}}\frac{\omega_{TO}}{dP}$ from calculations of the TO phonon frequency at four different values of V (Fig. 15). The rocksalt $E_{tot}(V)$ calculations are used to determine V(P) and B, the bulk modulus. The result is a Gruneisen parameter of about 7. Since the result is quite sensitive to the quantitative accuracy of the several quantities in the expression, this should be regarded as a very rough estimate and should not be used to determine definitely whether or not the observed large Gruneisen parameter is an intrinsic property of the material.

On the other hand, what these calculations definitely show is that $\omega_{TO}(P)$ is very close to linear. This is important because it would rule out explanations for the large Gruneisen parameter which require a strong nonlinearity of $\omega_{TO}(P)$ at small P.

VII. SUMMARY AND CONCLUDING REMARKS

We have presented relativistic self-consistent pseudopotential calculations of the electronic structure and total energies of PbTe and SnTe in the rocksalt and rhombohedral structures. Specifically, we have calculated both bandstructures and fully self-consistent ab initio charge densities. The latter were found to differ significantly from previous calculations. The structural properties calculated include equilibrium lattice parameters, bulk moduli, cohesive energies. phonon frequencies and the shear elastic constant. Good agreement with experiment was obtained. In addition, we found $\omega_{TO}(P)$ to be linear at small P, which is of interest in interpreting a recent experiment.

We discussed the sizes of numerical errors in Section II. An estimate of the accuracy to which the properties of the pseudocrystal reproduce those of the fully interacting electron-ion system is much harder to obtain. The validity of the frozen core approximation and the transferability of the pseudopotentials can be estimated by comparing pseudoatom results with all-electron calculations for different atomic configurations. The accuracy of the LDA in approximating the true functional is also difficult to estimate. One hope is that, in calculating energy differences between similar structures, the errors cancel out to some degree. In the final analysis, the validity of the approximations and rough sizes of errors are judged by agreement with appropriate experimental quantities.

Finally, we note that we have found that for these materials, it is a

valid approximation to neglect spin-orbit splitting in total energy calculations resulting in a great savings in computational effort. This is important for the application of this technique to more complicated problems, e.g., pseudobinary alloys, defects such as vacancies and impurities, phonon calculations for $\vec{k} \neq 0$, and discussion of finite temperature effects. The possibility of doing first principles calculations on these materials should help in sorting out the variety of physical effects which determine their properties and thus in realizing their potential as simple systems for the study of structural transitions.

VIII. APPENDIX

More extensive convergence tests, conducted after the completion of the work described in this paper, showed that the results for $E(\tau)$ given in Fig.10a for SnTe at the calculated equilibrium volume are not converged with respect to k-point set sizw. In fact, the converged results shown in Fig.16 are qualitatively different in that the energy curve is flat in the neighborhood of $\tau=0$ within the accuracy of the calculation rather than having a minimum at finite τ. Thus we cannot with this method make a firm prediction of a distorted structure at T=0, the existence of which is clearly indicated by experiment.

What went wrong? Allowing V and α also to vary leads to only tiny adjustments in these parameters and negligible energy gain. Rather than simply blaming it on the pseudopotential approximation and the LDA, we have been able to identify at least one important contributing factor. The prediction for the lattice constant is 1.5% smaller than the experimental value. While for most properties, this small discrepancy has a negligible effect, it can have a significant effect on the distortion energy, changing the delicate balance between the distorted and the rocksalt structures in favor of the latter. This is suggested by the experimental observation that $dT_c/dP < 0$, showing the favoring of the rocksalt structure by the pressure- induced compression.

In Fig.16 we also show $E(\tau)$ calculated at the experimental

lattice constant 6.30Å, with a minimum around $\tau = 0.015$, showing that the effect of the volume change is significant. Unfortunately, this prediction of a distorted structure at T=0 is no longer completely ab initio, and a first principles study of the 100K structural phase transition is not possible. Fortunately, because the distortion energy is an order of magnitude larger, the problem is not a serious one in GeTe, which will be the subject of future investigations.

REFERENCES

1. G. Nimtz and B. Schlicht, in Narrow Gap Semiconductors Springer Tracts in Modern Physics #98 (1983) and references therein.
2. W. Jantsch, in Dynamical Properties of IV-VI Compounds Springer Tracts in Modern Physics #99 (1983) and references therein.
3. A. Bussmann-Holder, H. Bilz and P. Vogl, in Dynamical Properties of IV-VI Compounds Springer Tracts in Modern Physics #99 (1983) and references therein.
4. M. E. Lines and A. M. Glass, Principles and Applications of Ferroelectrics and Related Materials Int. Series of Monographs on Physics, Clarendon, Oxford (1977).
5. N. J. Parada and G. W. Pratt, Jr., Phys. Rev. Lett. 22 180 (1969).
6. S. Sugai, K. Murase, S. Katayama, S. Takaoka, S. Nishi and H. Kawamura, Solid State Commun. 24 407 (1977).
7. K. L. I. Kobayashi, Y. Kato, Y. Katayama and K. F. Komatsubara, Phys. Rev. Lett. 37 772 (1976).
8. L. Muldawer, J. Nonmetals 1 177 (1973).
9. T. B. Zhukova and A. I. Zaslavskii, Sov. Phys. - Crystallogr. 12 28 (1967).
10. M. Iizumi, Y. Hamaguchi, K. F. Komatsubara and Y. Kato, J. Phys. Soc. Japan 38 443 (1975).
11. H. A. Alperin, S. J. Pickart, J. J. Rhyne and V. J. Minkiewicz, Phys. Lett. 40A 295 (1972).
12. W. Cochran, R. A. Cowley, G. Dolling and M. M. Elcombe, Proc. Roy. Soc. (London) 293 433 (1966).
13. G. S. Pawley, W. Cochran, R. A. Cowley and G. Dolling, Phys. Rev. Lett. 17 753 (1966).
14. H. Burkhard, G. Bauer and A. Lopez-Otero, Solid State Commun. 18 773 (1976).
15. S. W. McKnight and M. K. El-Rayess, Proc. 17th Int. Conf. Phys. of Semiconductors, San Francisco (1984).

16. S. Sugai, K. Murase and H. Kawamura, Solid State Commun. 23 127 (1977).

17. T. Shimada, K. L. I. Kobayashi, Y. Katayama and K. F. Komatsubara, Phys. Rev. Lett. 39 143 (1977).

18. A. D. C. Grassie, J. A. Agapito and P. Gonzalez, J. Phys. C 12 L925 (1979).

19. K. L. I. Kobayashi, Y. Kato, Y. Katayama and K. F. Komatsubara, Solid State Commun. 17 875 (1975).

20. I. Hatta and K. L. I. Kobayashi, Solid State Commun. 22 775 (1977).

21. W. Cochran, Adv. Phys. 9 387 (1960).

22. P. W. Anderson, in Fizika Dielectrikov, ed. G. I. Skanavi (Moscow, Akad. Nauk, 1960).

23. G. Lucovsky and R. M. White, Phys. Rev. B 8 660 (1973).

24. P. B. Littlewood, J. Phys. C 13 4855 (1980)(I); J. Phys. C 13 4875 (1980)(II); in Physics of Narrow Gap Semiconductors Springer Lecture Notes in Physics #152 (1982) p. 238.

25. W. Porod and P. Vogl, in Physics of Narrow Gap Semiconductors Springer Lecture Notes in Physics #152 (1982) p. 247.

26. G. Mula, in Physics of Narrow Gap Semiconductors Springer Lecture Notes in Physics #152 (1982) p. 252.

27. See Ref. 3, Section 3.3.1.

28. M. E. Lines, Phys. Rev. 177 797 (1969).

29. H. Kawamura in Narrow Gap Semiconductors: Physics and Applications Springer Lecture Notes in Physics #133, ed. W. Zawasdki, p. 470. See also Ref. 24 (II).

30. H. Bilz, A. Bussman, G. Benedek, H. Buttner, and D. Strauch, Ferroelectrics 25 339 (1980).

31. A. Bussmann-Holder, W. Kress, and H. Bilz in Physics of Narrow Gap Semiconductors Springer Lecture Notes in Physics #152 (1982) p. 257.

32. A. Zunger and M. L. Cohen, Phys. Rev. B 19 568 (1979).

33. D. M. Bylander and L. Kleinman, Phys. Rev. B 27 3152 (1983); Phys. Rev. B 29 1534 (1984).

34. P. K. Lam and M. L. Cohen, Phys. Rev. B 24 4224 (1981); Phys. Rev. B 25 6139 (1982).

35. M. T. Yin and M. L. Cohen, Phys. Rev. B 26 3259 (1982); Phys. Rev. B 26 5668 (1982).

36. S. Froyen and M. L. Cohen, Solid State Commun. 43 447 (1982); Physica B & C 117-118 pt. 2 561 (1983); Phys. Rev. B 28 3258 (1983).

37. D. Vanderbilt and J. D. Joannopoulos, Solid State Commun. 35, 535 (1980); Phys. Rev. 27 6296 (1983).

38. J. Ihm and J. D. Joannopoulos, Phys. Rev. Lett. 47 679 (1981).

39. M. T. Yin and M. L. Cohen, Phys. Rev. B 24 6121 (1981).

40. G. B. Bachelet, H. Greenside, G. A. Baraff and M. Schluter, Phys. Rev. B 24 4745 (1981).

41. W. Andreoni, K. Maschke and M. Schluter, Phys. Rev. B 26 2314 (1982).

42. S. Froyen and M. L. Cohen, Phys. Rev. B 29 3770 (1984).

43. For a review of work up to 1982, see M. L. Cohen, Phys. Scr. T 1 5 (1982).

44. M. T. Yin and M. L. Cohen, Phys. Rev. B 25 7403 (1982).

45. D. Vanderbilt, Ph.D thesis, Massachusetts Institute of Technology 1981.

46. J. Ihm, A. Zunger and M. L. Cohen, J. Phys. C 12 4409 (1979).

47. G. B. Bachelet, D. R. Hamann, and M. Schluter, Phys. Rev. B 26 4199 (1982).

48. D. M. Ceperley, Phys. Rev. B 18 3126 (1978); D. M. Ceperley and B. J. Alder, Phys. Rev. Lett. 45 566 (1980); J. Perdew and A. Zunger, Phys. Rev. B 23 5048 (1981).

49. P. O. Lowdin, J. Chem. Phys. 19 1396 (1951).

50. H. J. Monkhorst and J. D. Pack, Phys. Rev. B 13 5188 (1976).

51. L. Kleinman, Phys. Rev. B 21 2630 (1980).

52. G. B. Bachelet and M. Schluter, Phys. Rev. B 25 2103 (1982).

53. M. Schluter, G. Martinez, and M. L. Cohen, Phys. Rev. B 11 3808 (1975).

54. B. Houston, R. E. Strakna, and H. S. Belson, J. App. Phys. 39 3913 (1968).

55. D. R. Hamann, M. Schluter, and C. Chiang, Phys. Rev. Lett 43 1494 (1979).

56. R. Hultgren et. al., Selected Values of the Thermodynamic Properties of the Elements (American Society for Metals, Ohio, 1973).

57. D. D. Wagman, ed., NBS Technical Notes Nos. 270-3 (Washington, D. C., USGPO, 196

58. R. F. Bis and J. R. Dixon, J. Appl. Phys. 40 1919 (1969).

59. T. Seddon, S. C. Gupta, and G. A. Saunders, Solid State Commun. 20 69 (1976).

60. A. G. Beattie, J. Appl. Phys. 40 4818 (1969).

61. B. Houston and R. E. Strakna, Bull. Amer. Phys. Soc. 9 646 (1964).

62. G. Hausch, M. Gsanger and E. Luscher, Zeitschrift fur Angewandte Physik 25 261 (1968).

63. R. Dalven, Infrared Physics 9 141 (1969).

64. A. N. Mariano and K. L. Chopra, Appl. Phys. Lett. 10 282 (1967).

Figure 1: The low temperature rhombohedral structure of SnTe and GeTe can be obtained as a small distortion of the rocksalt structure by a) displacing the two fcc sublattices relative to each other by $a_o\tau$ (111), corresponding to a frozen-in k = 0 optic phonon, followed by b) a rhombohedral shear in the (111) direction which changes the rhombohedral angle from its fcc value of 60^o to α.

Figure 2: Nonlocal ionic pseudopotentials for Sn, Pb and Te. In the top row are shown the fully relativistic potentials constructed by BHS[47] which are nonlocal in j and l, requiring five different potentials $s_{1/2}$, $p_{1/2}$, $p_{3/2}$, $d_{3/2}$, $d_{5/2}$. Scalar relativistic s, p, d potentials are obtained from the weighted average $\tilde{V}_\ell = \frac{1}{2\ell+1}\left(\ell\hat{V}_{\ell-\frac{1}{2}} + (\ell+1)\hat{V}_{\ell+\frac{1}{2}}\right)$ and are not shown here.

In the bottom row are shown the nonrelativistic pseudopotentials constructed according to Ref. 55, with detailed information given in Table 1. In all crystal calculations, the p potential is used as the local potential.

Figure 3: Total energy (in Ry) in the rocksalt structure as a function of volume per atom (in $(Br)^3$) for SnTe. Each vertical tick equals 10^{-3} Ry. The upper data points are calculated using the NR potentials. The lower points are obtained using the SR potentials. Cubic polynomial fits are shown as solid lines.

Figure 4: Contributions to the SR total energy of SnTe in the rocksalt structure as described in the text. Each vertical tick equals 0.1 Ry.

Figure 5: Total energy in the rocksalt structure as a function of atomic value for PbTe. Same convention as in Fig. 3.

Figure 6: Contributions to the SR total energy of PbTe in the rocksalt structure. Same convention as in Fig. 4.

Figure 7: Pseudopotential bandstructures in the rocksalt structure of a)-c) SnTe and d)-f) PbTe. For each material, three calculations are shown: NR, SR, and FR respectively.

Figure 8: Total valence pseudocharge densities plotted in the (100) plane of the rocksalt structure for a) SnTe and b) PbTe, in units of electrons per unit cell.

Figure 9: Band-by-band pseudocharge densities plotted in the (100) plane of the rocksalt structure of PbTe for a)-e) bands 1-6 respectively, in units of electrons per unit cell.

Figure 10: Total energy in Ry of SnTe ($V = 203.0(Br)^3$) and PbTe ($V = 210.0(Br)^3$) as a function of τ with α fixed at 60^o. Each vertical tick equals 10^{-3} Ry. Fits to polynomials cubic in τ^2 are shown as solid lines.

Figure 11: Contributions to the total energy at $\alpha = 60^o$ as a function of τ for SnTe and PbTe. Same convention as in Figure 4.

Figure 12: Contour plot of the fit $\Delta E_{tot}(\alpha, \tau) = E_{tot}(\alpha, \tau) - E_{tot}(\alpha = 60^o, \tau = 0.00$ for a) SnTe and b) PbTe. Energies shown are in units of 10^{-5} Ry.

Figure 13: Total valence pseudocharge densities in (110) plane of SnTe for a) $\tau = 0.000$ and b) $\tau = 0.015$. This section is advantageous since it slices through the bonds like the (100) section and the atoms stay in the plane for $\tau \neq 0.000$. Charge densities are given in units of electrons per unit cell.

Figure 14: Pseudopotential bandstructure of SnTe with $\alpha = 59.5$ and $\tau = 0.015$ using fully relativistic potentials. The levels near the gap at the L and T points are compared in the detail.

Figure 15: $\omega_{TO}(V)$ in cm^{-1} in PbTe. The range in V corresponds to a range in P from 0 to 8 kbar. The solid line is a good fit to the four calculated points. The calculation was done with 19 k-points.

Figure 16: Total energy in meV/atom as a function of τ for SnTe at the calculated equilibrium volume (solid circles) and the experimentally observed volume (vertical crosses). Calculations were performed with a 44 k-point set.

Table 1: Construction of nonrelativistic pseudopotentials for Sn, Pb and Te. s, p and d potentials are calculated from a single atomic configuration. r_c is the core radius parameter described in Ref. 55, adjusted to optimize the smoothness and shallowness of the potentials. The energy eigenvalues of the non-relativistic pseudoatom are compared with those of the BHS FR pseudoatoms given in parentheses.

	Eigenvalues (in Ry)				r_c (in a.u.)		
	configuration	s	p	d	s	p	d
Sn	$s^1p^{0.75}d^{0.25}$	-1.96276 (-2.05024)	-1.40928 (-1.46054,-1.40408)	-0.71013 (-0.70427,-0.69930)	1.41	1.57	1.80
Pb	$s^1p^{0.75}d^{0.25}$	-1.88196 (-2.16814)	-1.35142 (-1.52106,-1.34200)	-0.68616 (-0.67282,-0.65820)	1.25	1.40	1.80
Te	$s^1p^{2.75}d^{0.25}$	-2.40357 (-2.52152)	-1.72558 (-1.79768,-1.71331)	-0.83167 (-0.82143,-0.81388)	1.28	1.35	1.50

Table 2: Structural properties of SnTe and PbTe calculated using nonrelativistic (NR), scalar relativistic (SR) and fully relativistic (FR) atomic pseudopotentials, compared to experimental values.

	crystal energy in Ry/atom	cohesive energy (eV)	lattice constant (Å)	bulk modulus (Mbar)
SnTe NR	-11.60314	7.5	6.14	0.59
SR	-11.80814	7.2	6.21	0.49
FR	-11.81250	6.9	6.23	0.51
expt	-	5.7[a)]	6.295 (0K)[8] 6.327 (300K)[58]	0.378, 0.278 (300K)[59] 0.46 (0K)[60] 0.42 (300K)[61] 0.47 (4.2K)[62]
PbTe NR	-11.45875	7.5	6.31	0.48
SR	-11.88251	7.2	6.31	0.48
FR	-11.89644	6.4	6.29	0.45
expt	-	4.7[a)]	6.443 (300K)[64] 6.462 (300K)[63]	0.456 ± .004 (0K)[54]

a) cohesive energy is obtained from cohesive energies of the elements [56] and heats of formation of the compounds.[57]

Table 3: contributions to total energy for undistorted and τ-distorted structures in SnTe and PbTe.

	SnTe (E_1=10.5, 19k-points)		PbTe (E_1=10.5, 32k-points)	
	τ=0.000	τ=.015	τ=0.000	τ=.015
E_{kin}	3.49239	3.49722	3.52250	3.52709
E_{xc}	-2.82877	-2.83086	-2.81985	-2.82175
E'_{H}	0.61630	0.62315	0.66629	0.67316
E'_{ei}	-2.79686	-2.81804	-3.10296	-3.12363
E'_{ii}	-12.36657	-12.35509	-12.22762	-12.21627
E_{tot}	-11.80887	-11.80898	-11.88329	-11.88305

a)

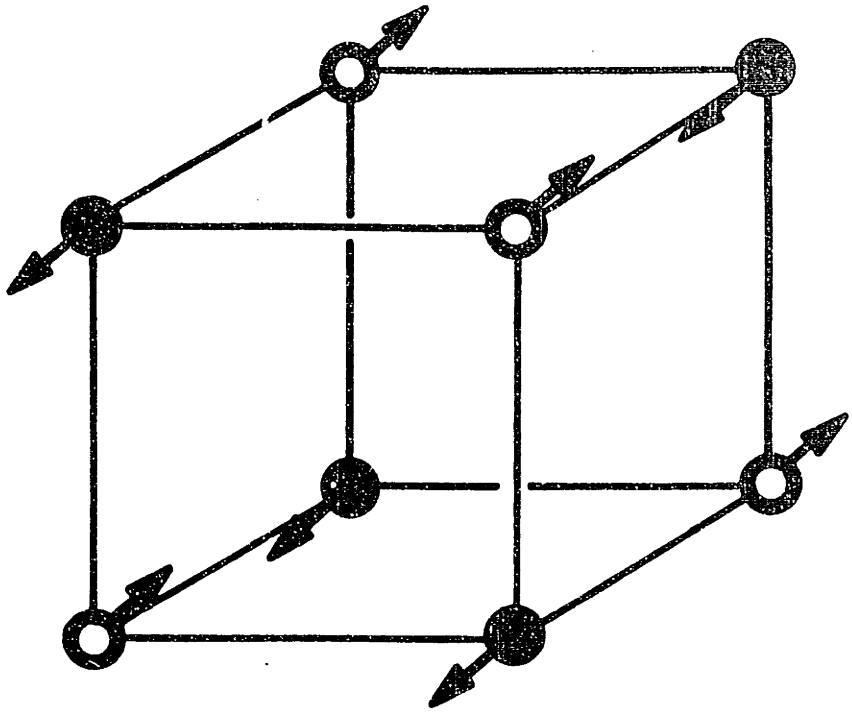

b)

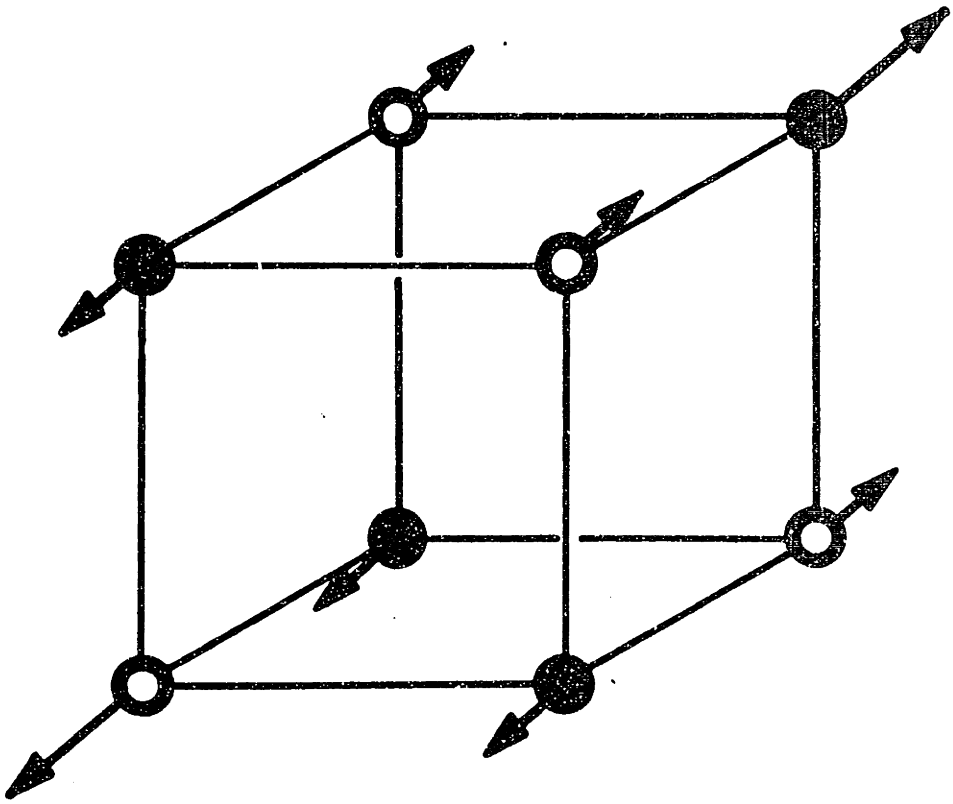

Figure 1

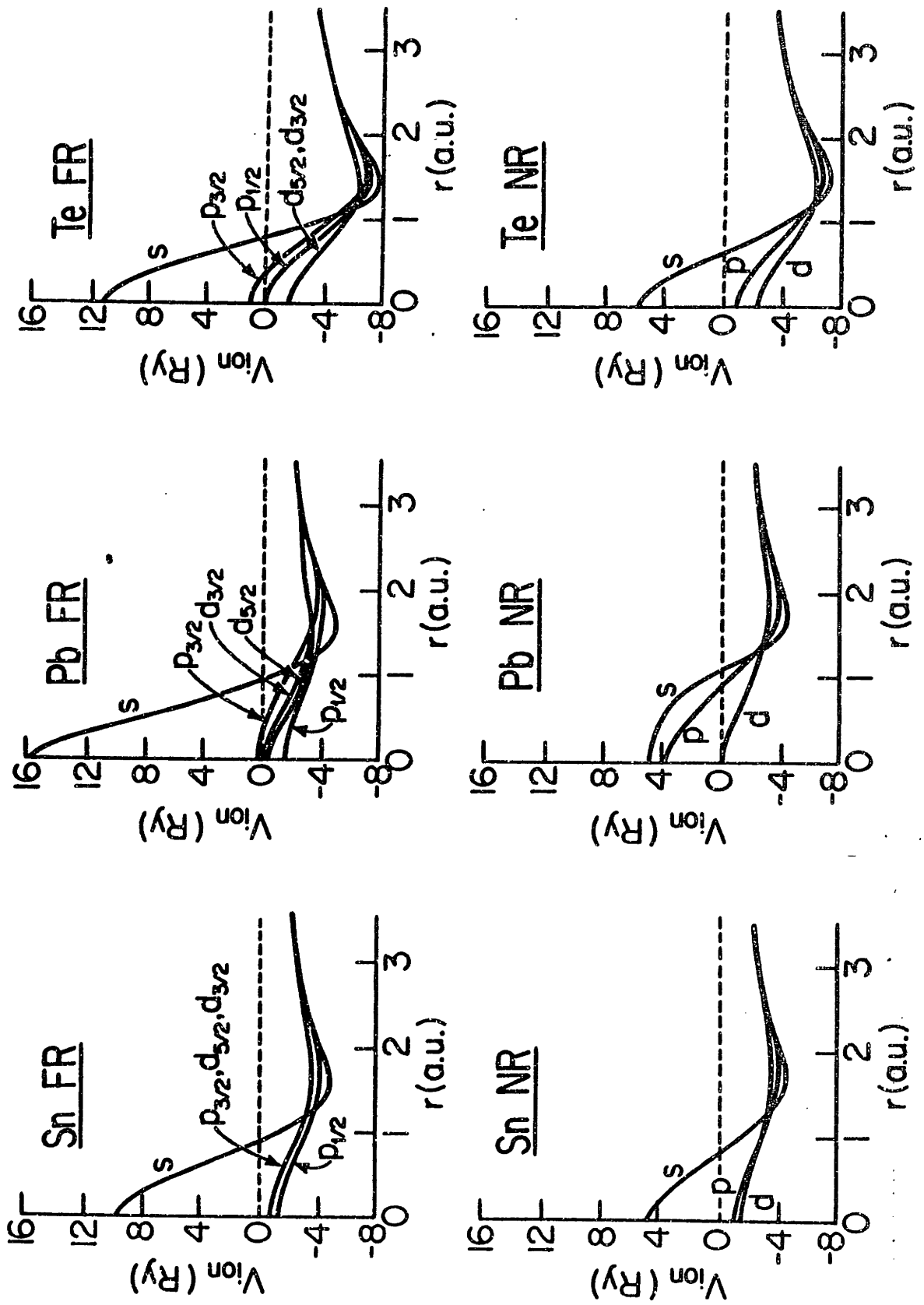

Figure 2

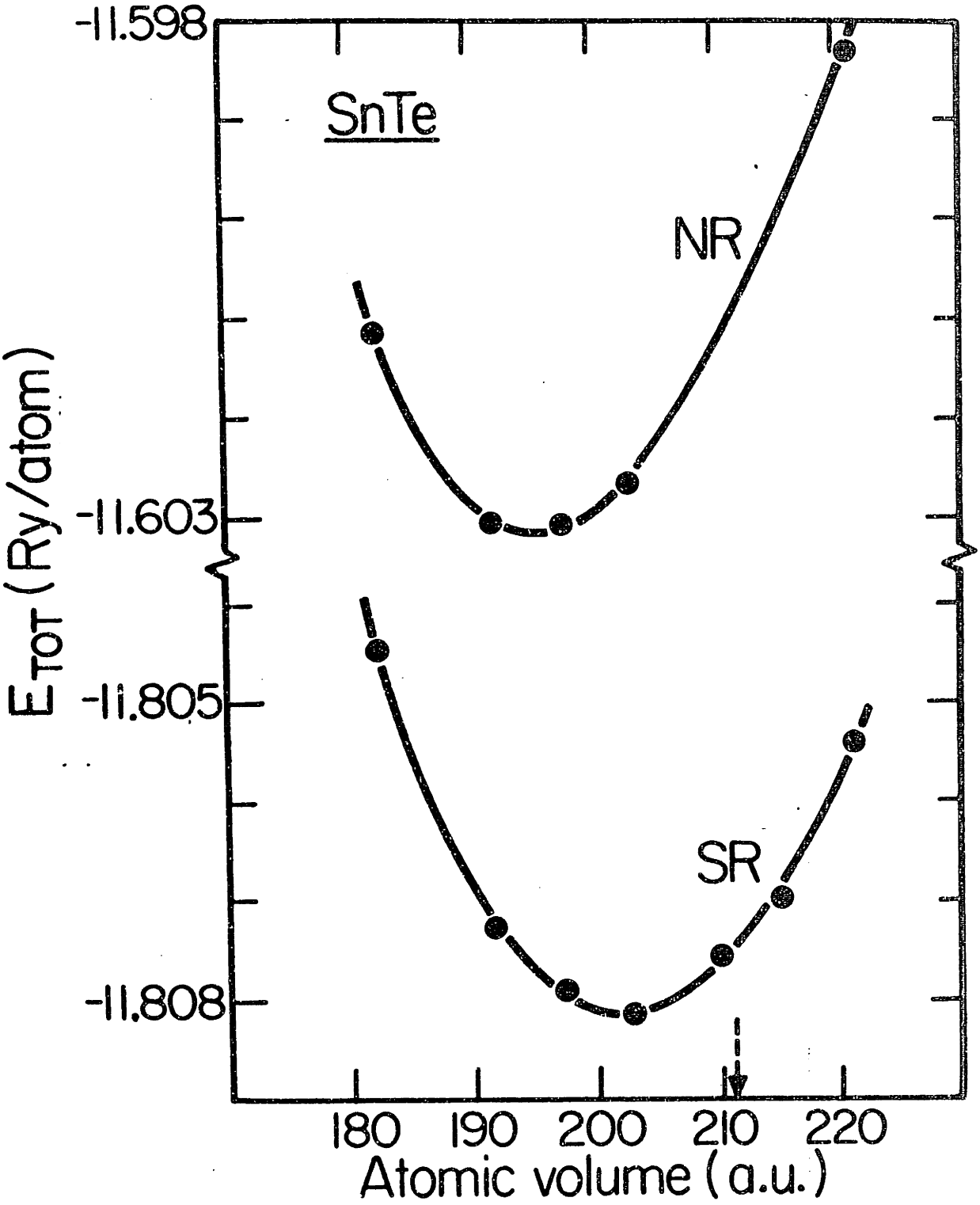
-11.598
-11.603
-11.805
-11.808
SnTe
NR
SR
E TOT (Ry/atom)
180
190
200
210
220
Atomic volume (a.u.)

Figure 3

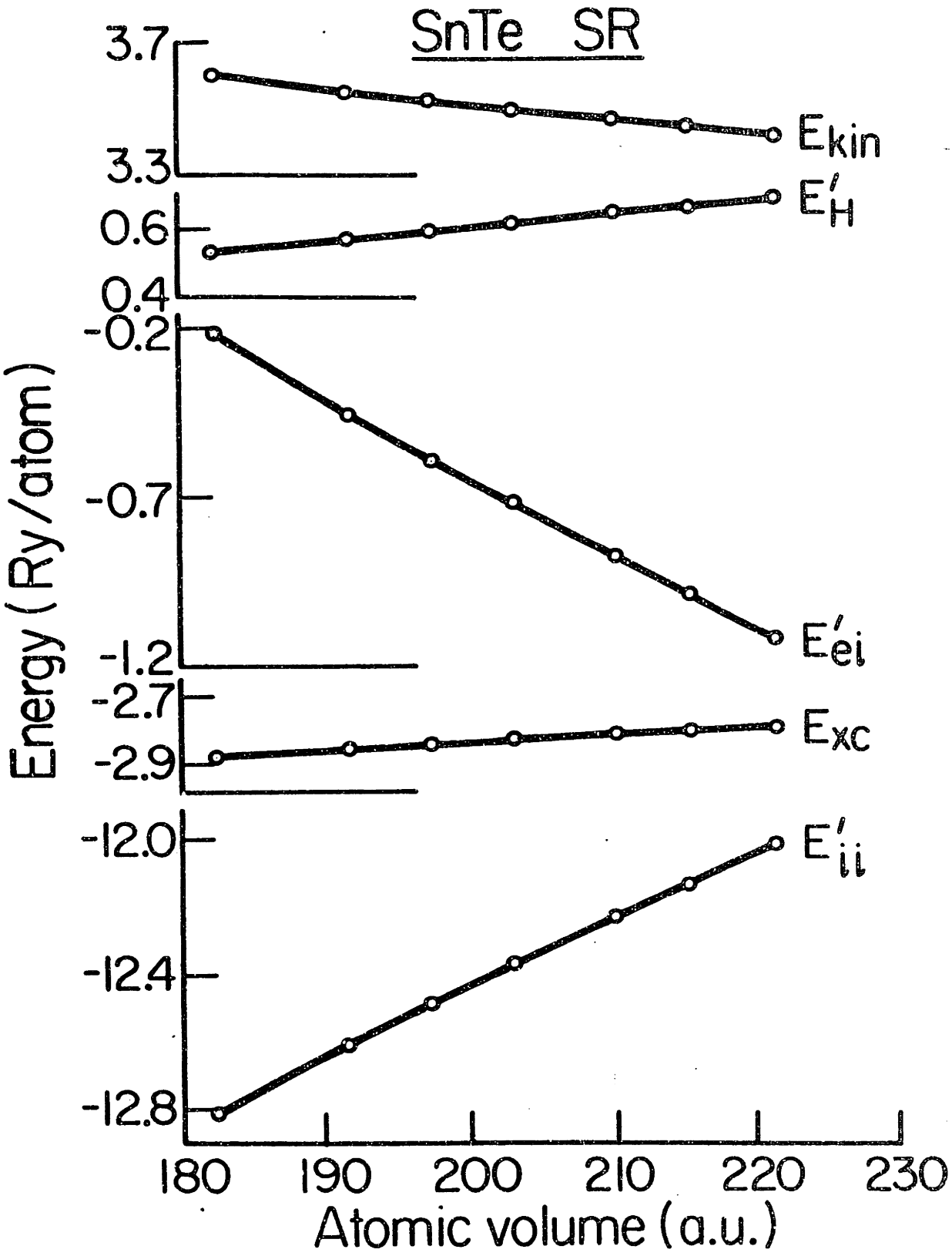
SnTe SR
3.7
3.3
0.6
0.4
-0.2
-0.7
-1.2
-2.7
-2.9
-12.0
-12.4
-12.8
Energy (Ry/atom)
Ekin
E'H
E'ei
Exc
E'ii
180
190
200
210
220
230
Atomic volume (a.u.)

Figure 4

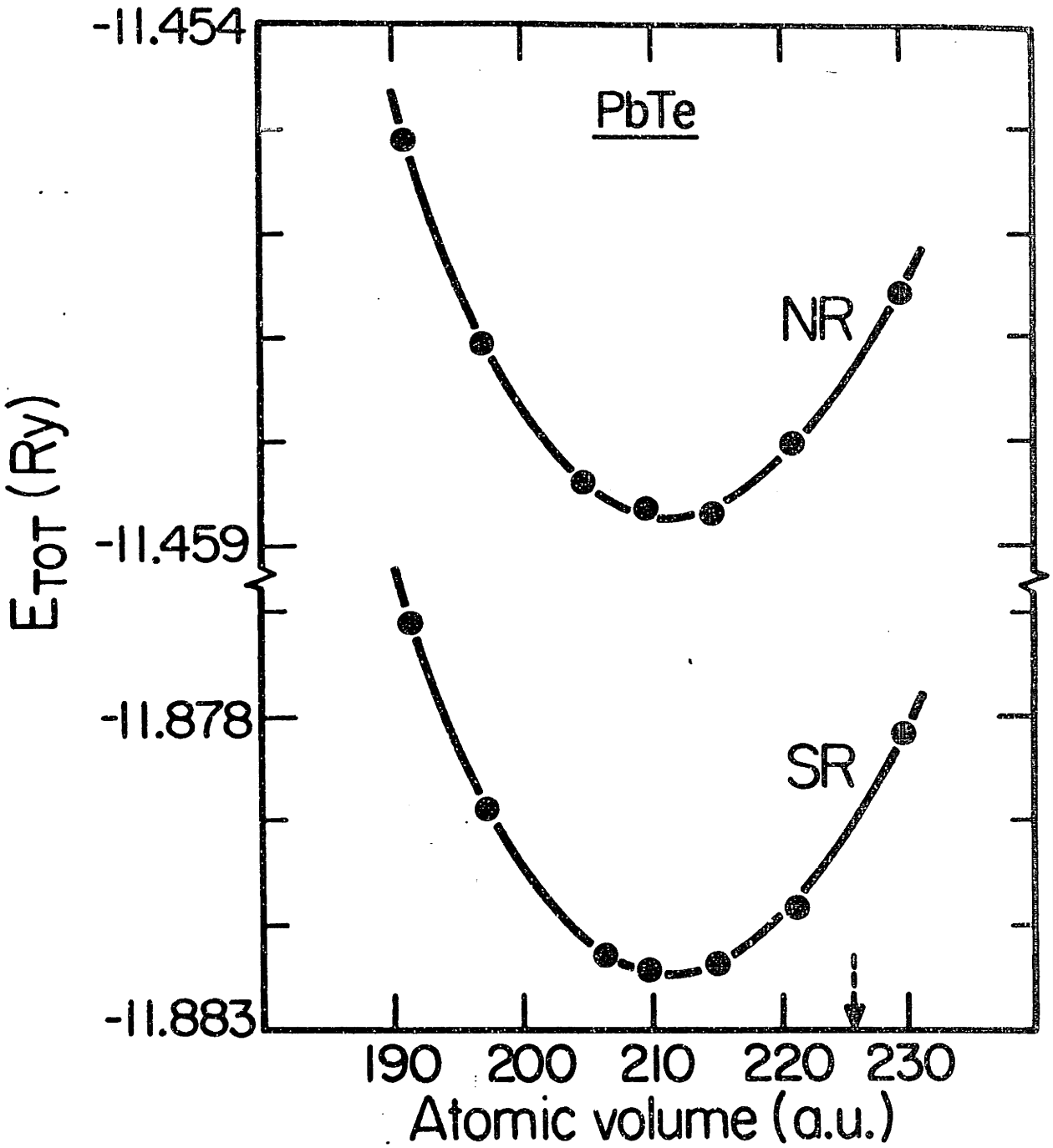
-11.454
-11.459
-11.878
-11.883
PbTe
NR
SR
E_{TOT} (Ry)
190
200
210
220
230
Atomic volume (a.u.)

Figure 5

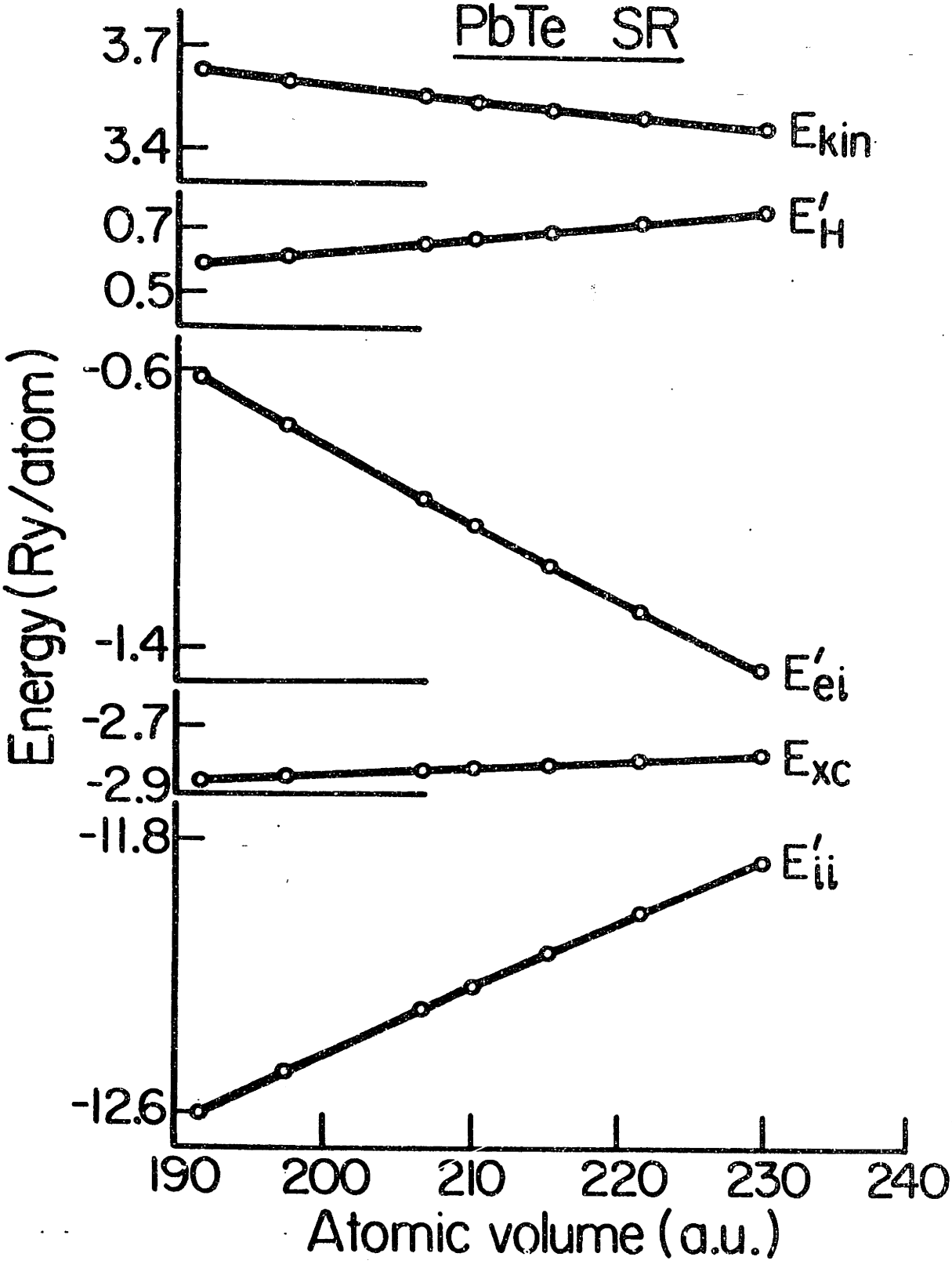
PbTe SR
3.7
3.4
0.7
0.5
-0.6
-1.4
-2.7
-2.9
-11.8
-12.6
Ekin
E'H
E'ei
Exc
E'ii
Energy (Ry/atom)
190
200
210
220
230
240
Atomic volume (a.u.)

Figure 6

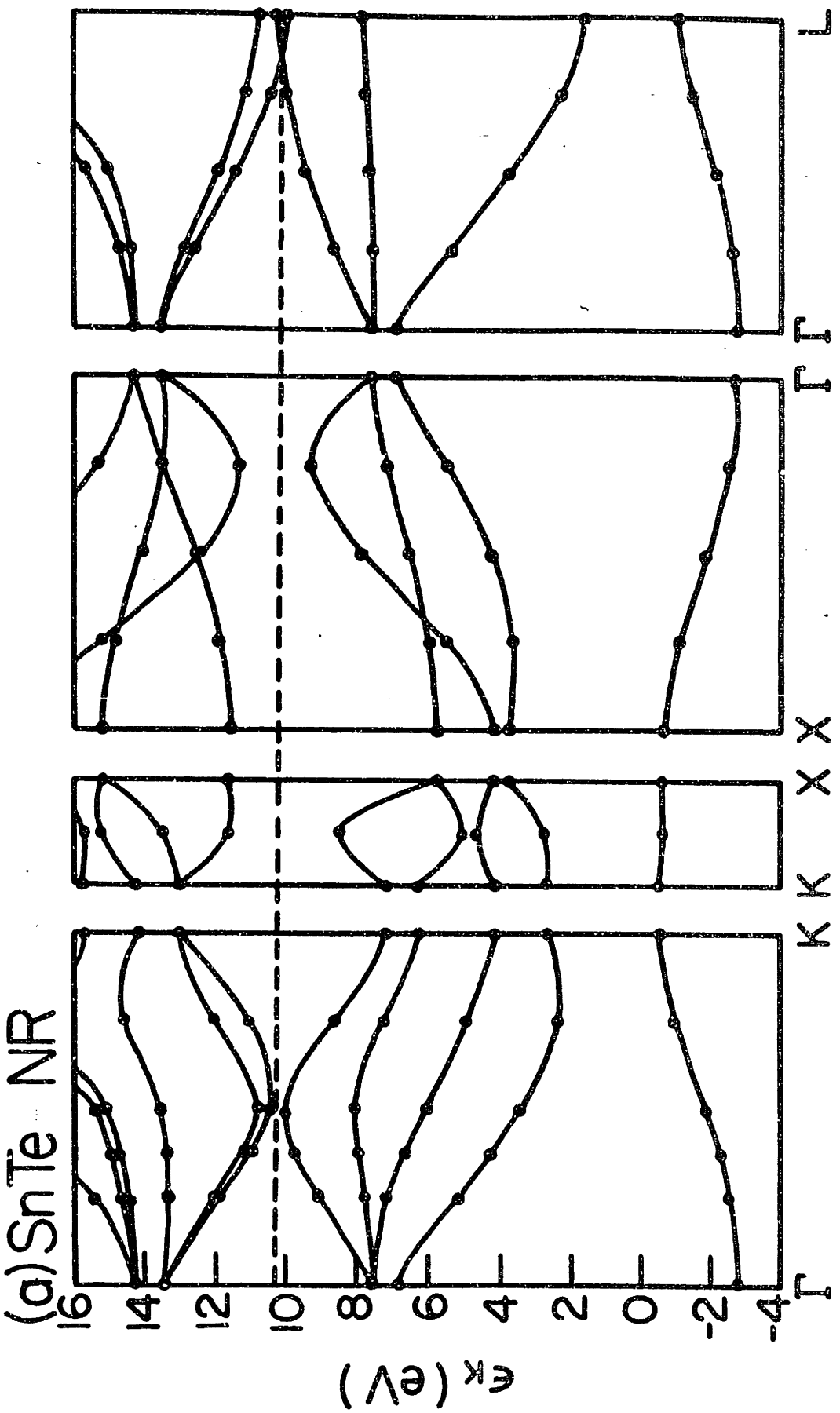

Figure 7

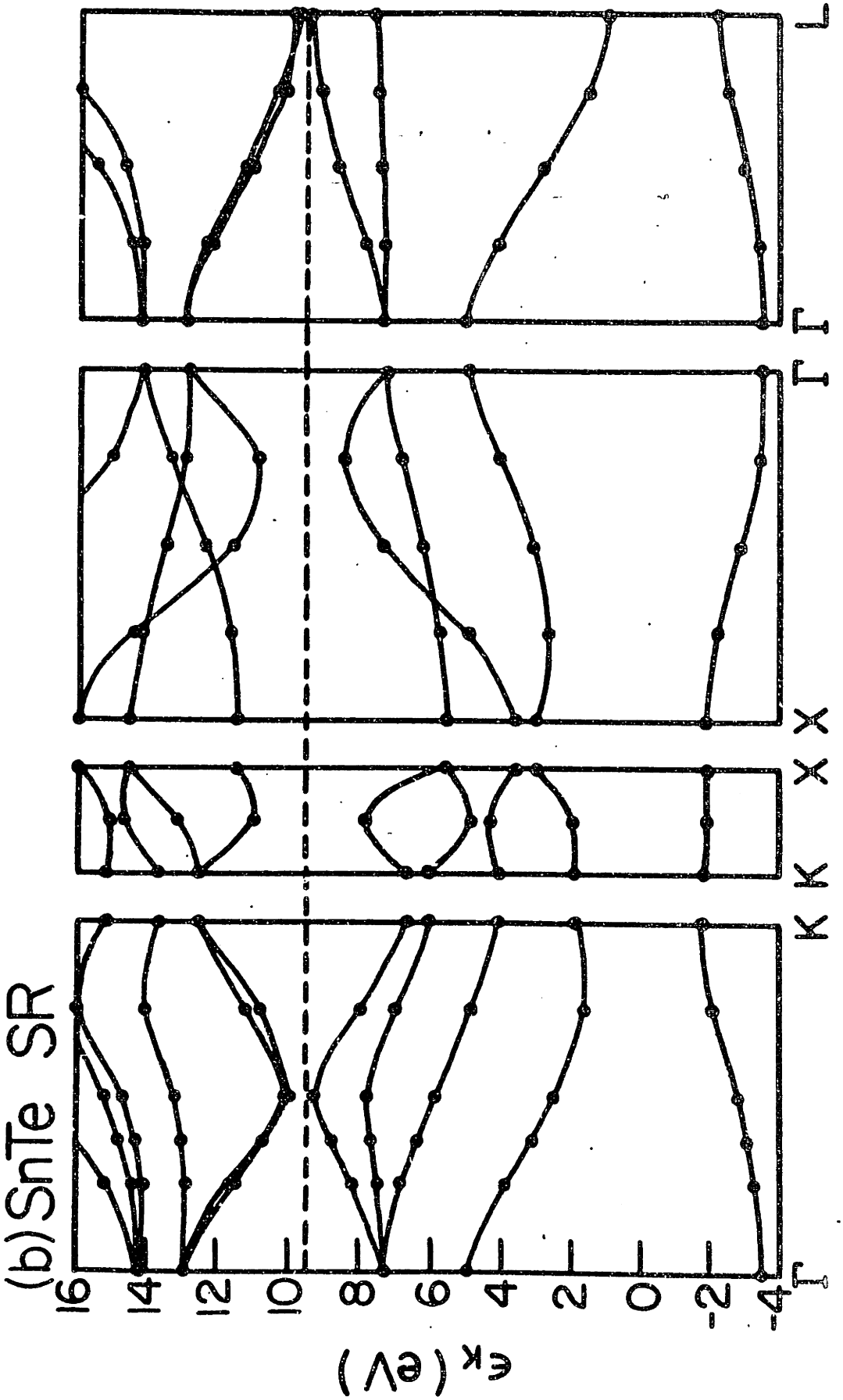

Figure 7

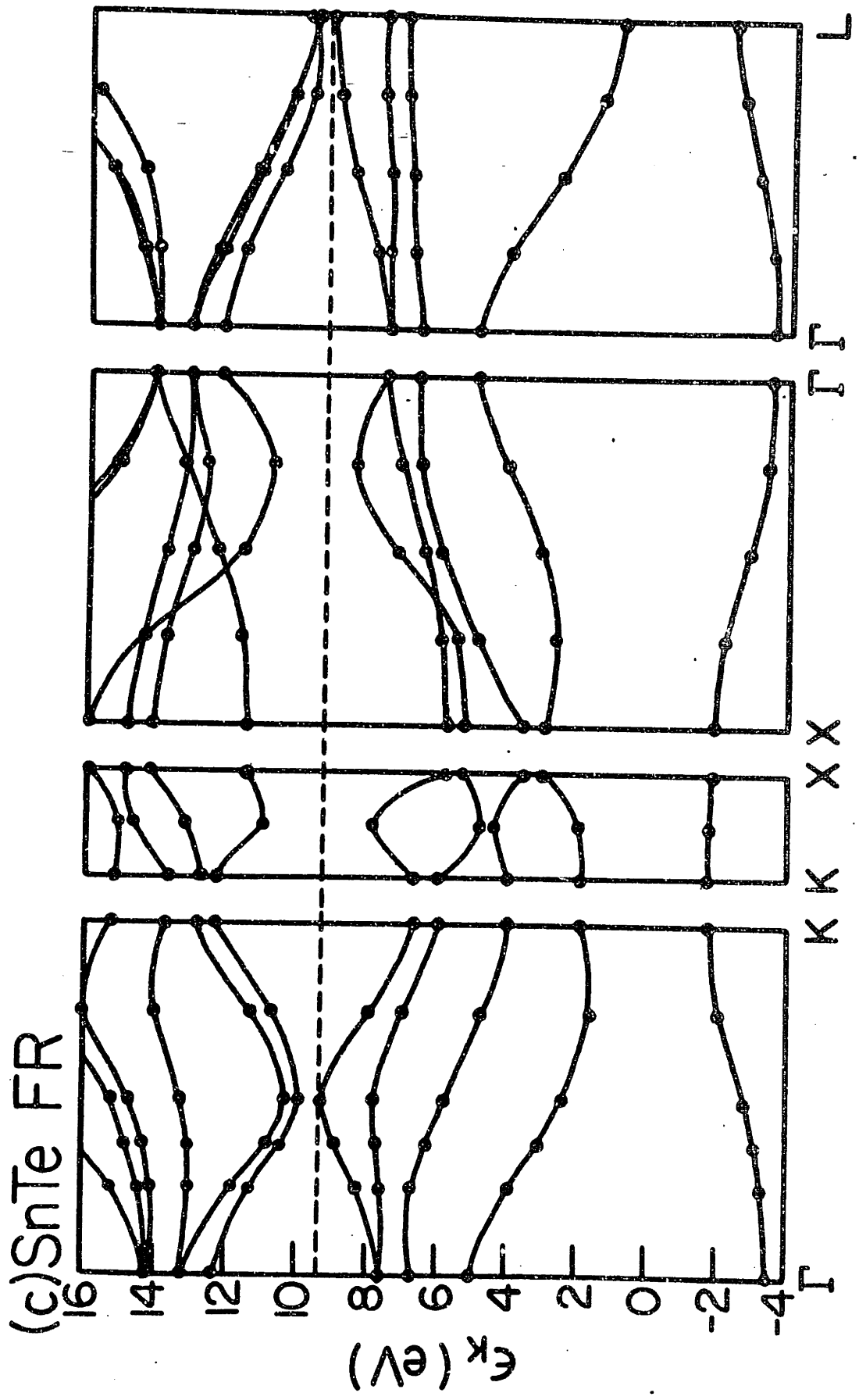

Figure 7

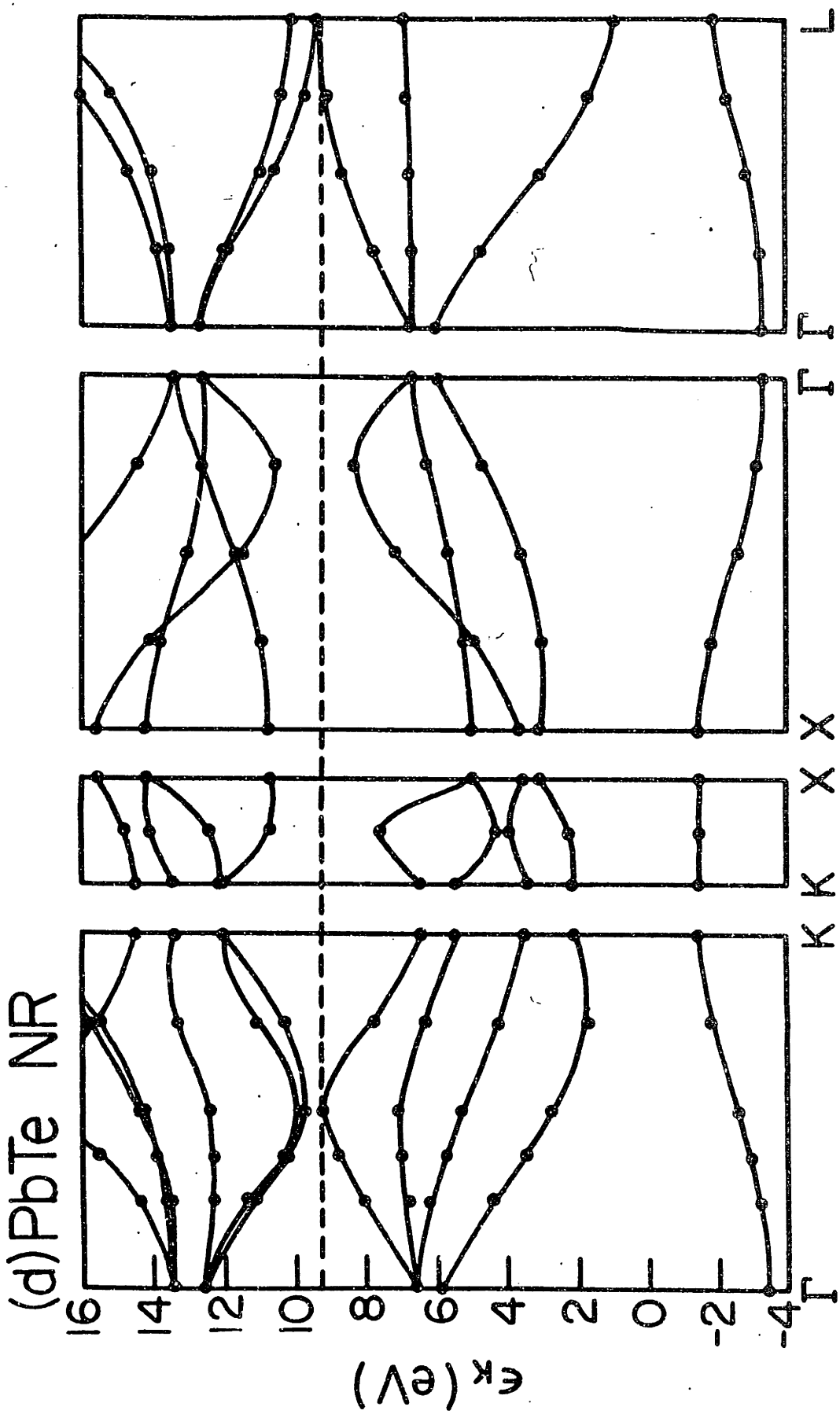

Figure 7

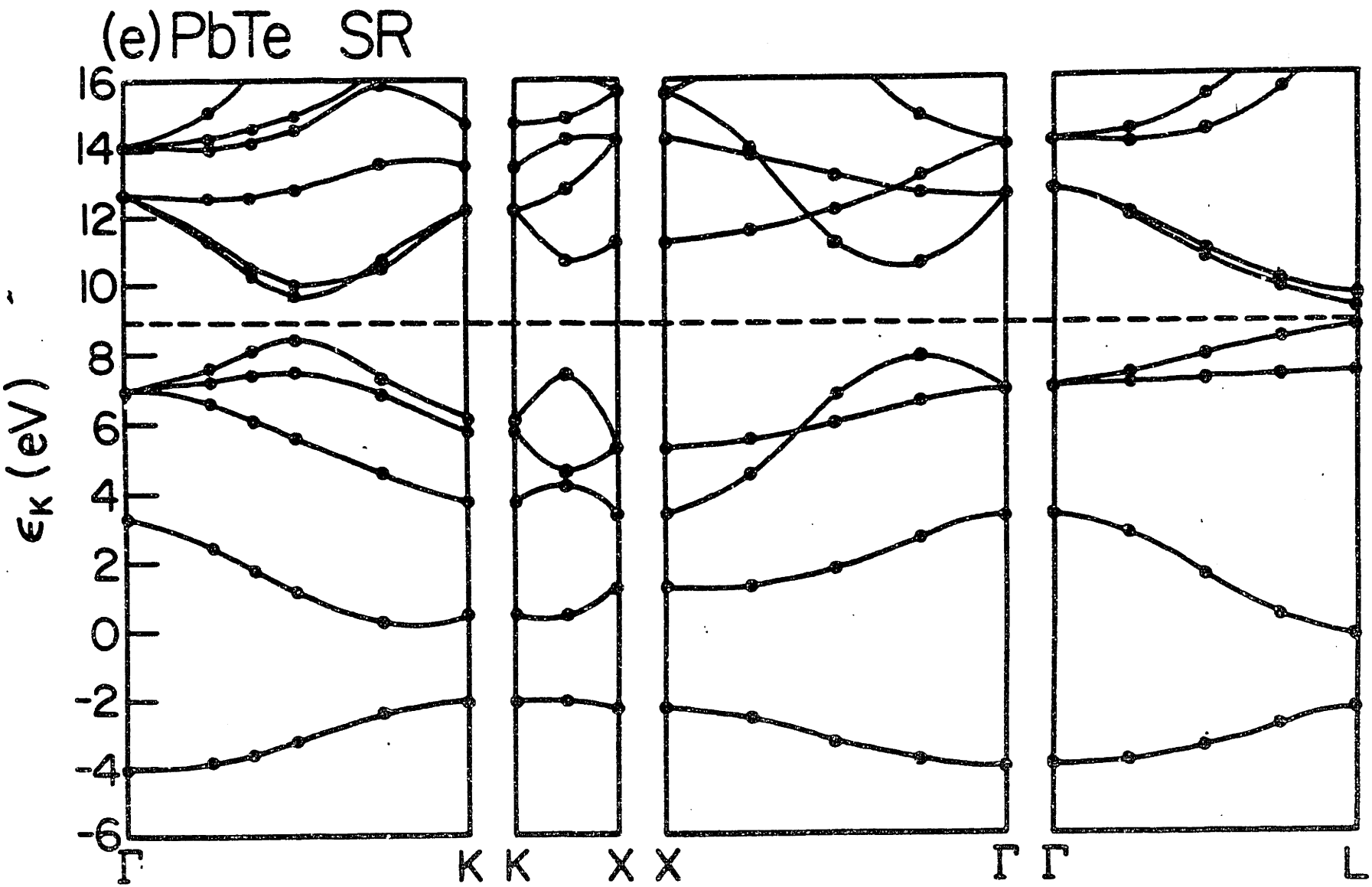

Figure 7

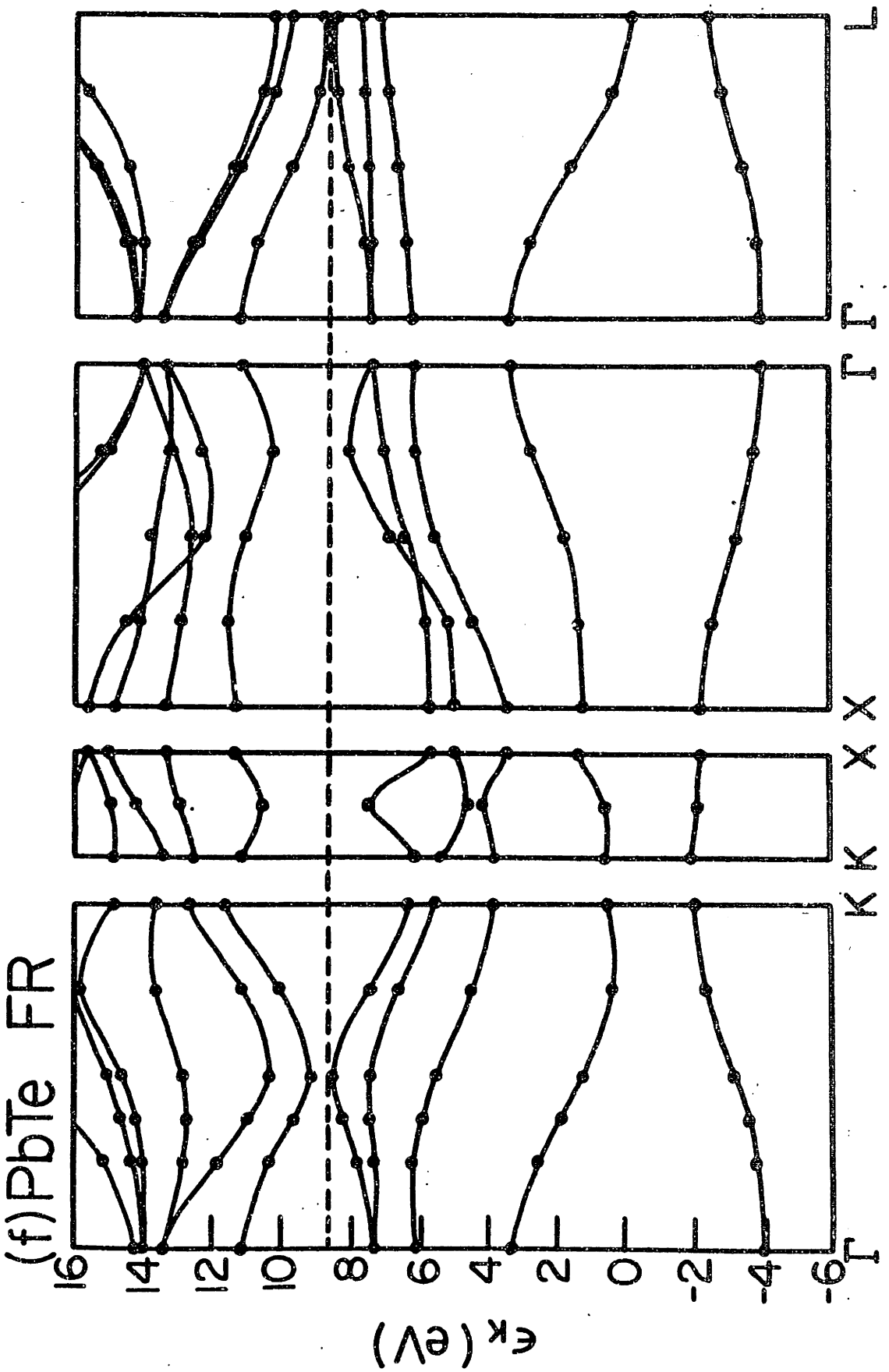

Figure 7

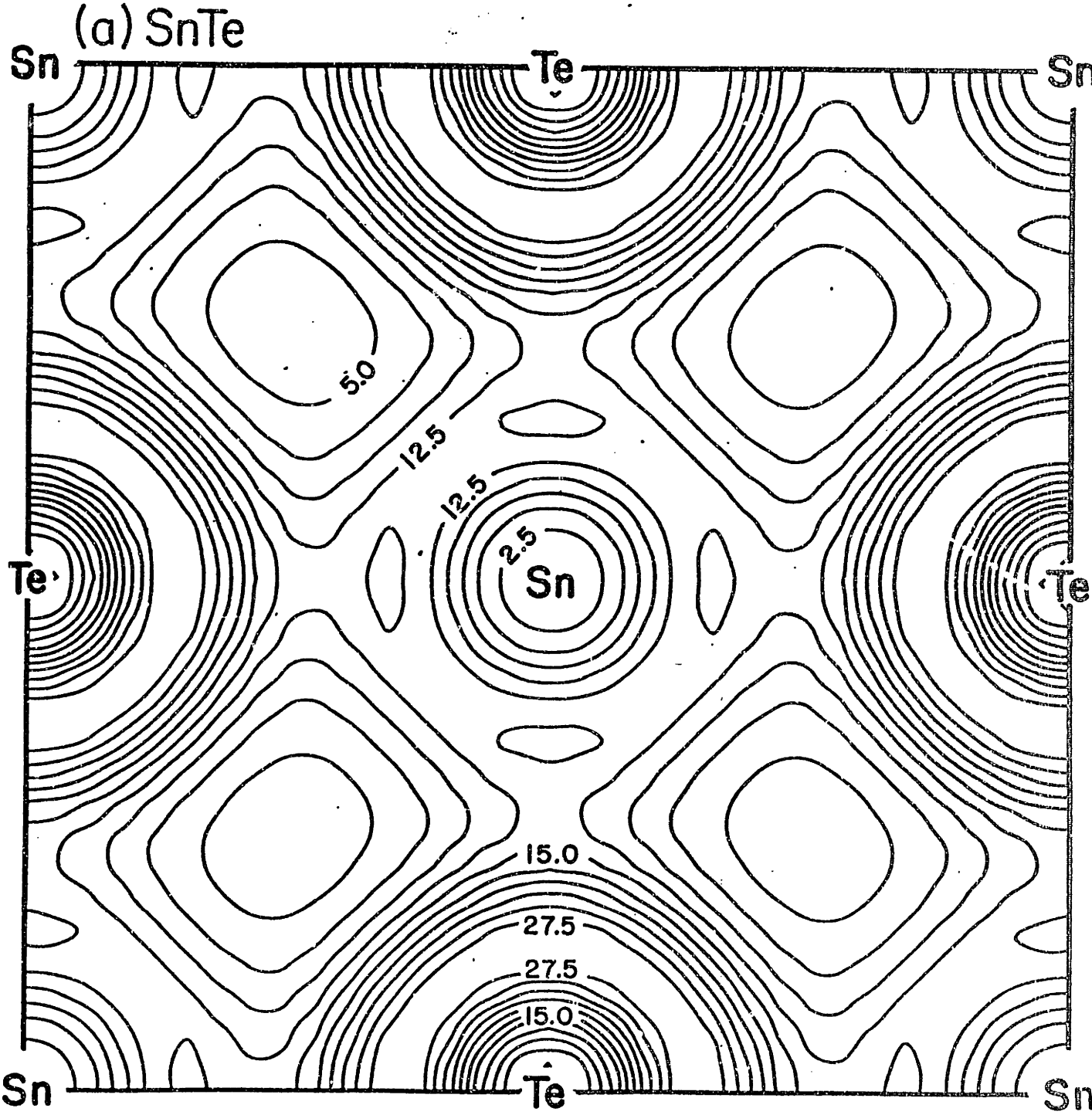

Figure 8

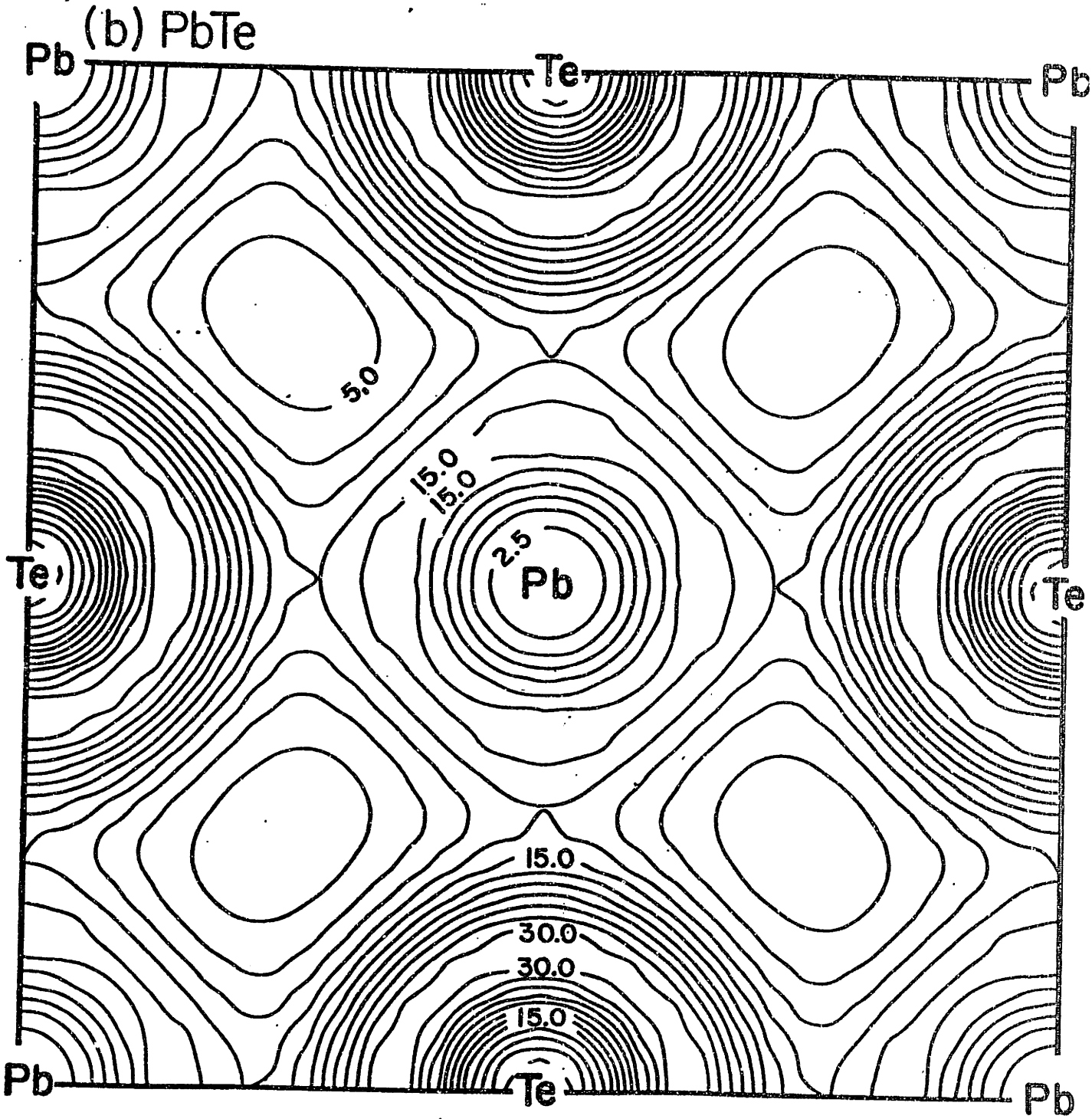

Figure 8

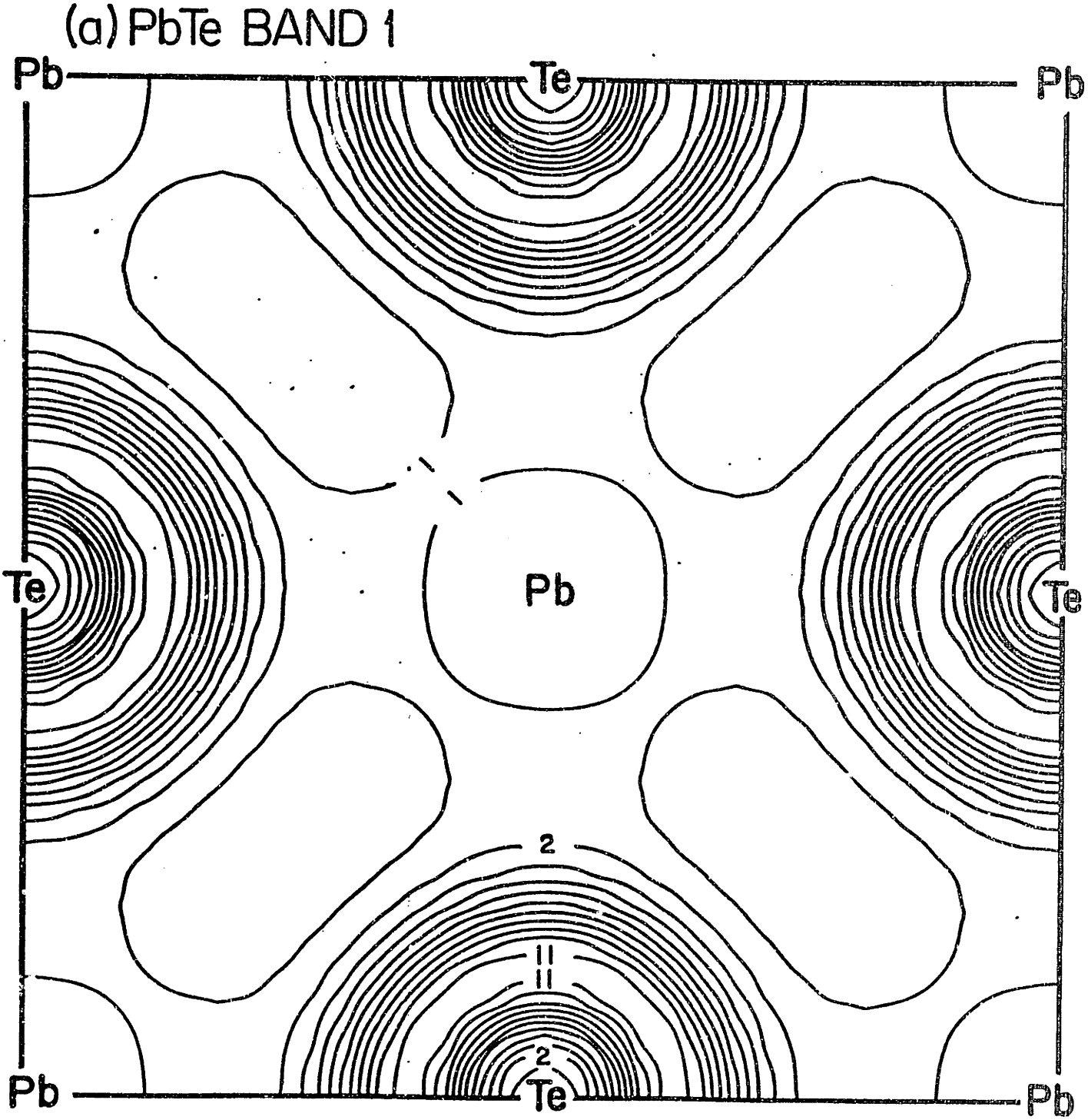

Figure 9

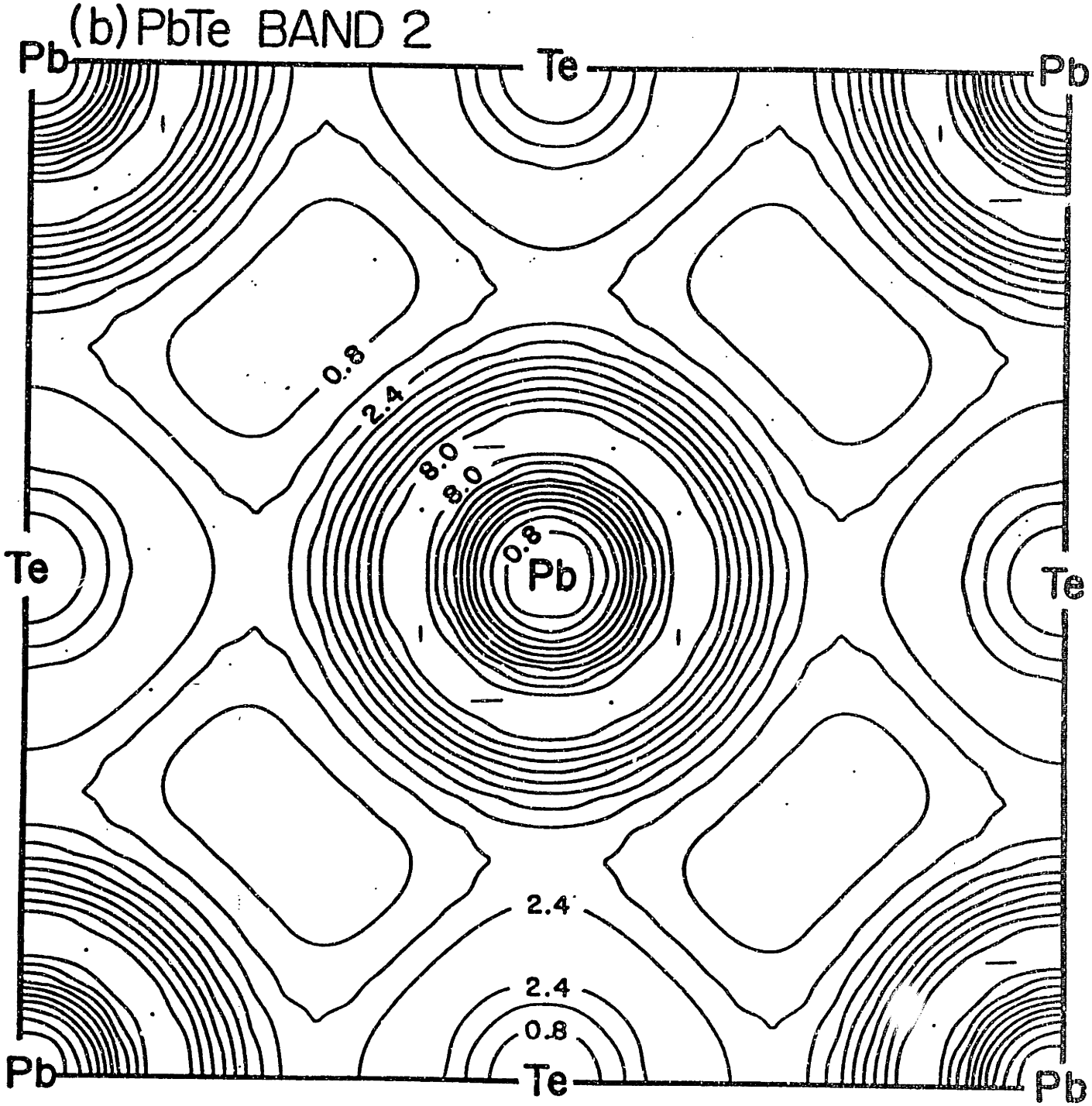

Figure 9

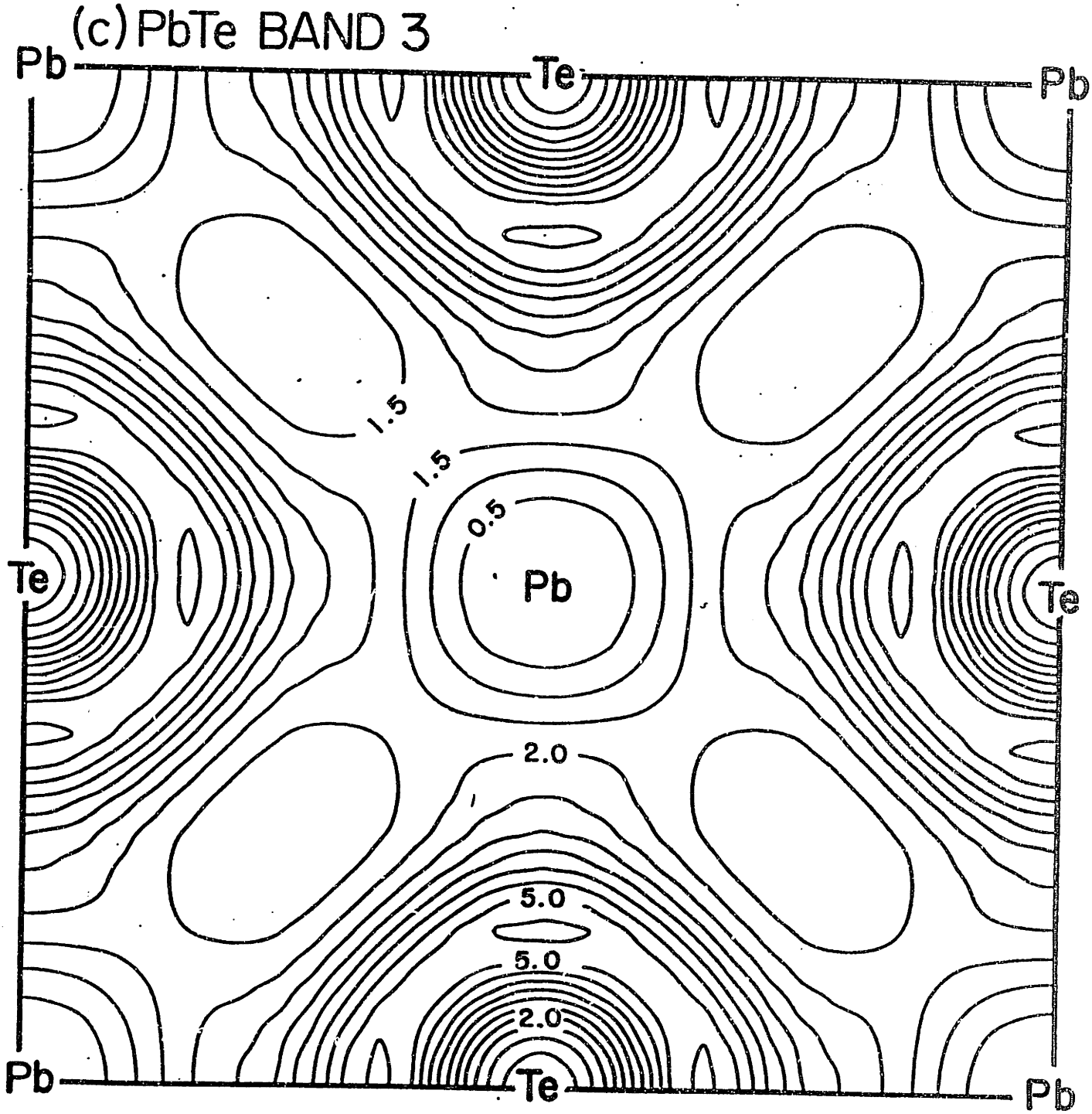

Figure 9

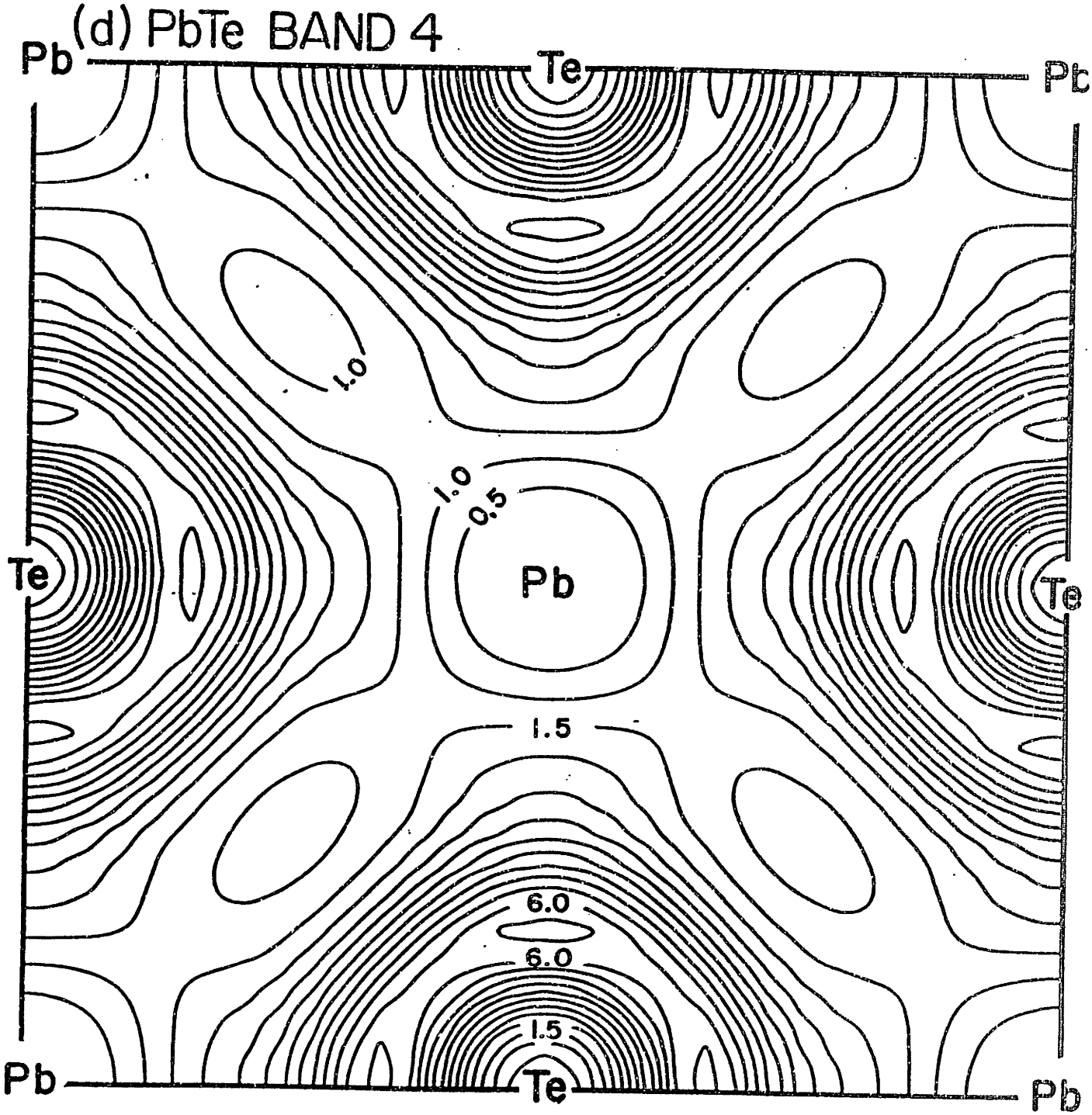

Figure 9

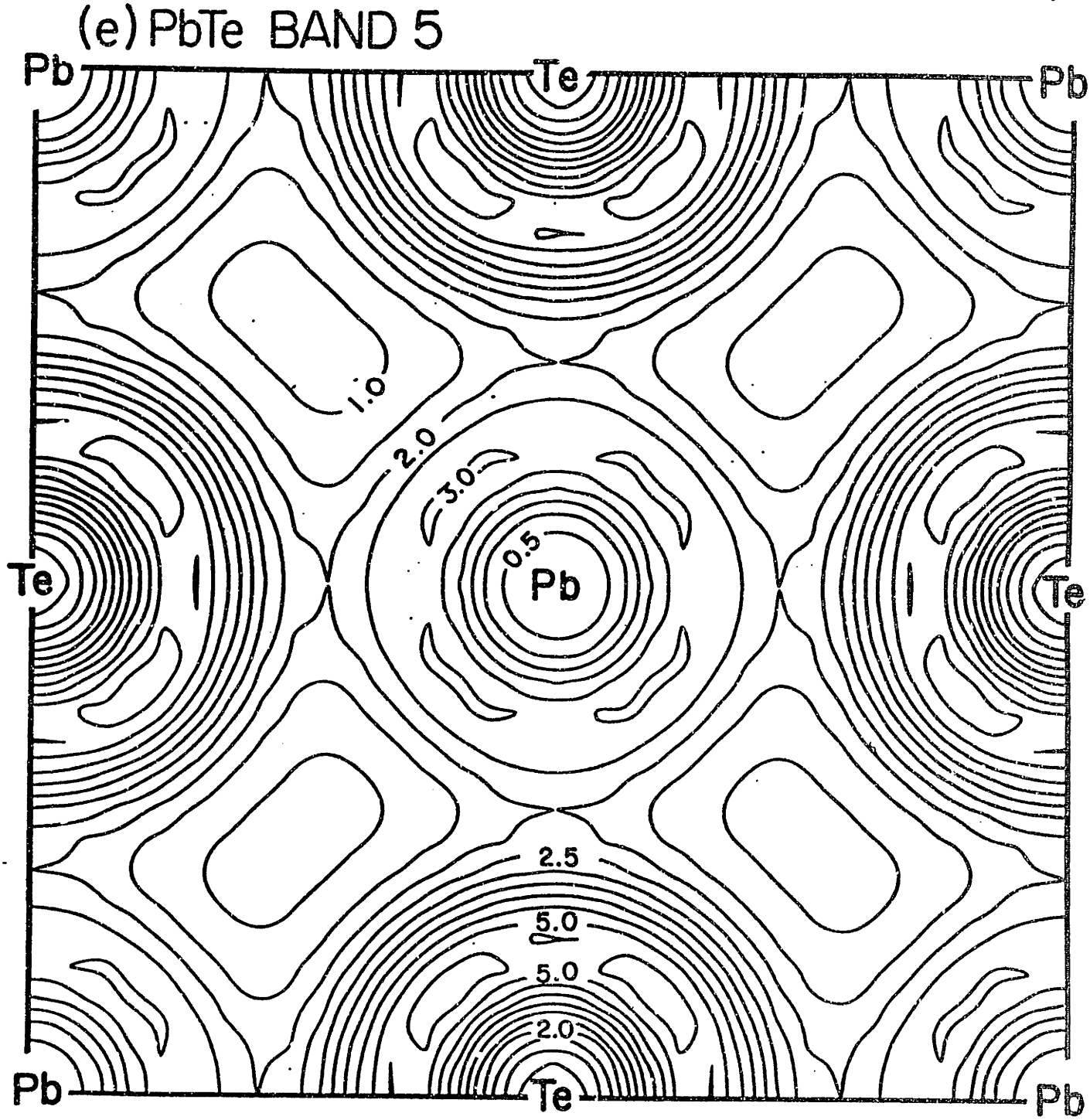

Figure 9

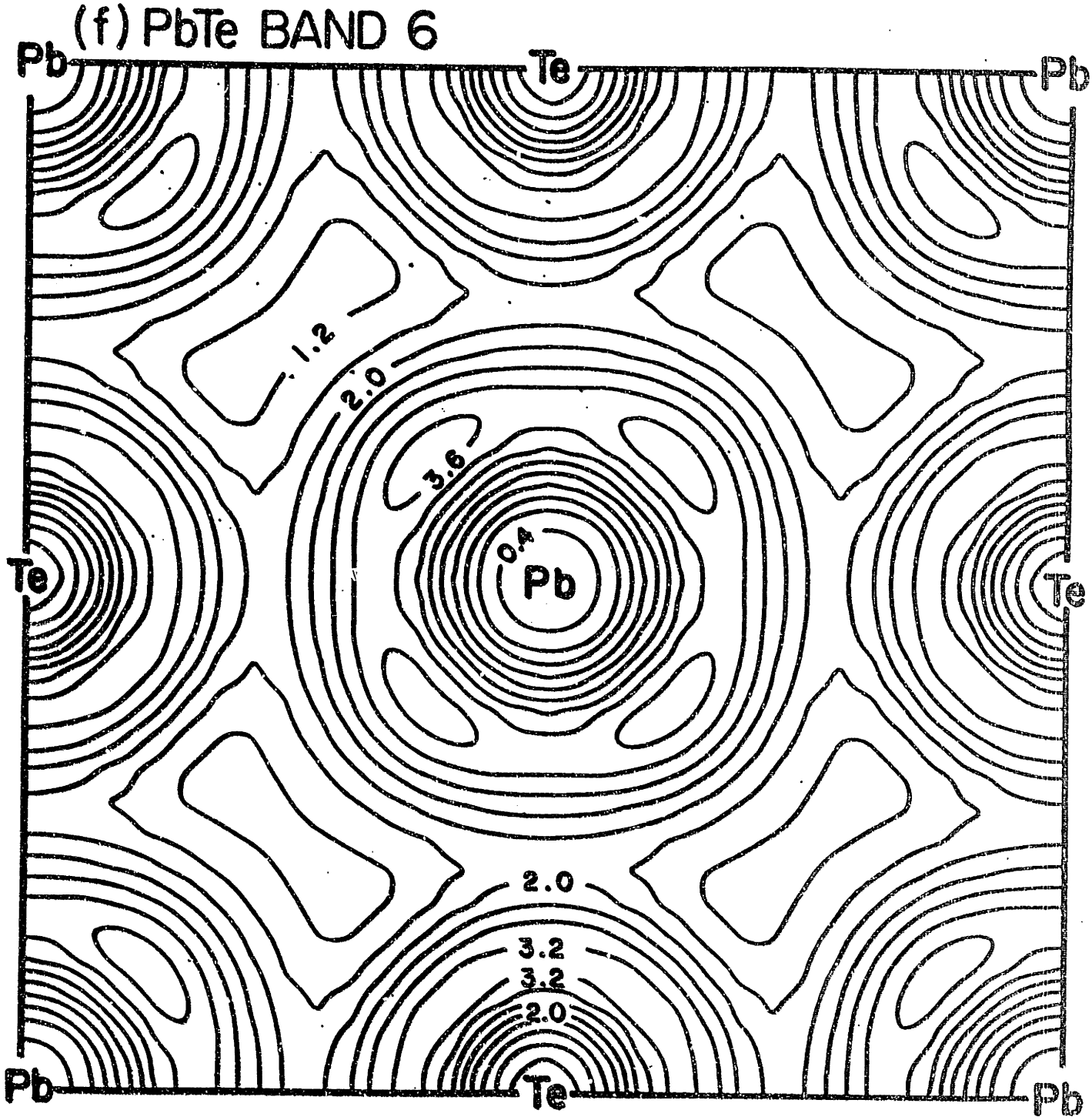

Figure 9

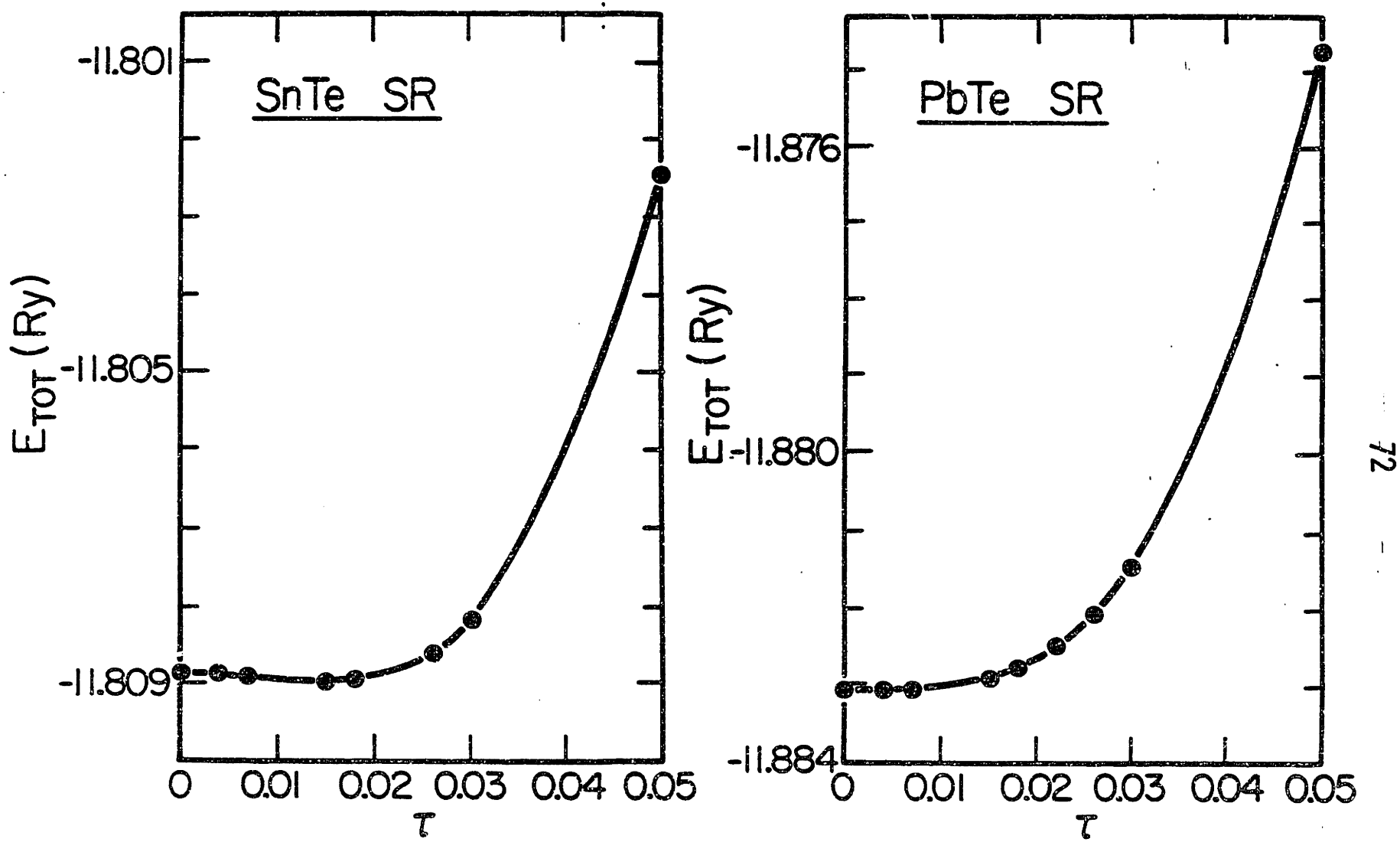
SnTe SR
PbTe SR
E_{TOT} (Ry)
-11.801
-11.805
-11.809
-11.876
-11.880
-11.884
0
0.01
0.02
0.03
0.04
0.05
τ

Figure 10

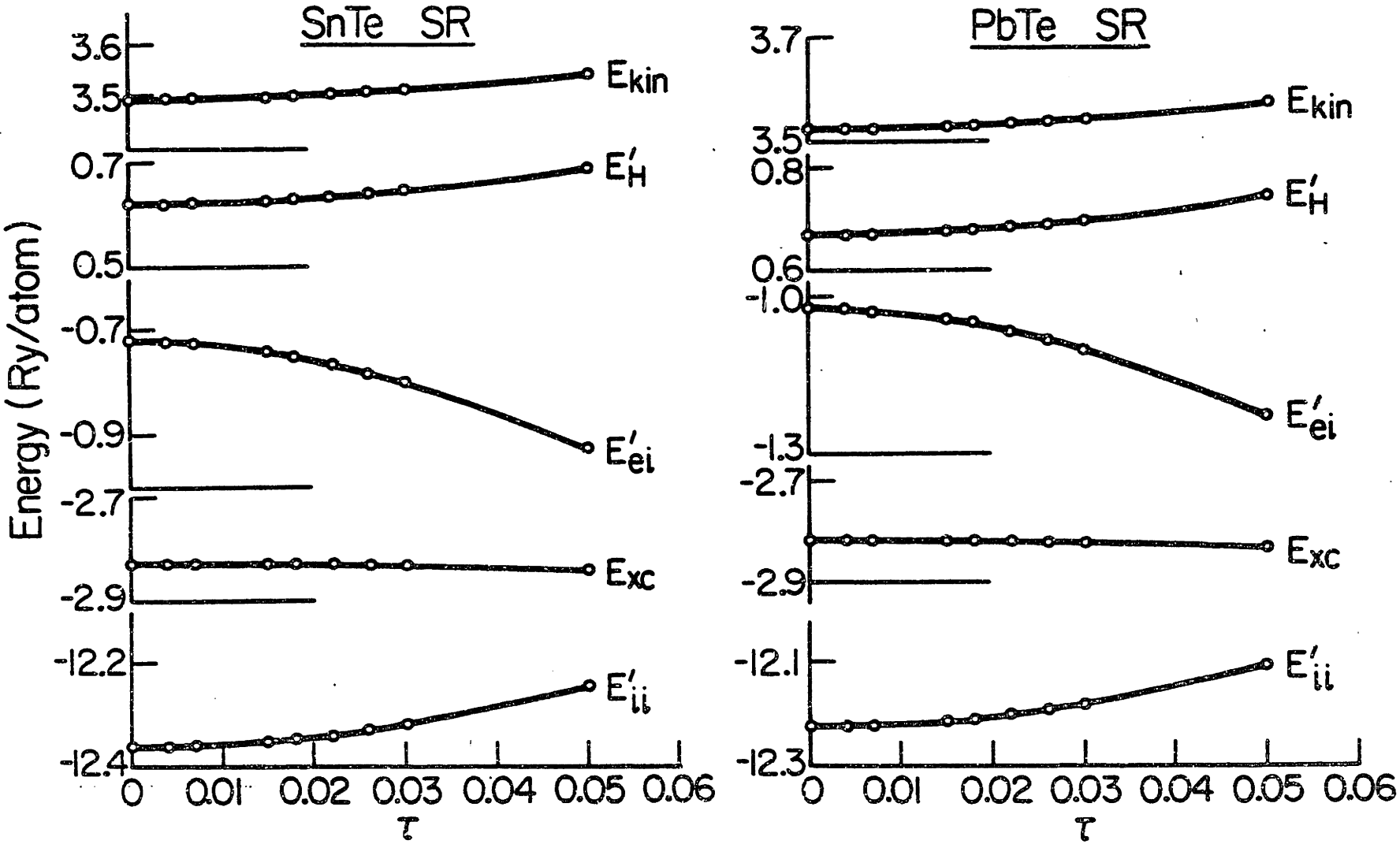
SnTe SR
PbTe SR
Energy (Ry/atom)
3.6
3.5
0.7
0.5
-0.7
-0.9
-2.7
-2.9
-12.2
-12.4
3.7
3.5
0.8
0.6
-1.0
-1.3
-2.7
-2.9
-12.1
-12.3
Ekin
E'H
E'ei
Exc
E'ii
0
0.01
0.02
0.03
0.04
0.05
0.06
τ

Figure 11

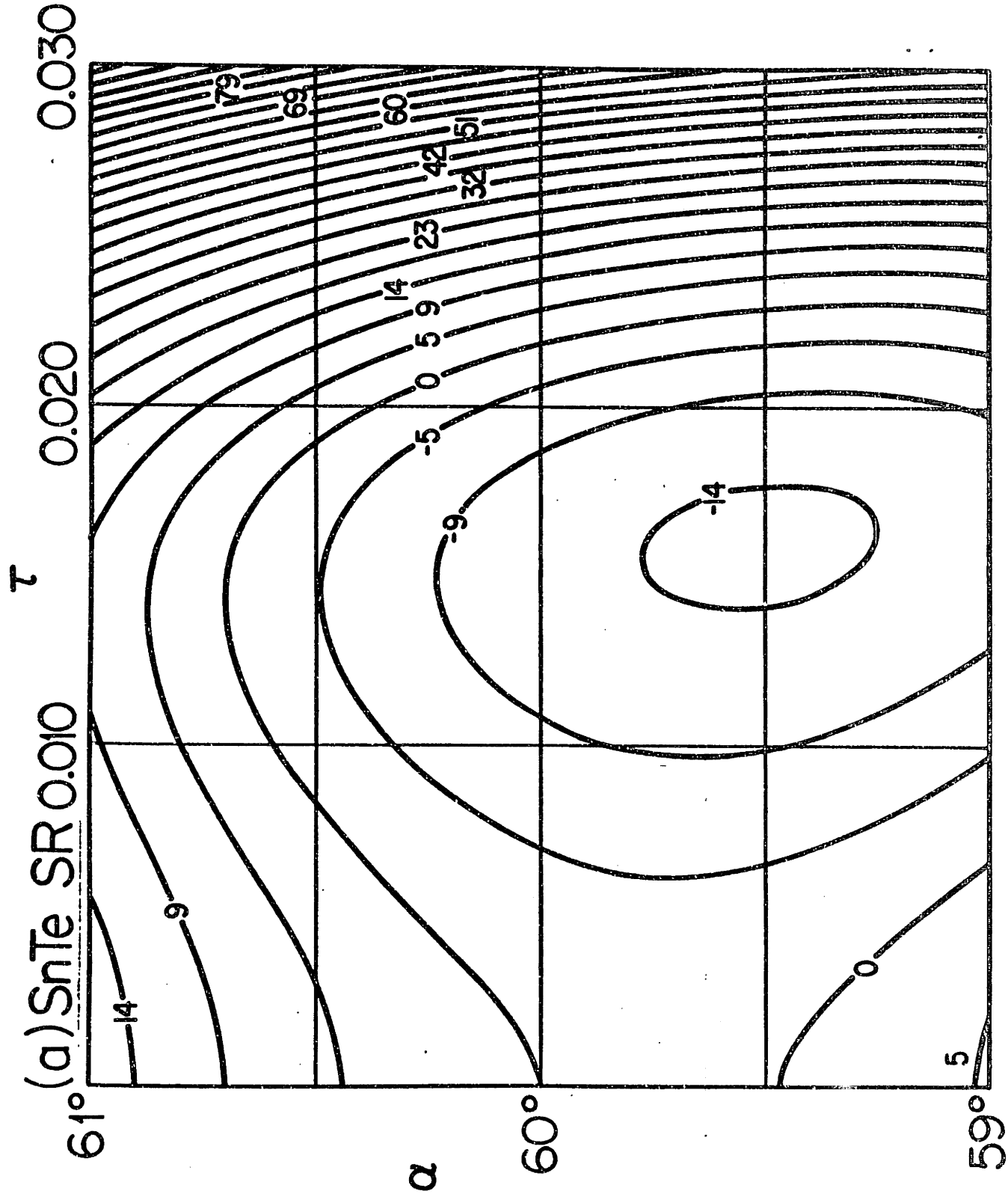
(a) SnTe SR 0.010
τ
0.030
0.020
α
61°
60°
59°
79
69
60
51
42
32
23
14
9
5
0
-5
-9
-14
14
9
0
5

Figure 12

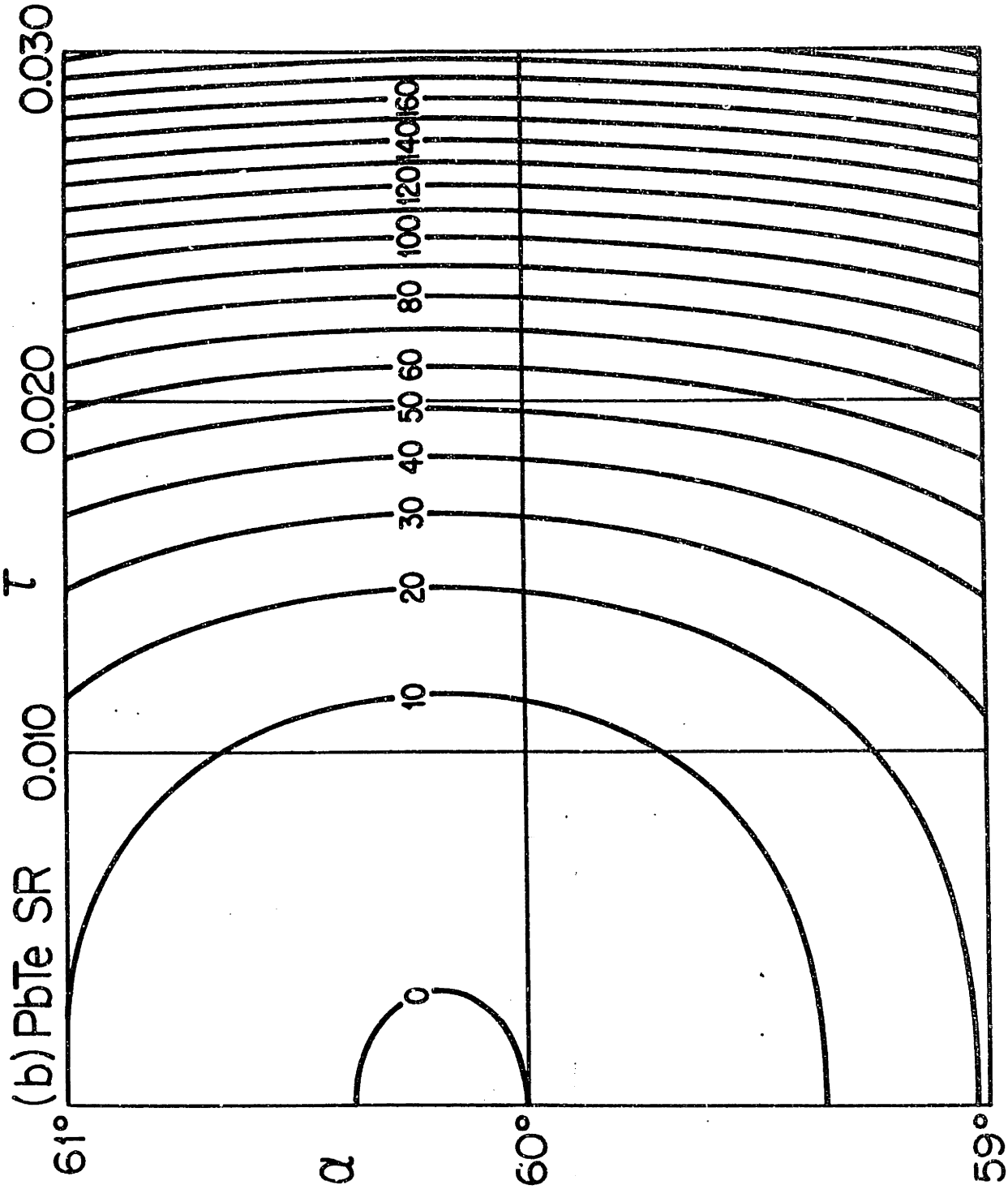
(b) PbTe SR
0.010
0.020
0.030
τ
0
10
20
30
40
50
60
80
100
120
140
160
61°
60°
59°
α

Figure 12

(a) $\tau = 0.000$

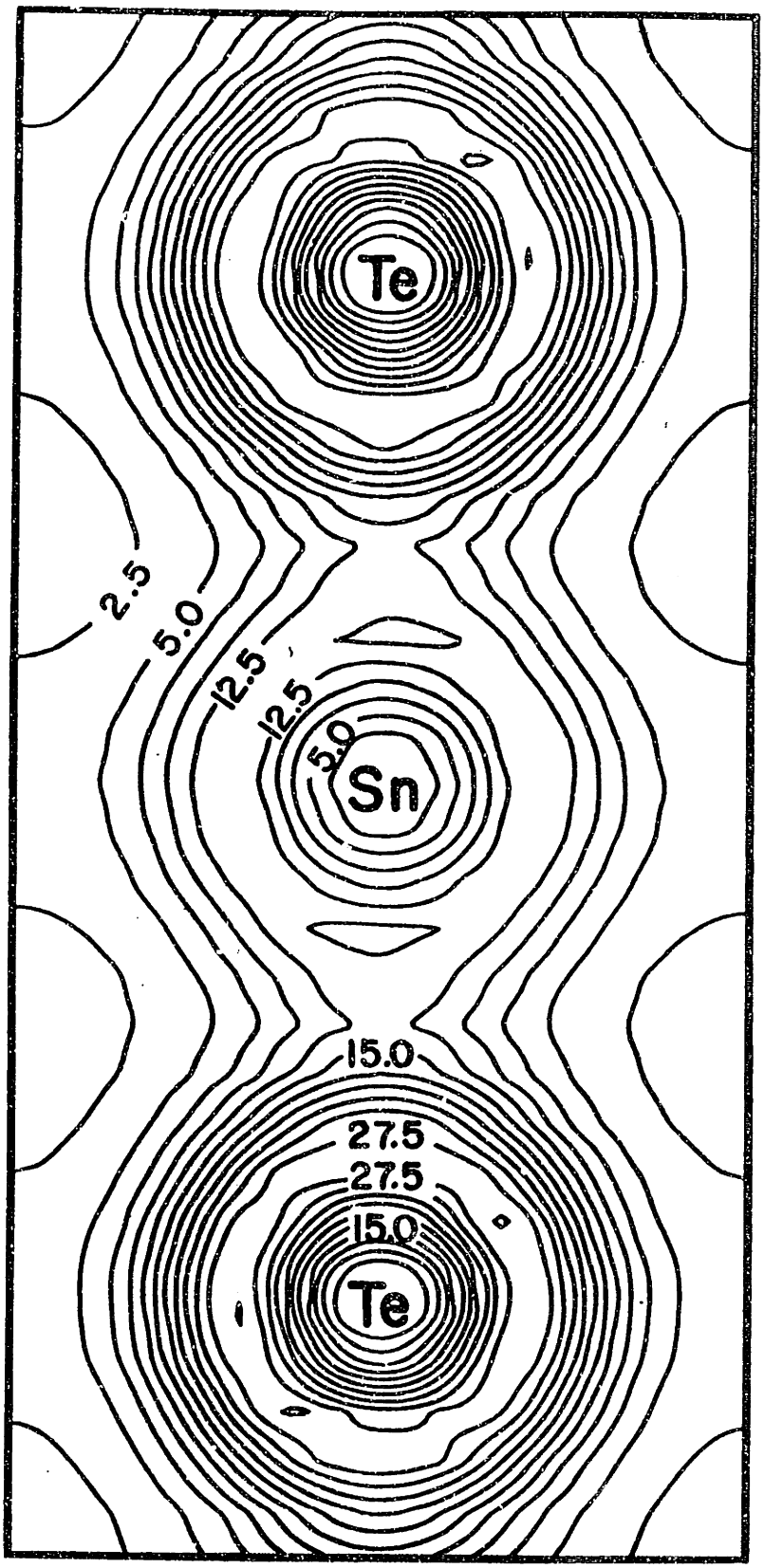

(b) $\tau = 0.015$

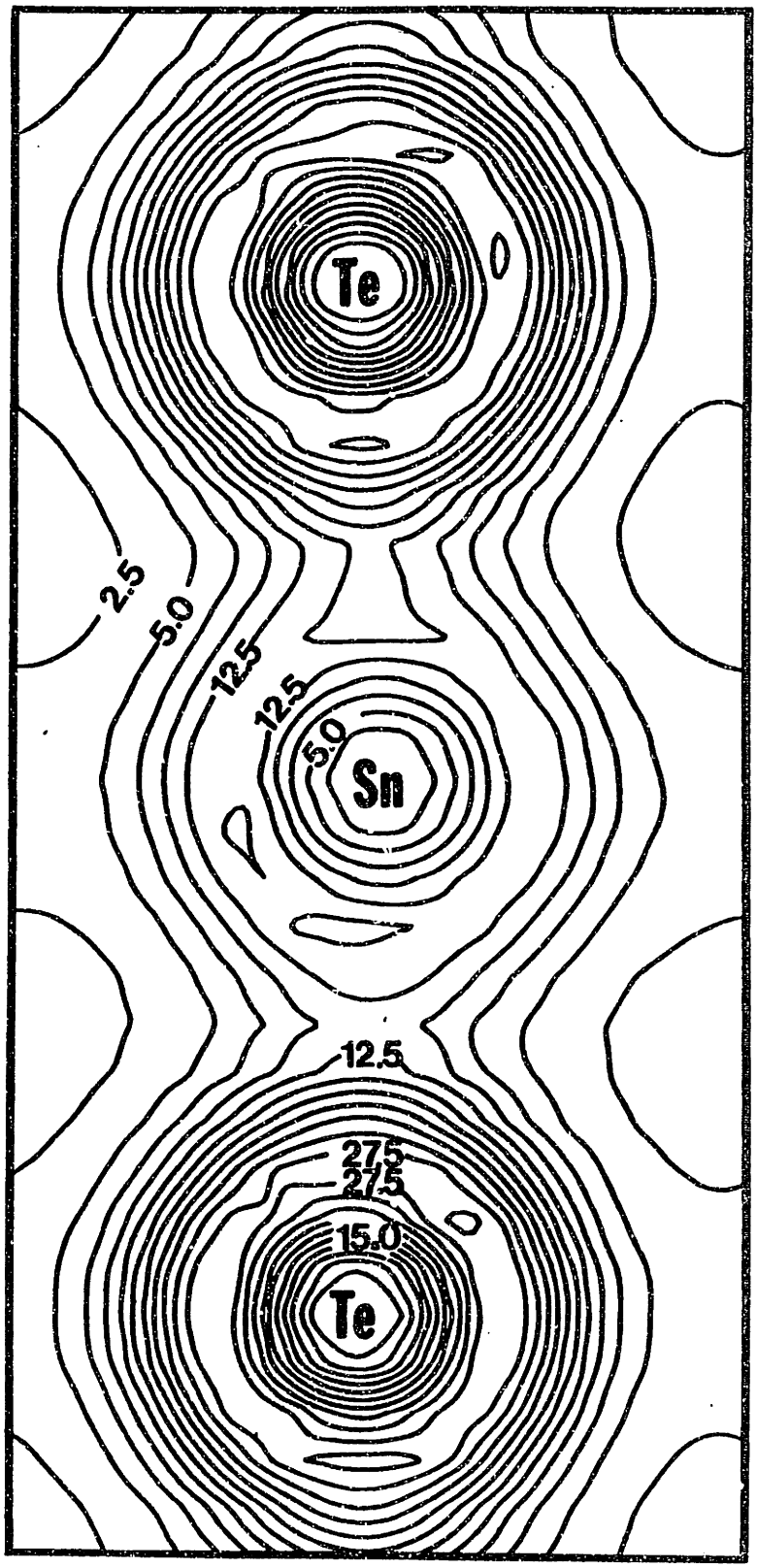

Figure 13

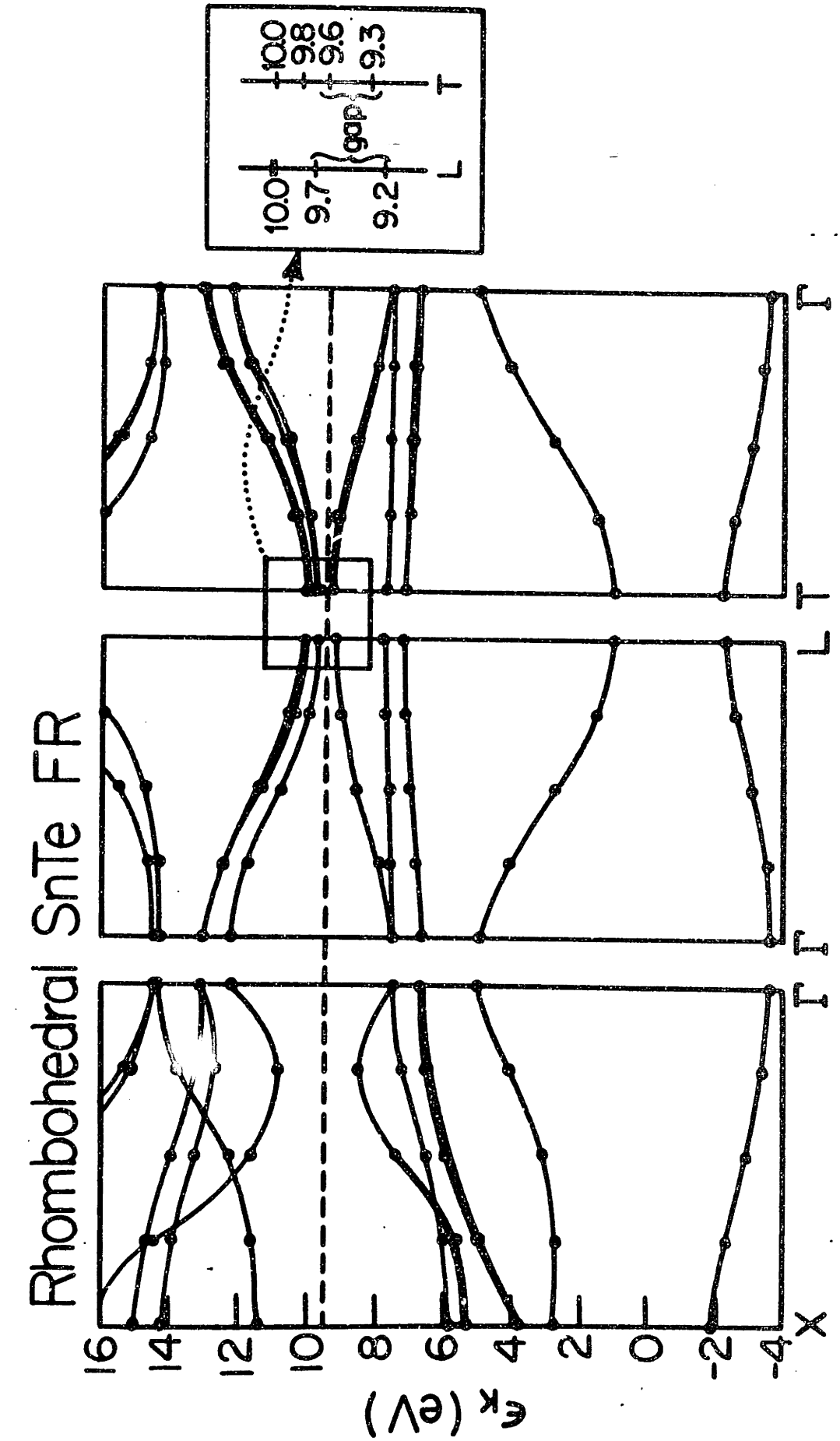
Rhombohedral SnTe FR
ϵ_k (eV)
16
14
12
10
8
6
4
2
0
-2
-4
X
Γ
L
Γ
T
Γ
10.0
9.8
9.6
9.3
gap
10.0
9.7
gap
9.2
L
T

Figure 14

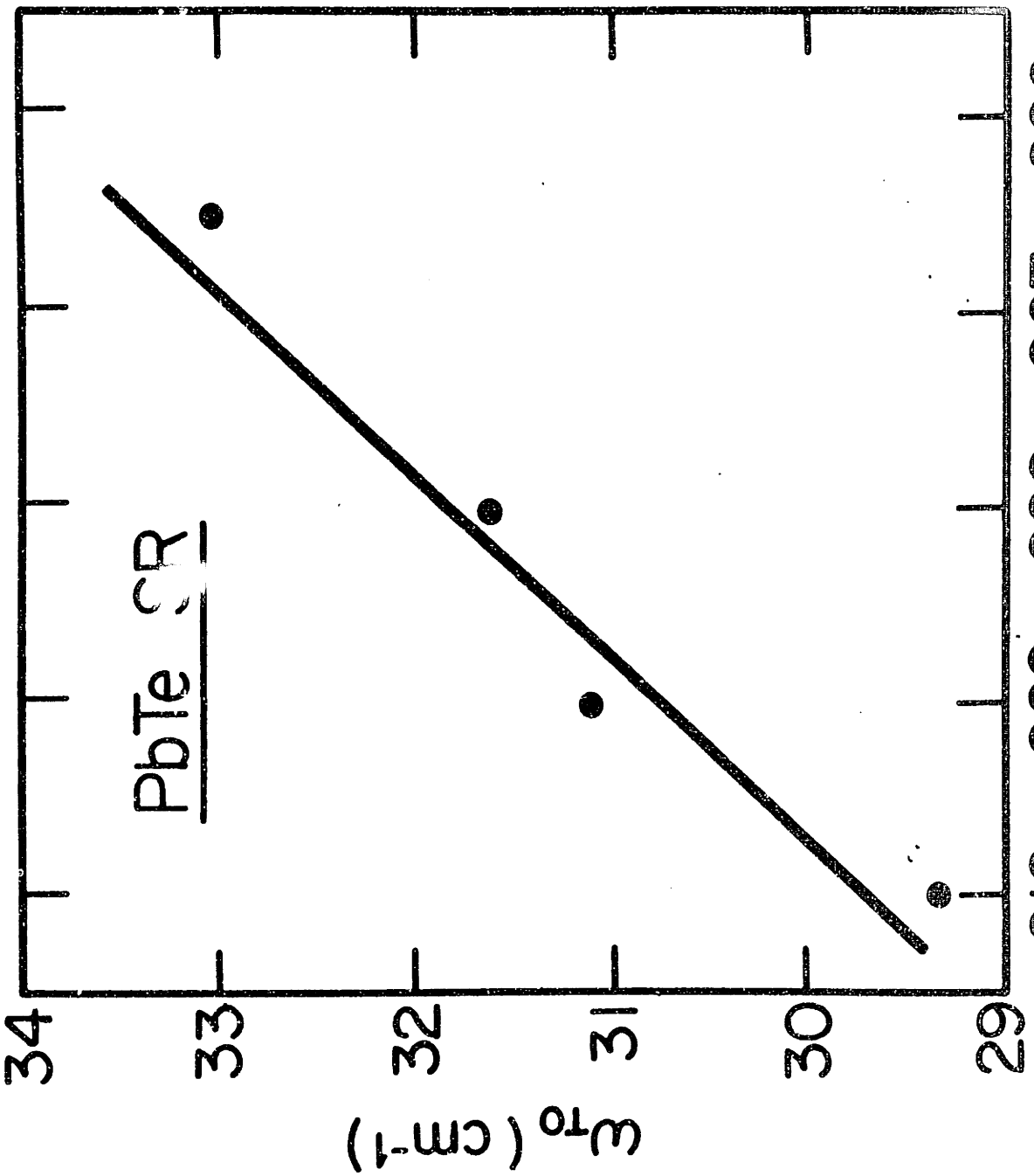
PbTe CR
ω_{TO} (cm^{-1})
34
33
32
31
30
29
210
209
208
207
206
Volume per atom (a.u.)

Figure 15

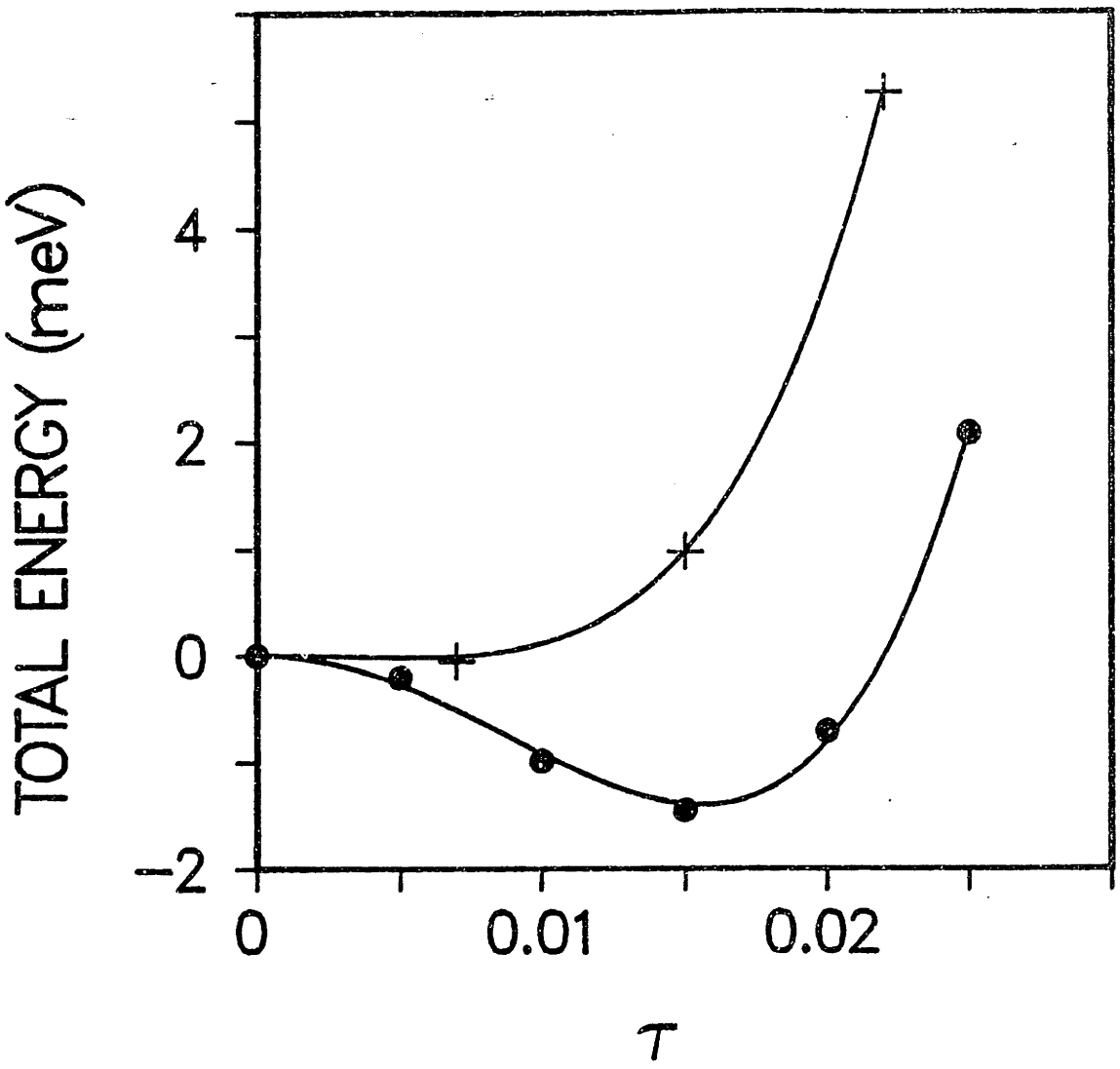

Fig. 16

CHAPTER III:

STRUCTURAL PROPERTIES OF GeTe AT T=0

I. Introduction

The structural properties of the group IV tellurides GeTe, SnTe and PbTe are of interest because these compounds have a lattice instability which results in a rocksalt-rhombohedral transition at finite temperature for SnTe and GeTe. Recently we reported the application of the ab-initio pseudopotential total-energy method to the study of the structural properties of the IV-VI compounds SnTe and PbTe at T=0[1]. Here, we present the extension of this work to the analogous compound GeTe. In particular, we discuss calculations of the lattice constant, bulk modulus, cohesive energy, total charge density and band structure for the high temperature rocksalt form, and then study the distortions corresponding to the observed low-temperature rhombohedral structure and resulting changes in the bandstructure. This work forms the foundation of an ab-initio study of the structural transition in GeTe, to be reported elsewhere[2].

The format of this paper is as follows. In Sec.II we give information about the computation of total energies and bandstructures. In Sec.III and Sec.IV. we give the results of calculations in the rocksalt and distorted structures, respectively. Sec.V contains a discussion of various issues pertaining to the calculations and their interpretation, and concluding remarks.

II. Method

As described previously[1], we obtain quantum mechanical total energies of various ionic configurations of GeTe using the self-consistent ab-initio-pseudopotential total-energy method with the local density approximation (LDA) in the momentum space formalism. For total energies and self-consistent potentials, we use the spin-orbit averaged pseudopotentials of Bachelet, Hamann and Schluter[3] (Fig.1) while for bandstructures, the spin-orbit splitting is included. We use the Ceperley- Alder- Perdew- Zunger form[4] for the exchange-correlation potential. Brillouin zone averages are performed using the special $\vec{k}$-point scheme of Monkhorst and Pack[4] with 7^3=343 points in the full BZ. Wavefunctions are expanded in a basis set of plane waves with energy less than E_1=10.5 Ry, while the effects of plane waves with energy above E_1 and below E_2 =16.5 Ry are included using Lowdin perturbation theory[5]. Computations were performed using an IBM 370/4381 with 8-byte word length.

III. Results: Rocksalt Structure

At temperatures above T_c~670 K, GeTe is observed to crystallize in the rocksalt structure[6,7]. By calculating E(V) at various atomic volumes V (Fig.2a) and fitting to a

polynomial quadratic in V we can extract the lattice constant and bulk modulus of a hypothetical rocksalt form at T=0, given in Table I. After making a rough thermal expansion correction of -1.5% to the experimental lattice constant values also given in Table I, corresponding to a linear thermal expansion coefficient of 20×10^{-6} for $T>T_c$[8] we see that the calculated values are ~1% too small. Though there are no measurements of the bulk modulus for GeTe, the calculated value of 0.51 Mbar is, as expected, roughly the same as measurements in SnTe and PbTe, which fall in the range 0.4-0.5 Mbar.[9,10]

By calculating the energies of free Ge and Te pseudoatoms, we obtain 6.9 eV/pair for the cohesive energy of GeTe, compared to the experimental value 6.1 eV/pair[11,12]. The overestimate can mostly be attributed to difficulties in calculating the free atom energy, both from the use of the LDA and from the approximate treatment of the spin-orbit interaction energy, as discussed previously[1].

In order to study convergence, in addition to calculations with energy cutoffs (10.5Ry, 16.5Ry) and 7^3 k-points (set A), we include in Fig.2 and Table I the results of calculations with (10.5Ry, 16.5Ry) and 6^3 k-points (set B) and (11.5Ry, 18.0Ry) and 6^3 k-points (set C). The convergence of the lattice constant is excellent. The examination of the convergence of the bulk modulus is

complicated by uncertainty in our fitted values, arising from two sources. First, because of discrete changes in the basis set at each k-point as V changes, there is scatter in the calculated E(V) points, the amplitude of which depends both on the energy cutoffs and the k-point set. Secondly, the given comparisons include only volumes in the narrow range 168 a_B^3 to 180 a_B^3, since for smaller volumes the bands cross near L, a point included in the 6^3 k-point set, and the crossing at this volume is probably an artifact of the LDA band-gap underestimate. Thus the set A result of 0.51 Mbar is the most reliable, and direct comparison with the calculated energies in set B and C given in Fig.2, with allowance for the larger scatter in these sets, indicates that the convergence should be considered acceptable.

The general features of the calculated bandstructure at V_{min} = 169 a_B^3, shown in Fig.3, compare well with previous empirical-pseudopotential-method calculations[13-15]. We see that rocksalt GeTe is a narrow-gap-semiconductor with the gap at L=0.04 eV, spin-orbit splitting of the upper valence bands at Γ of 0.78eV and a secondary maximum or saddle point along Γ-K at (0.3)$(2\pi/a_0)$(1 1/4 -1/4), 0.25 eV below the valence band maximum at L. Unfortunately, measurements of the gap in rocksalt GeTe are not currently available, so no direct comparison with experiment is possible. However, our

calculated value of 0.04 eV will almost certainly prove to be an underestimate. This is due in part to the generic underestimate of band gaps in density-functional calculations and in part to the use of the energy-minimizing volume rather than the larger experimental value for the volume, for which a calculation of the bands at L gives a gap of 0.12 eV.

The total scalar-relativistic pseudocharge density, shown in Fig.4, reflects the mixed ionic/covalent bonding also characteristic of SnTe and PbTe[1]. The charge transfer from Ge to Te is less than that from Pb to Te, indicating that the bonding in GeTe is less ionic, while in GeTe the deviation from spherical symmetry of the Te ion, associated with covalent bonding, is slightly more pronounced than in PbTe.

The difference between GeTe and PbTe is particularly apparent in the band-by-band charge densities shown in Fig.5. The lowest four bands are similar in the two compounds-- the first is Te s-like, the second Ge(Pb) s-like, and the third and fourth are Te p-like. However, the fifth band, which is a mixture of Ge(Pb)-p and Te-p, has much more charge associated with the cation in the case of GeTe, while the lowest conduction band, a roughly equal mixture of Pb-p and Te-s in PbTe, is predominantly Ge p-like in GeTe. The increased involvement of Ge-p levels is probably associated with the greater instability of GeTe

against the distortions corresponding to the rhombohedral structure, described below.

IV. Results: Rhombohedral structure

The observed low-temperature structure of GeTe can be considered as a distortion of the rocksalt structure by the relative displacement of the two fcc sublattices by $a_0\tau(111)$ and a subsequent rhombohedral shear along (111) which changes the rhombohedral angle from its fcc value of 60° to α (Fig.6). The first question we address is the stability of the rocksalt structure against this distortion. First, we vary τ, holding α at 60° and volume at the rocksalt structure energy minimum 169 a.u. (Fig.7). We see that the energy gain from this distortion alone is significant. Since this distortion energy is particularly sensitive to k-point convergence, we show the calculations explicitly for three sets of increasing size (6^3=196, 7^3=343, 9^3=729) with energy cutoffs (10.5Ry,16.5Ry). In a polynomial fit to $E(\tau)$, the quadr tic coefficient is converged to about 10%. On the other hand, energy convergence is extremely good. Calculations with cutoffs of (11.5Ry,18.0Ry) and 6^3 k-points (set C of Table I) coincide with points calculated with the lower energy cutoff on the scale of the figure, with the

deviation increasing with τ to a maximum of 1 meV at τ = 0.04.

Next, we vary α, with τ=0 and volume=169 a.u. (Fig.8). The rocksalt structure is seen to be stable against rhombohedral shear, and we obtain a value for the shear elastic constant of the rocksalt structure, C_{44}=1.8x10^{11} dyne/cm^2. Since there is no experimental measurement of C_{44} for GeTe, we compare the calculation to the SnTe value C_{44}=1.4x10^{11} dyne/cm^2 [16], finding reasonable agreement. We demonstrate convergence in k-point set and basis set size by including the results of other calculations (sets B and C of Table I) in the figure. Again, because the shape of the unit cell is changing, we see some scatter in the points which, as in the rocksalt structure, is especially noticeable for set B. Otherwise, the convergence appears to be good, with C_{44} converged to about 10%.

Finally, we study a range of values of τ and α to determine the zero-temperature equilibrium lattice parameters. The results are fit to within 10^{-4} Ry and the fit is shown in Fig.9 as a contour plot. The resulting lattice parameters are α = 58.8° and τ = 0.025 to be compared with the experimental values (57.9°,0.026)[17] and

(58.0°, 0.034)[7].

The bandstructure at the minimum-energy configuration is shown in Fig.10. Because inversion symmetry is slightly broken, the bands are spin-split. For this distortion, we find a gap at L of 0.4 eV, with a secondary valence band maximum 0.18 eV lower at T, and another maximum or saddle point 0.27 eV lower along Γ-K . Tunnelling spectroscopy gives a value of 0.1-0.2 eV for the fundamental gap[19]. Since the gaps at L and T and the existence of an indirect gap are quite sensitive to the distortion, our overestimate of the gap might be accounted for by the difference between the structural parameters of the calculated minimum-energy configuration and those of the thin polycrystalline films in which the tunnelling experiments were performed.

We have studied the trends in band edges at L and T with distortion in more detail. For $\alpha = 60°$, as τ increases the conduction band minima increase and the valence band maximum at L decreases slightly, while the valence band maximum at T decreases strongly. For $\tau = 0$, as α decreases, the gaps at L and T increase slightly and the levels at L drop while those at T rise, keeping the weighted average constant. Fitting the results for varying α to a straight line, we can obtain the shear deformation potential constant, defined as Ξ =

$(\sqrt{3}/2)(\Delta/\phi)$, where Δ is the L-T energy splitting and ϕ is the deviation of α from $2\pi/3$. Our calculated value Ξ = 10 eV is comparable to Ξ = 5-7 eV derived from measurements of the anisotropy of the resistivity below T_c[20,21].

V. Discussion

The lack of complete experimental data on elastic constants and bandstructure of GeTe is partly a consequence of the intrinsic limitations on the quality of samples and, for rocksalt GeTe, the high temperature at which the form exists. These limitations arise because the range of homogeneity of the alloy does not include the stoichiometric composition, but lies on the Te-rich side[22-24]. The Ge vacancies and other lattice defects, in addition to possibly modifying the structural properties of the material directly, give rise to a large concentration of free holes. In fact, tunnelling spectroscopy shows that ε_f lies 0.4-0.5 eV below the top of the valence band[19], and Hall measurements[25] typically show $p \sim 10^{20}$-10^{21} cm^{-3}.

The effects of non-stoichiometry can be important in the comparison of experimental and calculated quantities. For example, in going from the rocksalt to the rhombohedral structure, there is an energy gain from the redistribution

of holes among the L and T maxima, called the 'inter-valley Jahn-Teller effect.'[26] The lowering of C_{44} for typical hole concentrations is measured in SnTe to be as large as 35%[16], and is expected to be important in GeTe as well.

Aside from the use of finite basis and k-point sets, the most important approximations in the calculation are the pseudopotential and local-density approximations. As mentioned earlier, the use of the LDA overestimates the cohesive energy of GeTe due to the inaccuracy in the calculation of the free-atom energy. Moreover, since density functional theory underestimates the gaps in semiconductors, we fill the five lowest bands completely, even when the gap is slightly negative. This occurs for small volumes in the rocksalt structure or for the rhombohedral structure when τ is 0 and α is not equal to 60°. By the same token, it is reasonable, even when we use this method to study finite temperature properties, to keep the electrons at zero temperature despite the fact that our calculated gap for the rocksalt structure is $<kT_c$. Finally, as is known from experience in a variety of systems[18], this method underestimates the lattice constant. Though this underestimate is not in itself very significant, when we determine the structural parameters of the rhombohedral form the errors in the calculation of the distortion energy are

convoluted with the volume error. Since a decrease in volume should favor the more symmetric rocksalt structure and dT_c/dp is observed to be negative, the result is that for all three materials, GeTe, SnTe and PbTe, the stability of the rocksalt structure is greater than that inferred from experiment.

In summary, we have calculated and studied the convergence of lattice parameters, elastic constants and bandstructures of the rocksalt and rhombohedral forms of GeTe, and obtained good agreement with experimental measurements, when available. We conclude that the ab-initio scalar relativistic pseudopotential total-energy method can be used to provide an accurate description of the structural properties of GeTe.

Table I. Minimum crystal energy, lattice constant and bulk modulus in the rocksalt structure extracted from quadratic polynomial fits to calculations done with three different sets of energy cutoffs and k-points, compared to experiment.

Energy cutoffs (Ry)	k-point set	mimimum crystal energy (Ry/atom)	lattice constant (Å)	bulk modulus (Mbar)
(10.5,16.5)	7^3	-12.22884	5.85	0.51
(10.5,16.5)	6^3	-12.22818	5.83	0.41
(11.5,18.0)	6^3	-12.22734	5.87	0.60
EXPERIMENT		---	6.01(670 K)[7]	--

REFERENCES

1. K.M.Rabe and J.D.Joannopoulos, Phys.Rev. B32, 2302 (1985).

2. K.M.Rabe and J.D.Joannopoulos, submitted to Phys.Rev.B.

3. G.B.Bachelet, D.R.Hamann and M.Schluter, Phys.Rev.B 26, 4199 (1982).

4. D.M.Ceperley, Phys.Rev.B 18, 3126 (1978); D.M.Ceperley and B.J.Alder, Phys.Rev.Lett. 45, 566 (1980); J.Perdew and A.Zunger, Phys.Rev.B 23, 5048 (1981).

4. H.J.Monkhorst and J.D.Pack, Phys.Rev.B 13, 5188 (1976).

5. P.O.Lowdin, J.Chem.Phys. 19, 1396 (1951).

6. J.N.Bierly, L.Muldawer and O.Beckman, Acta.Met. 11,447 (1963).

7. T.B.Zhukova and A.I.Zaslavskii, Kristallografiya 12,37 (1967). [Sov.Phys.--Crystallogr. 12, 28 (1967)].

8. S.I.Novikova, A.E.Shelimova, N.Kh.Abrikosov, V.I.Galyutin and B.A.Evseev, Fiz.Tverd.Tel. 12,3623 (1970) [Sov.Phys.--Sol.St. 12,2945 (1971)].

9. A.G.Beattie, J.Appl.Phys. 40, 4818 (1969).

10. B.Houston, R.E.Strakna and H.S.Belson, J.App.Phys. 39, 3913 (1968).

11. R.Hultgren et.al., Selected Values of the Thermodynamic Properties of the Elements (American Society for Metals, Metals Park, Ohio, 1973).

12. D.D.Wagman, Natl. Bur. Stand. Tech. Note 270-3, 184 (1968); 270-3, 191 (1968).

13. M.L.Cohen, Y.Tung and P.B.Allen, J.de Phys. 29, C4-163 (1968).

14. Y.W.Tung and M.L.Cohen, Phys.Rev. 180, 823 (1969).

15. H.M.Polatoglou, G.Theodorou and N.A.Economou, in Physics of Narrow Gap Semiconductors, ed. E.Gornik, H.Heinrich and L.Palmetshofer (Springer-Verlag Lecture Notes in Physics #152, 1982).

16. T.Seddon, S.C.Gupta and G.A.Saunders, Solid State Commun. 20, 69 (1976).

17. J.Goldak, C.S.Barrett, D.Innes and W.Youdelis, J.Chem.Phys. 44, 3323 (1966).

18. M.L.Cohen, Phys.Scr. T1, 5 (1982).

19. S.K.Bahl and K.L.Chopra, J.App.Phys. 41, 2196 (1970).

20. M.A.Korzhuev, L.E.Shelimova and N.Kh.Abrikosov, Fiz. Tekh. Poluprovodn. 11, 296 (1977) [Sov.Phys.Semicond. 11, 171 (1977)].

21. M.A.Korzhuev and A.V.Arakcheeva, Fiz. Tekh. Poluprovodn. 12, 2192 (1978) [Sov.Phys.Semicond. 12, 1304 (1978)].

22. L.E.Shelimova, N.Kh.Abrikosov and V.V.Zhdanova, Russ. J. Inorg. Chem. 10, 650 (1965).

23. A.D.Bigava, A.A.Gabedava, E.D.Kunchuliya, S.S.Moiseenko and R.R.Shvangiradze, Neorg.Mater. 12, 835 (1976) [Inorg.Mater 12,708 (1976)].

24. N.Kh.Abrikosov, O.G.Karpinskii, L.E.Shelimova and M.A.Korzhuev, Neorg.Mater. 13, 2160 (1977) [Inorg.Mater.

13,1723 (1977)].

25. N.Kh.Abrikosov, M.A.Korzhuev and L.E.Shelimova, Neorg.Mater. 13, 1757 (1977) [Inorg.Mater. 13, 1418 (1977)].

26. M.A.Korzhuev,L.I.Petrova,G.K.Demenskii and O.A.Teplov, Fiz.Tverd.Tel. 23, 3387 (1981) [Sov.Phys.--Sol.St. 23, 1966 (1981)].

Figure Captions

1. Ab-initio non-local relativistic atomic pseudopotentials for Ge and Te as calculated by Bachelet, Hamann and Schluter[3].

2. Total energy of the rocksalt structure, in meV/atom, as a function of varying atomic volume. The points shown are calculated with (a) set A cutoffs, (b) set B cutoffs and (c) set C cutoffs. For each set, the minimum of the parabolic fit shown as a solid line is selected as the zero of energy.

3. Pseudopotential bandstructure of GeTe in the rocksalt structure with atomic volume 169 a_B^3, including spin-orbit coupling. In units of $2\pi/a_0$, Γ = (0,0,0), L = (1/2,1/2,1/2), W = (1,1/2,0), K = (1,1/4,-1/4) and X = (1,0,0). The gap of 0.04 eV at L is too small to be visible on this plot. The energy of the top of the valence band is indicated by a dashed line.

4. Total pseudocharge density of rocksalt GeTe with atomic volume 169 a_B^3 in the (100) plane. Densities are given in units of electrons per two-atom unit cell.

5. Band-by-band pseudocharge densities of rocksalt GeTe in the (100) plane for (a)-(e) bands 1-6, respectively, in units of electrons per unit cell. Positions of Ge and Te atoms are the same as in Fig.4.

6. Rhombohedral structure of GeTe is obtained from the

rocksalt structure by a two-step distortion: (a) relative displacement of the two fcc sublattices by $a_0\tau(111)$ and (b) rhombohedral shear along (111).

7. Total energy in meV/atom of GeTe as a function of τ with α fixed at 60°. The filled circles are points calculated with 7^3 k-points, vertical crosses with 6^3 k-points and diagonal crosses with 9^3 k-points. The fit to the points calculated with 7^3 k-points to a polynomial quartic in τ^2 is shown as a solid line. For each set, the calculated value at $\tau = 0$ is selected as the zero of energy.

8. Total energy in meV/atom of GeTe as a function of α with $\tau = 0$. The filled circles are points calculated with set A cutoffs, vertical crosses with set B and diagonal crosses with set C (see Table I). The solid line is a parabolic fit to the points in set A. For each set, the mimimum of a parabolic fit is selected as the zero of energy.

9. Contour plot of the fit to $\Delta E_{tot}(\alpha,\tau) = E_{tot}(\alpha,\tau) - E_{tot}(\alpha=60°,\tau=0)$. Energies shown are in meV/atom.

10. Pseudopotential bandstructure of GeTe in the rhombohedral structure with atomic volume 169 a_B^3 and

distortions α=58.8° and τ=0.025, including spin-orbit coupling. In units of $2\pi/a_0$, Γ = (0,0,0), T = (1/2,1/2,-1/2), L = (1/2,1/2,-1/2), W = (1,1/2,0), K = (1,1/4,-1/4) and X = (1,0,0). The energy of the top of the valence band is indicated by a dashed line.

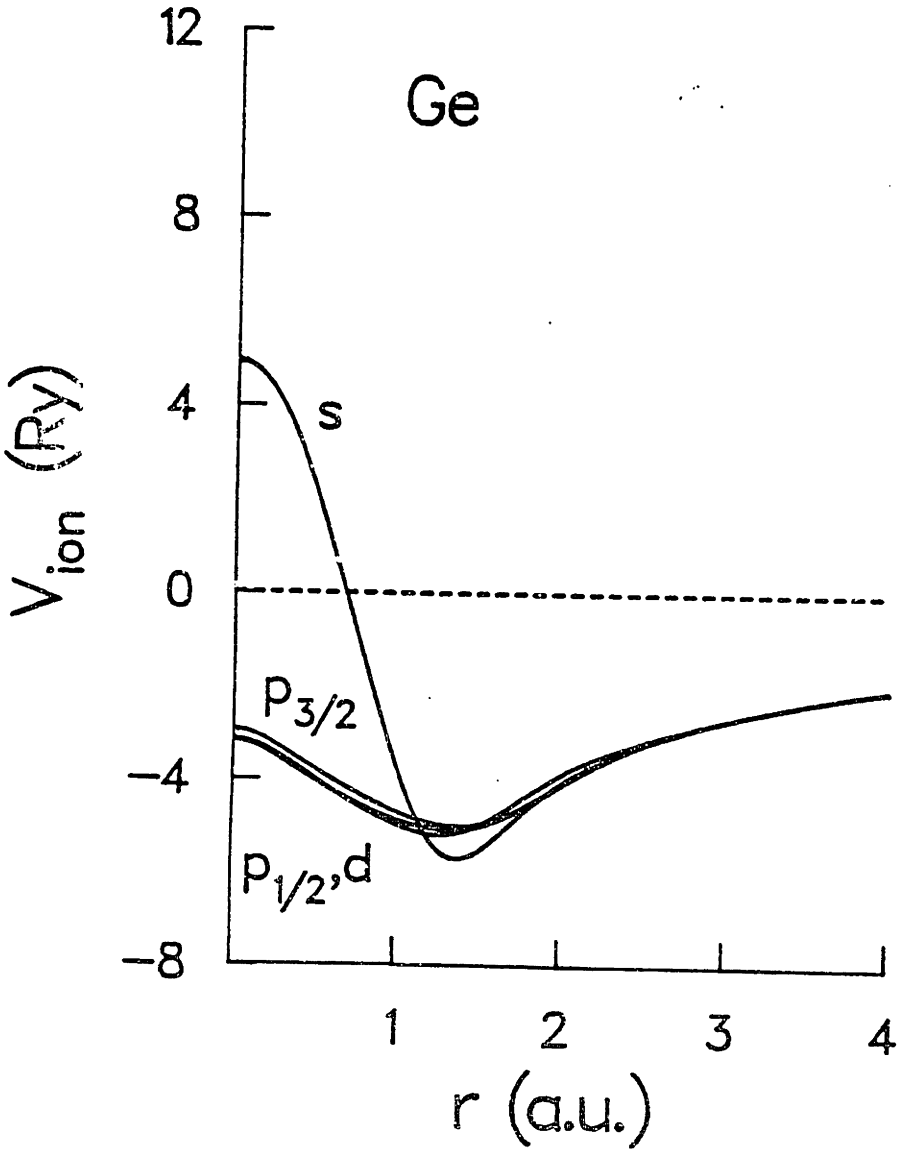
Ge
12
8
4
0
−4
−8
V_{ion} (Ry)
s
$P_{3/2}$
$P_{1/2}$,d
1
2
3
4
r (a.u.)

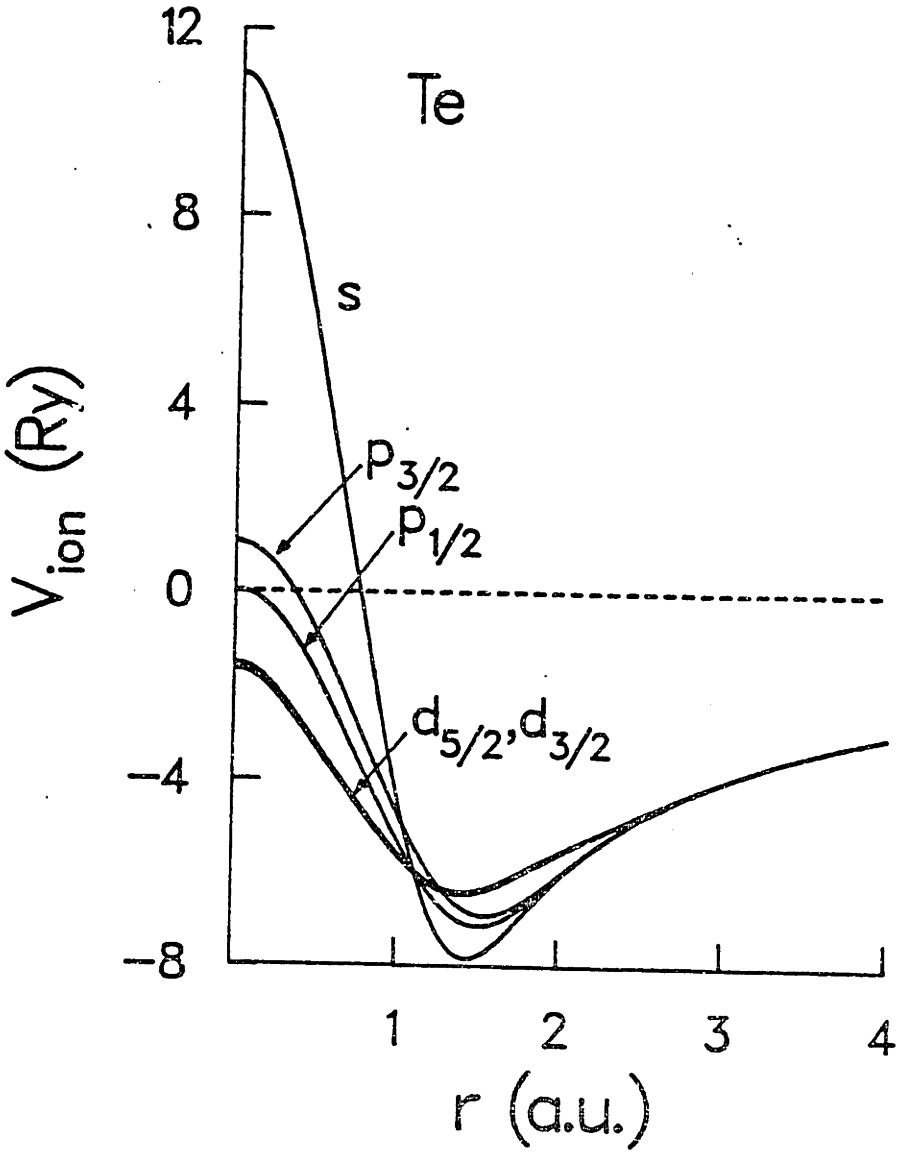
Te
12
8
4
0
−4
−8
V_{ion} (Ry)
s
$P_{3/2}$
$P_{1/2}$
$d_{5/2}$,$d_{3/2}$
1
2
3
4
r (a.u.)

100

Fig.1

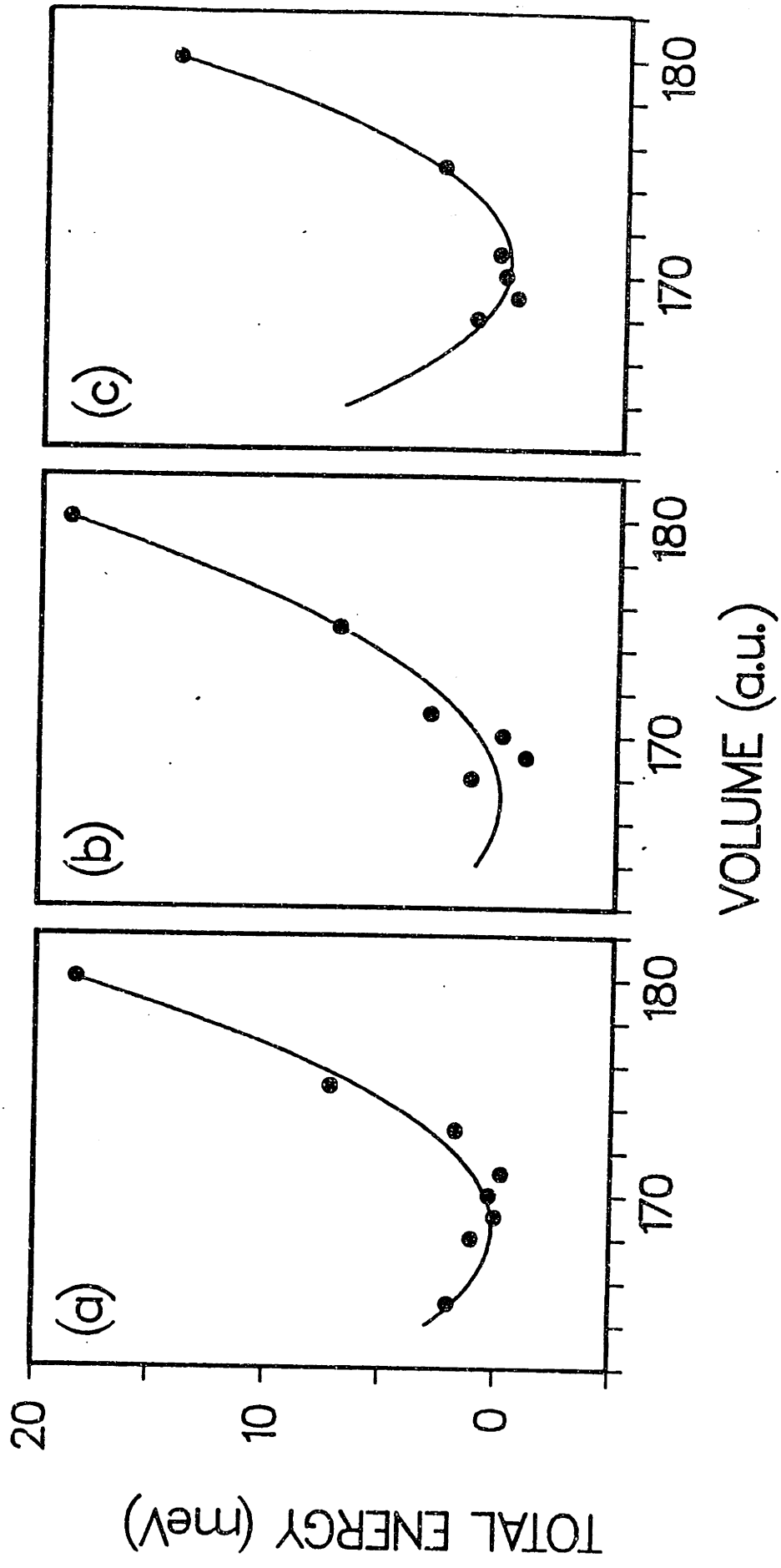

Fig. 2

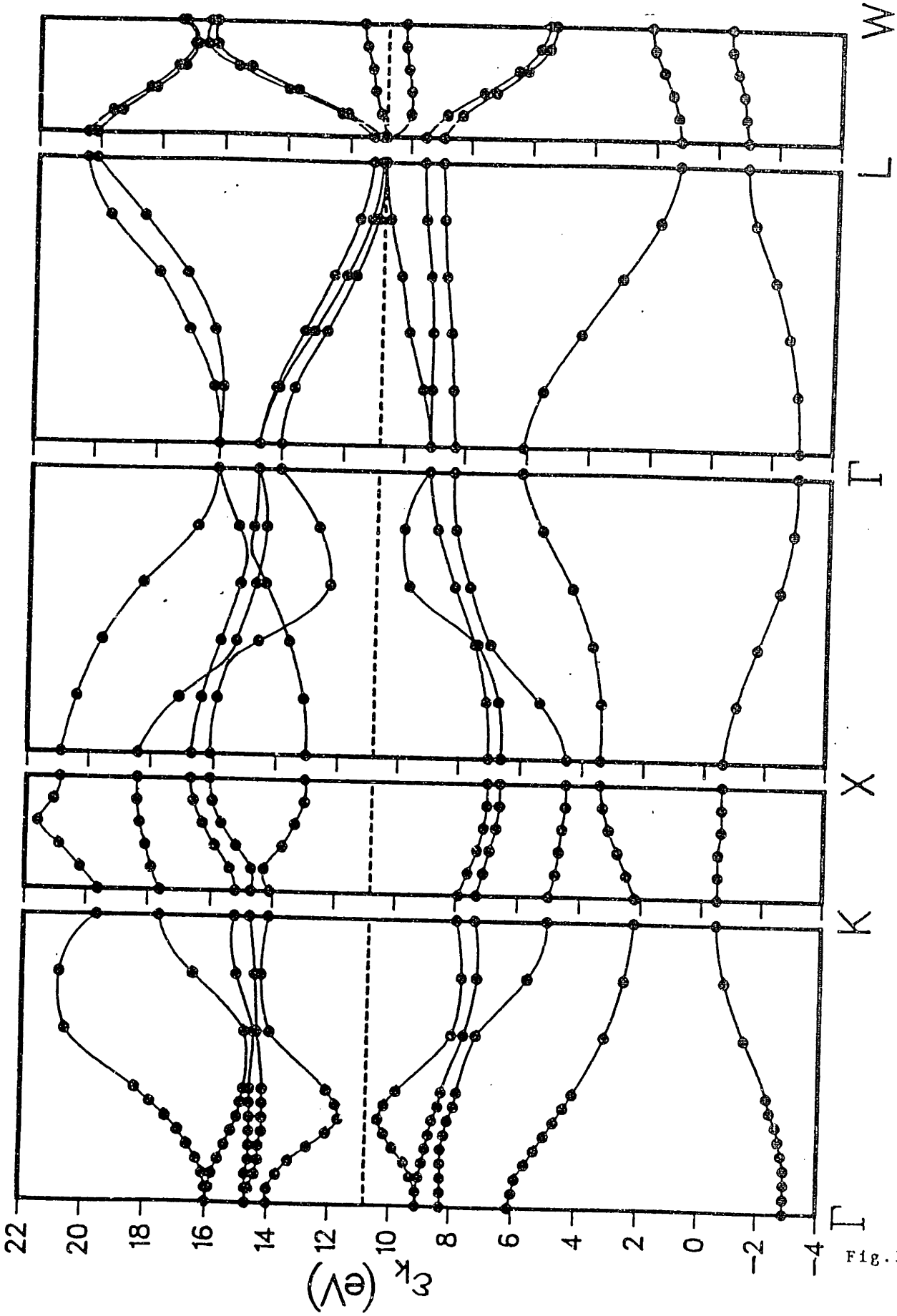

Fig.3

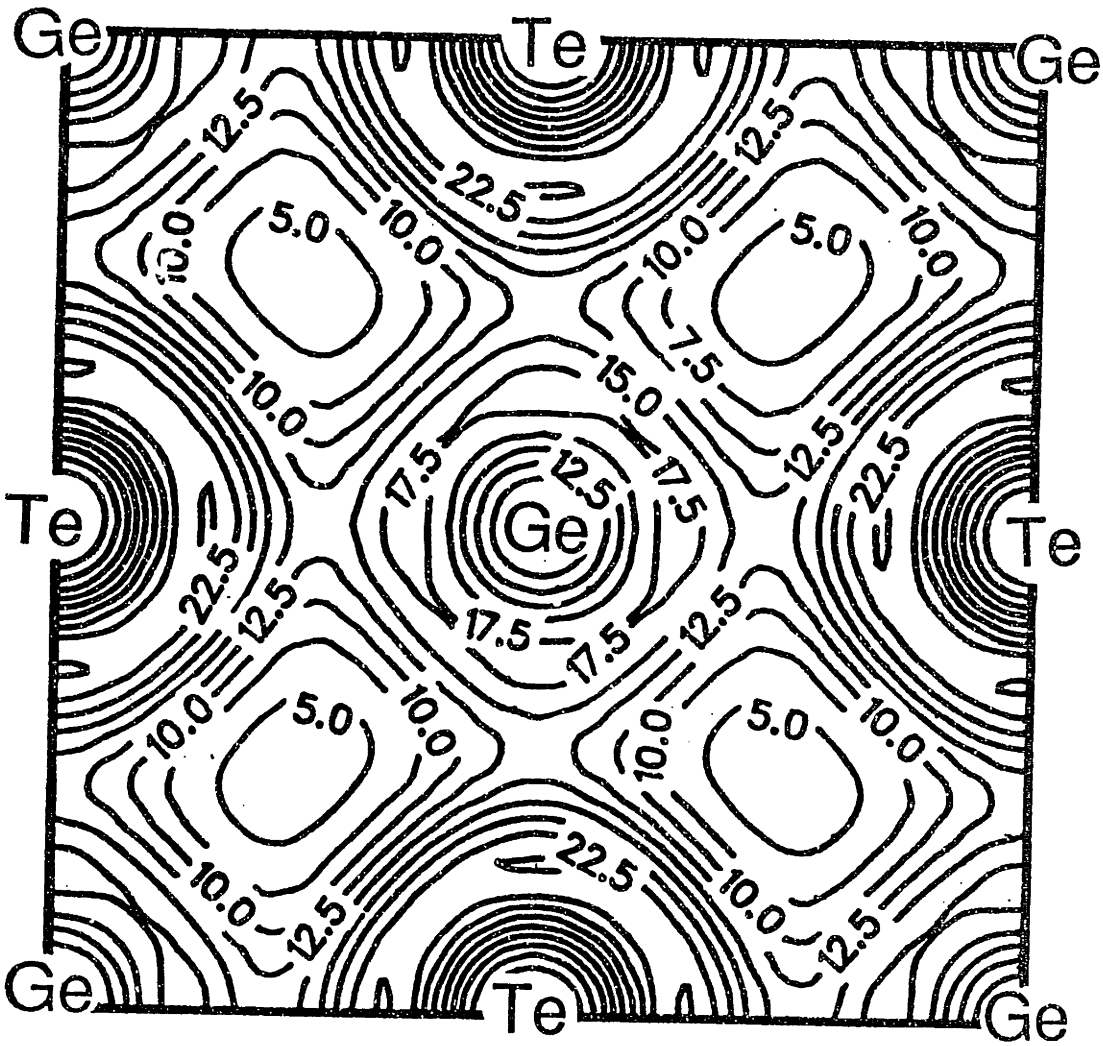

Fig. 4

(a) BAND 1

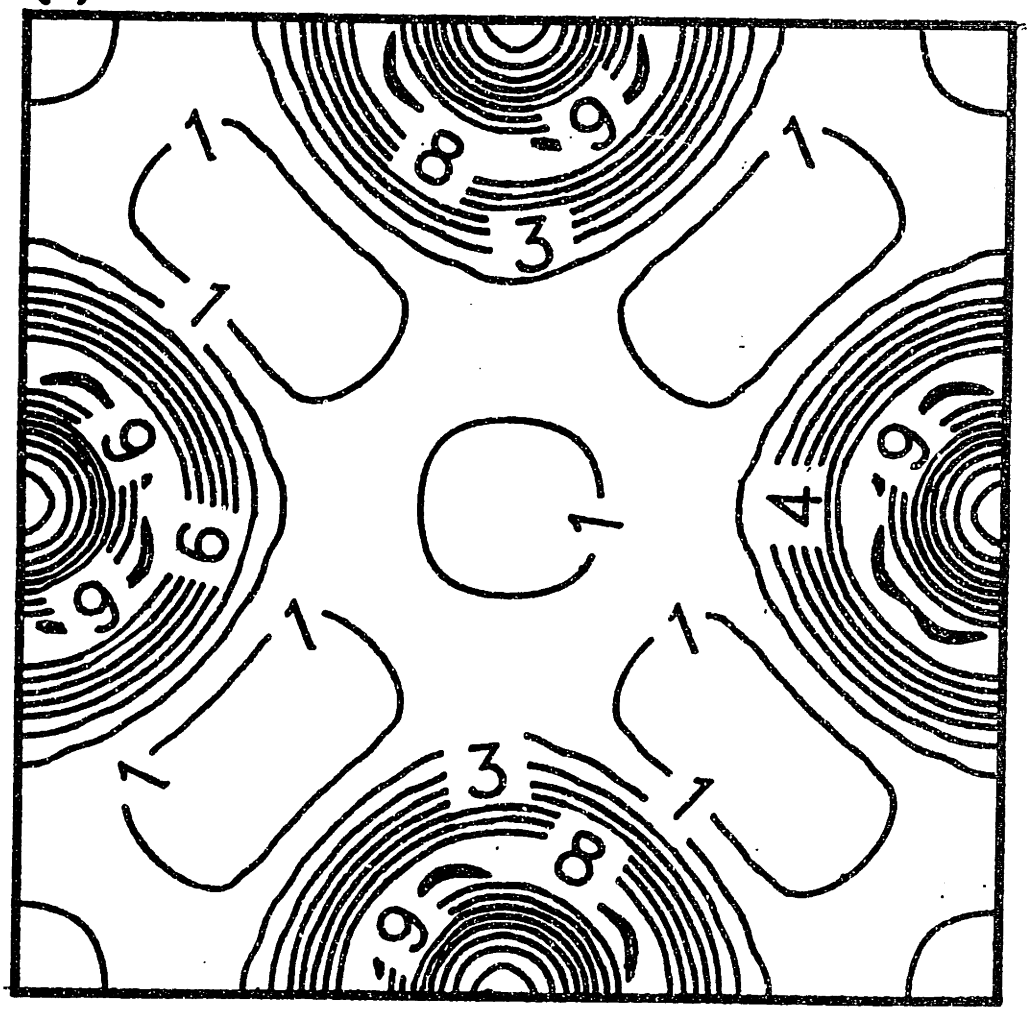

Fig. 5

(c) BAND 3

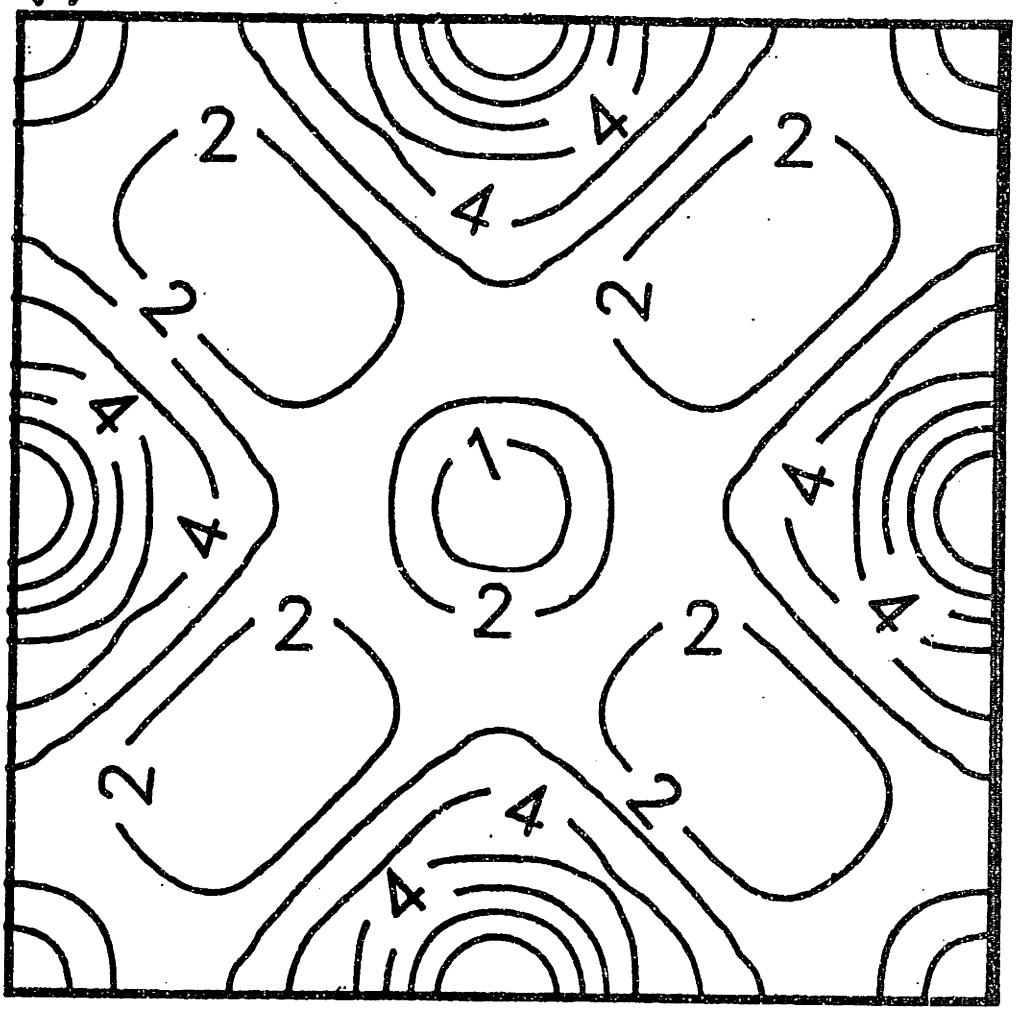

Fig.5

(b) BAND 2

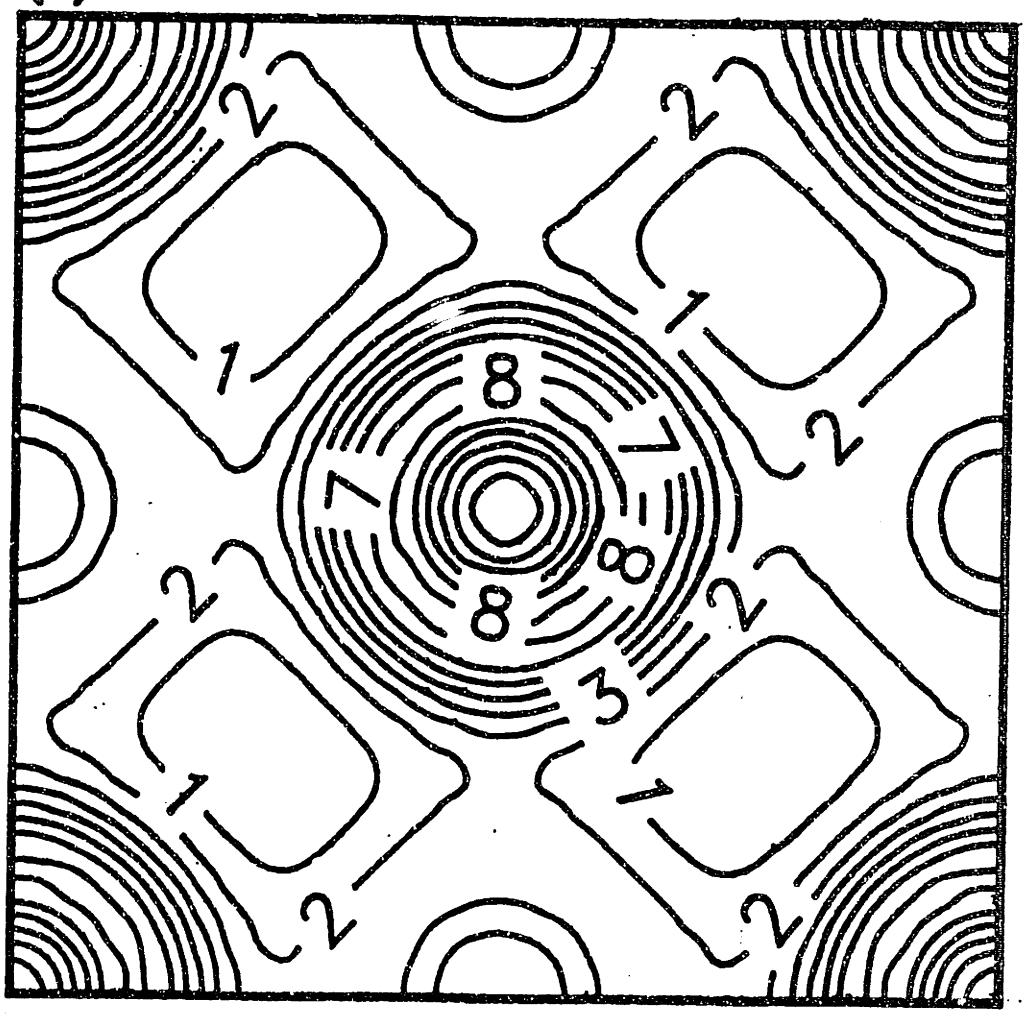

Fig.5

(d) BAND 4

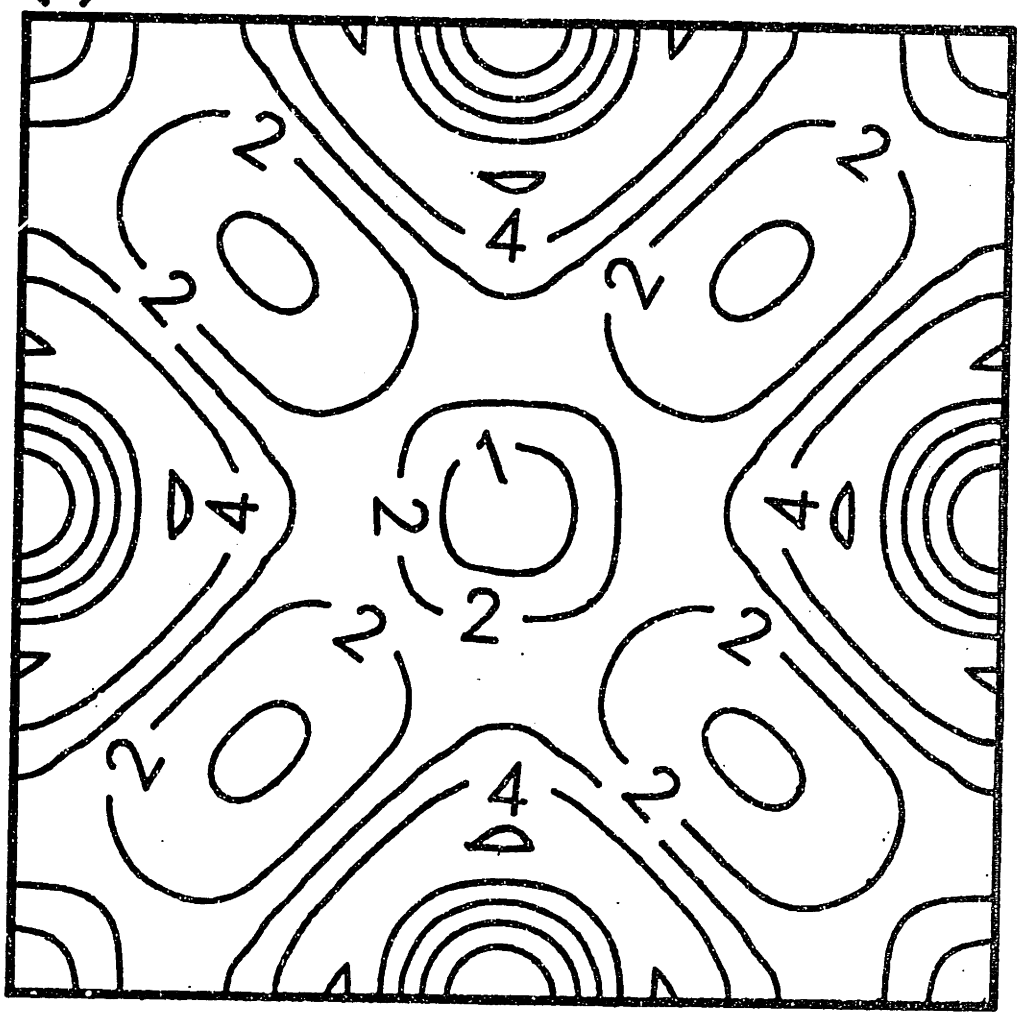

Fig.5

(e) BAND 5

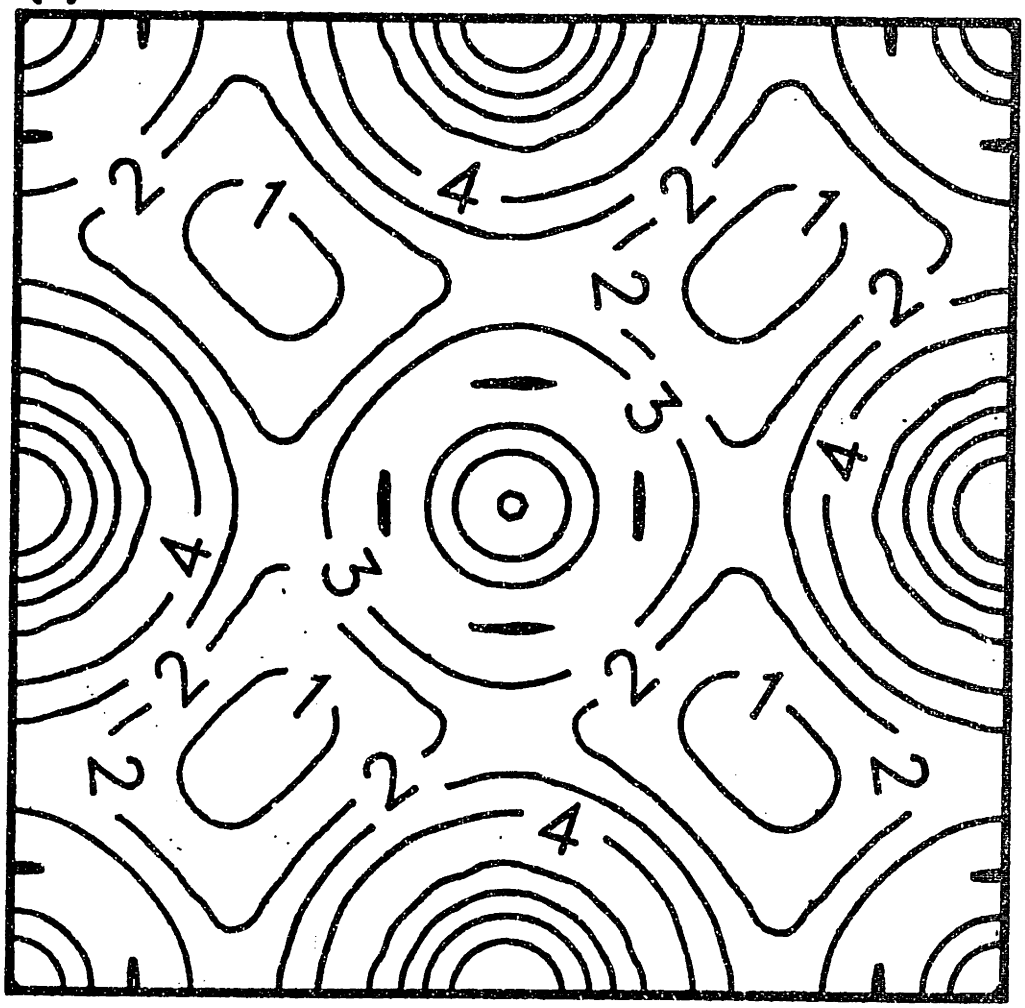

Fig. 5

(f) BAND 6

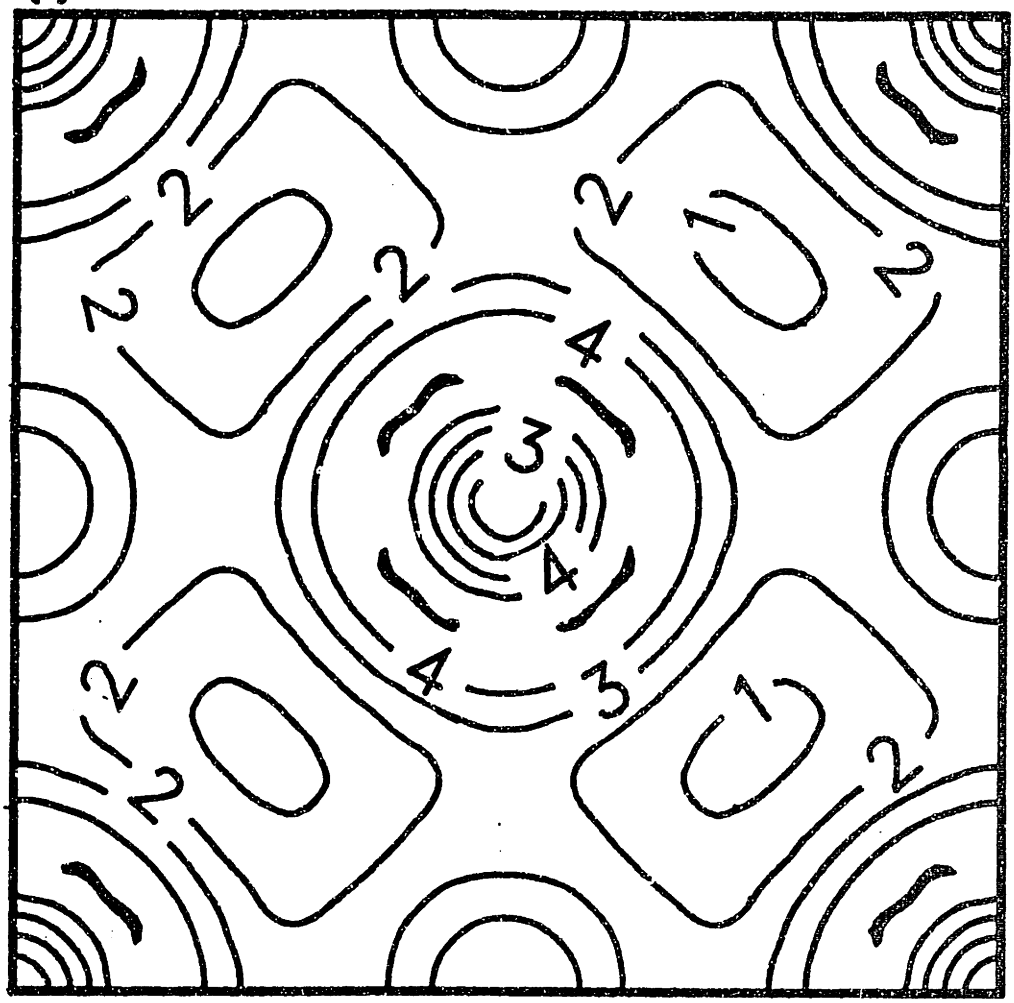

Fig.5

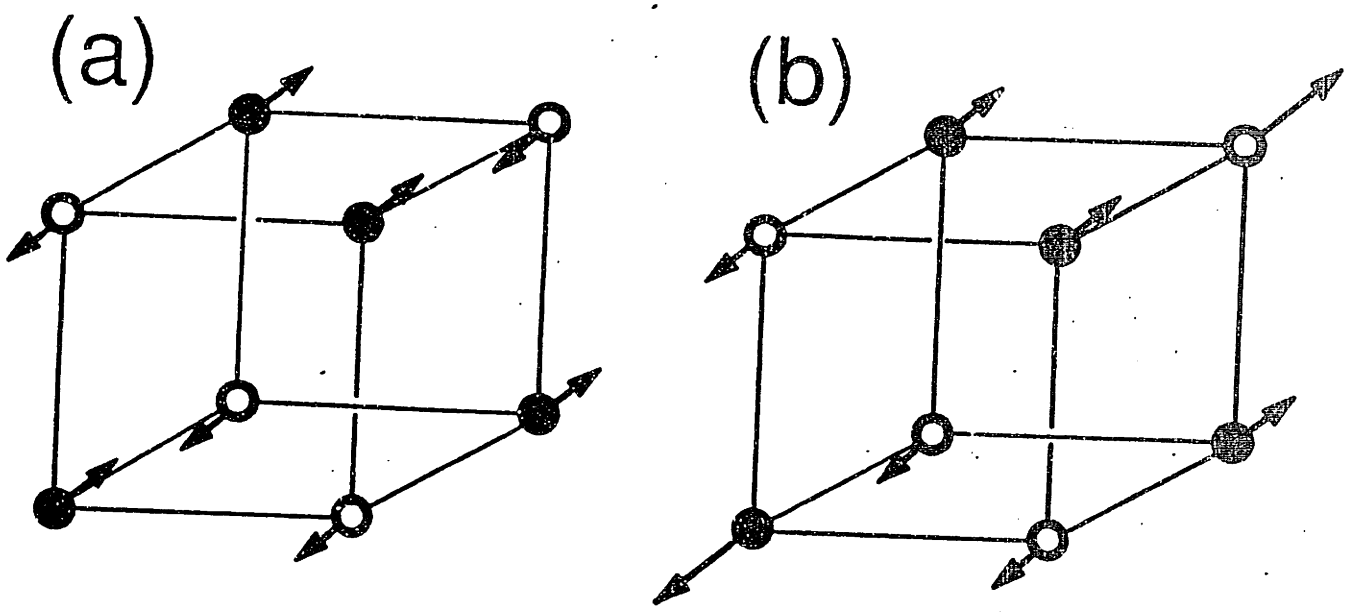

Fig.6

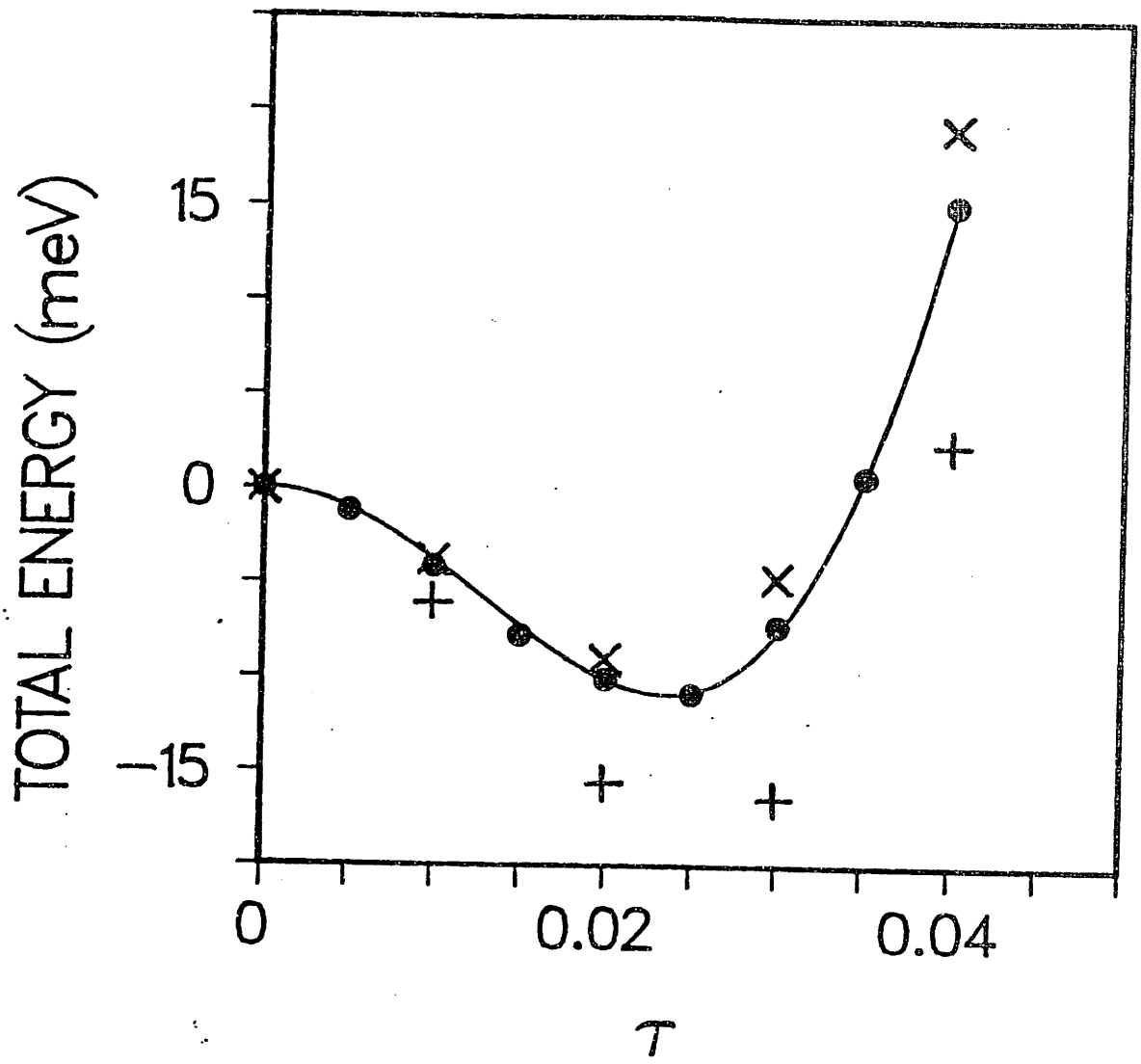

Fig. 7

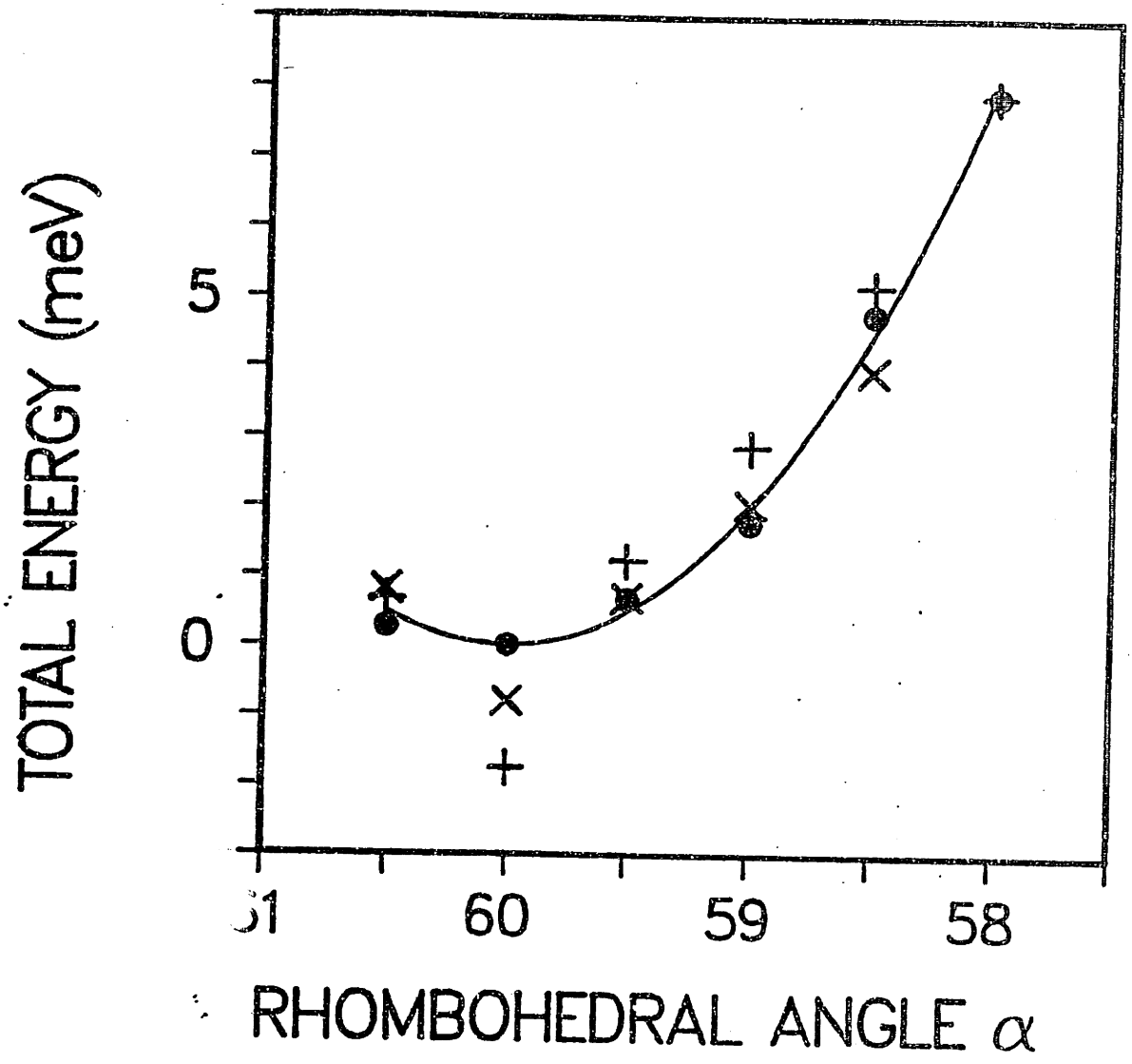

Fig.8

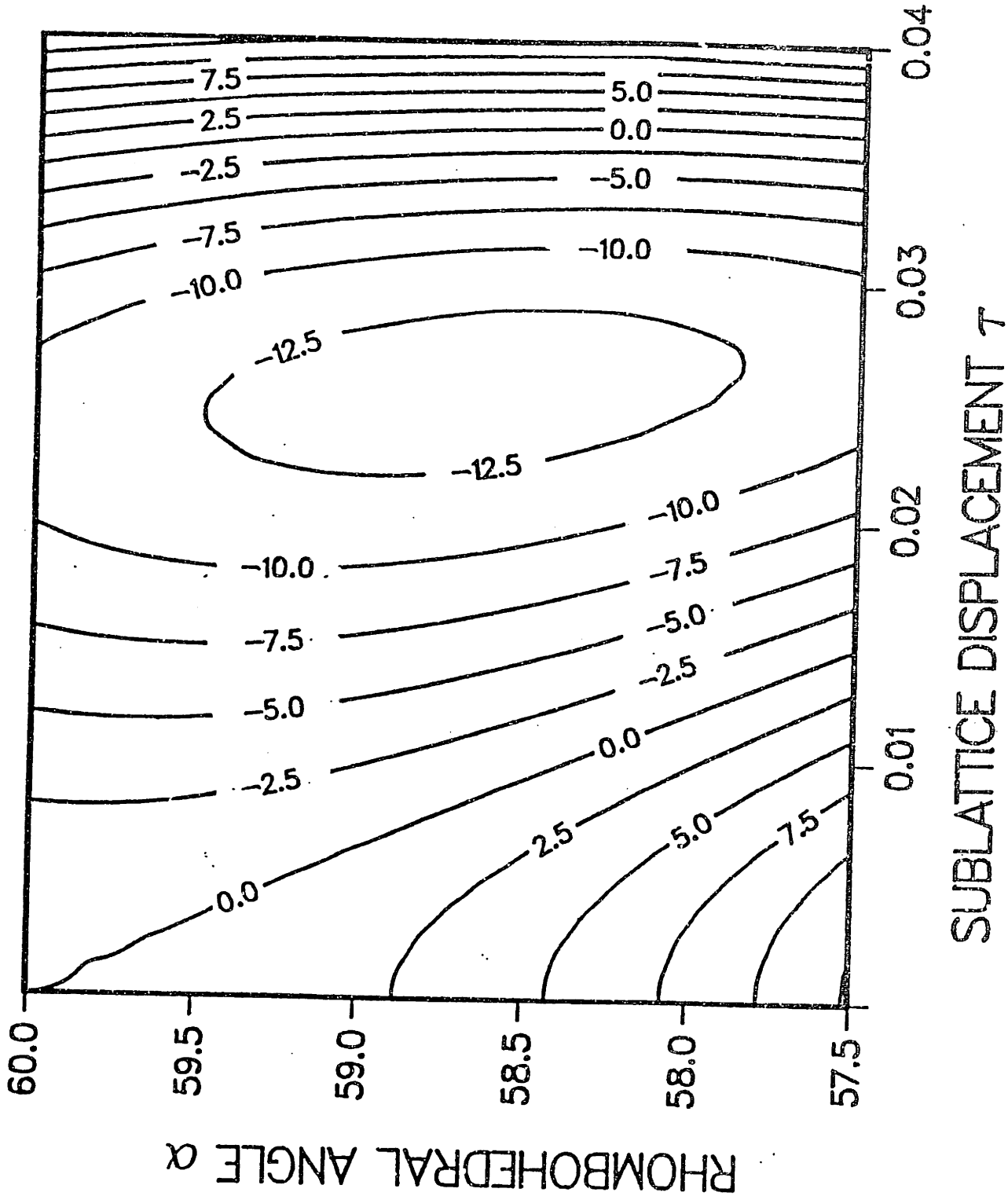
7.5
5.0
2.5
0.0
-2.5
-5.0
-7.5
-10.0
-10.0
-12.5
-12.5
-10.0
-10.0
-7.5
-7.5
-5.0
-5.0
-2.5
-2.5
0.0
0.0
2.5
5.0
7.5
0.04
0.03
0.02
0.01
SUBLATTICE DISPLACEMENT τ
60.0
59.5
59.0
58.5
58.0
57.5
RHOMBOHEDRAL ANGLE α

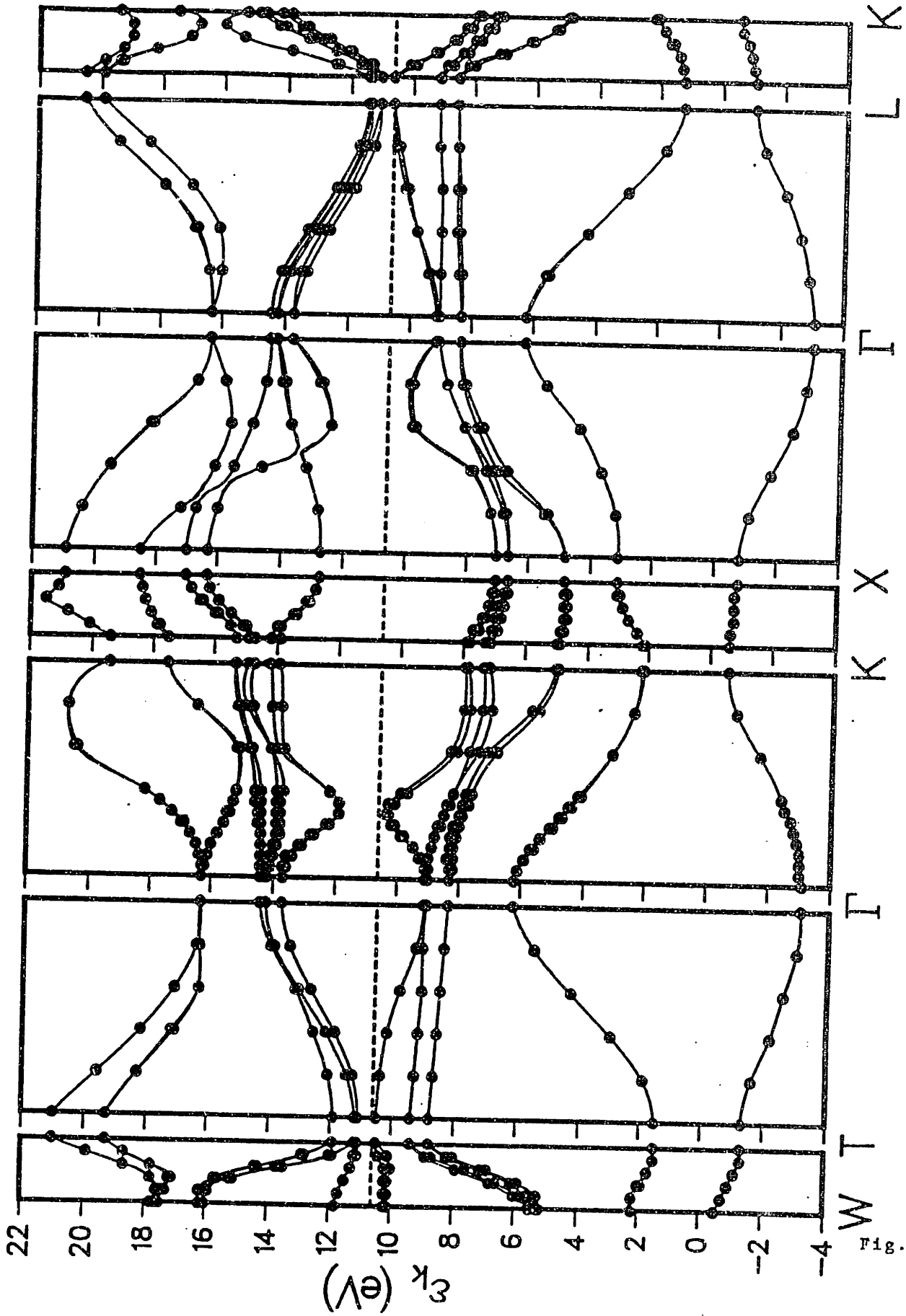

Fig.1(

CHAPTER IV:

THEORY OF
THE STRUCTURAL PHASE TRANSITION OF GeTe

I. INTRODUCTION

In the application of modern concepts of critical phenomena to the study of finite-temperature phase transitions in real materials, the calculation of the transition temperature and other non-universal critical properties is essential. This requires the combination of detailed microscopic quantitative knowledge of the properties of the material under consideration with an appropriate statistical mechanical treatment.

One way to obtain these properties is through first-principles total energy calculations. Previous attempts to calculate transition temperatures[1,2] have used total energy methods which rely on approximations limiting their accuracy and range of applicability. In contrast, the ab-initio pseudopotential method has been seen to be highly accurate in describing the zero-temperature structural properties of a wide variety of systems[3], including group IV tellurides[4]. In the present study of the structural phase transition of bulk GeTe, we combine this self-consistent method with a renormalization-group-theory (RG) approach to calculate T_c and predict other critical phenomena associated with the transition, in excellent agreement with available experimental data.

At high temperatures, the IV-VI narrow gap semiconductor GeTe has the rocksalt structure. At low temperatures the

system exists in a rhombohedral structure. This structure, shown in Fig.1, can be described as a rocksalt structure slightly distorted by freezing in a $\vec{k}=0$ optic phonon along the [111] direction, corresponding to the order parameter of the transition, with a subsequent shear relaxation along [111], corresponding to the secondary order parameter. Experimental studies of the transition and their interpretation are somewhat difficult because of the high transition temperature and intrinsic limitations on the quality of the sample. The latter arises because the compound GeTe is not in the range of homogeneity of the alloy, which for a nominal stoichiometric composition results in the coexistence of free Ge with a 50.3% Te phase[5-7]. This phase exhibits the rhombohedral-rocksalt transition and contains free holes arising mainly from Ge vacancies. The temperature dependence of the order parameter near the transition has not been observed, as it has in the analogous compound SnTe using elastic neutron scattering[8]. However,transition temperatures in the range 625 K to 700 K have been extracted from measurements of the temperature dependence of the volume and rhombohedral angle α using x-ray diffraction[6,9-11], calorimetric determinations of the heat evolution associated with the transition[12] and studies of anomalies in the thermal expansion[5,7,13-15] and electrical resistivity[16,17]. In some measurements[11], small

discontinuities in volume and α have been detected at the transition, suggesting that it may be weakly first order.

Our theoretical investigation of this transition proceeds in three steps. In section II, we show how to manipulate the full anharmonic lattice Hamiltonian into a form with a tractable number of coupling constants. In section III we determine the coupling constants for GeTe using pseudopotential total energy calculations for various structural configurations. Finally, in section IV we describe a renormalization-group calculation implemented in momentum space which yields T_c and the critical properties associated with the transition. Section V contains a discussion of the approximations in this approach and the considerations relevant to its application to finite-temperature structural transitions in other systems, and concluding remarks.

II. CONSTRUCTION OF MODEL HAMILTONIAN

As the starting point of a first-principles study, we seek a microscopic Hamiltonian for the system which incorporates a correct desription of the features leading to the structural transition[18]. For GeTe, it is appropriate to use an anharmonic lattice Hamiltonian[19,20] in which only the ionic degrees of freedom appear explicitly, and the electronic effects are included in the Born-Oppenheimer

approximation. However, even if this Hamiltonian is simplified by expanding to fourth order about the prototype configuration (the rocksalt structure), it is still too complicated for calculating numerical values of the coefficients or for evaluating the partition function and obtaining thermal properties. The local mode approximation[21] provides an intuitively appealing way of obtaining an equivalent model Hamiltonian with a simpler form and a greatly reduced number of parameters. For each unit cell, the local mode variable is defined as the projection of local ionic displacements onto the polarization vectors of the k=0 optic modes, referred to the mean positions in the high-temperature structure. The Hamiltonian is expanded in symmetry allowed powers of the local mode variables, with on-site terms kept up to some arbitrary order and intersite interactions to quadratic order only.

To a large extent, the requirement that the local mode have the lattice symmetry restricts the possible definitions. The approximation of purely local anharmonicity, essential for obtaining a Hamiltonian with a small number of parameters, necessitates that the precise choice of local mode incorporate a physical understanding of the lattice instability. The charge flow and energy gain resulting from the symmetry breaking by the distortion of the six equivalent nearest-neighbor bonds of the rocksalt structure involves primarily Te p-like states[4,22], while the

main anharmonic contribution to the energy originates in the nonlinear Te polarizability.[23] Thus, for GeTe, the best choice of local mode emphasizes the distortion of the Te ion environment:

$$\vec{\xi}_i = a_0^{-1}(\Delta\vec{r}_{Te}{}^i - \sum_{n.n\,j} \Delta\vec{r}_{Ge}{}^j/6)$$

where a_0 is the length of the side of the fcc conventional unit cell and the displacements $\Delta\vec{r}$ are measured relative to the rocksalt structure.

Before giving the explicit approximate expression for the model Hamiltonian H_{mod} which will be used in the calculation, we study its properties using the exact form, obtained from the relation:

$$\exp(-\beta H_{mod}(\{\vec{\xi}_i\})) = \int [\Pi(d\vec{\sigma}_i)]\ \exp(-\beta H_{lat}(\{\vec{\xi}_i\},\{\vec{\sigma}_i\}))$$

where $\vec{\sigma}_i = a_0^{-1}(\Delta\vec{r}_{Te}{}^i + \sum_{n.n.j} \Delta\vec{r}_{Ge}{}^j/6)$ and $H_{lat}(\{\vec{\xi}_i\},\{\vec{\sigma}_i\})$ is the full anharmonic lattice Hamiltonian. We note that at fixed $\{\vec{\xi}_i\}$, H_{mod} in principle depends on the energies of a 3N/2 dimensional space of ionic configurations and the temperature.

However, to a good approximation the situation is much simpler. We decompose H_{lat} as follows:

$H_{lat}(\{\xi_i\},\{\sigma_i\}) = H_1(\{\xi_i\}) + H_2(\{\sigma_i\}) + H_3(\{\xi_i\},\{\sigma_i\})$.

Because the physically important anharmonicity is associated with the $\{\vec{\xi}_i\}$, it should be sufficient to include the $\{\vec{\sigma}_i\}$ in the expansion of H_{lat} up to quadratic order only. The Gaussian integration over the $\{\vec{\sigma}_i\}$ replaces $\{\vec{\sigma}_i\}$ by the values which minimize H_{lat} at fixed $\{\vec{\xi}_i\}$, and therefore the coefficients of H_{mod} are independent of temperature in this approximation.

The relation of $H_{mod}(\{\vec{\xi}_i\})$ to the energies of ionic configurations $H_{lat}(\{\vec{\xi}_i\},\{\vec{\sigma}_i\})$ can be further simplified by keeping only the lowest order term in H_3, $\int d^3k V^{\alpha\beta}(\vec{k})\sigma^{\alpha}(\vec{k})\xi^{\beta}(-\vec{k})$. Then, with $\vec{\xi}(\vec{k})$ nonzero, only the minimization with respect to the component of $\vec{\sigma}(-\vec{k})$ which transforms according to the same representation of the group of $\vec{k}$ is nontrivial. For small $\vec{k}$, however, $V(\vec{k})$ vanishes like k^2, so there we keep instead the term proportional to $\int d^3k \int d^3k' V^{\alpha\beta\gamma\delta} k^{\delta} \sigma^{\alpha}(\vec{k}) \xi^{\beta}(\vec{k}') \xi^{\gamma}(\vec{k}-\vec{k}')$ which describes the lowest order coupling of $\vec{\xi}$ to long-wavelength strain. Rather than

integrate this term out immediately, we will for the time being keep the long-wavelength strains explicitly in order to study the physics arising from this coupling.

The construction of H_{mod} for the GeTe transition proceeds as follows. The local mode variables sit on the sites of an fcc lattice and only cubic-symmetry invariants appear in the expansion of the Hamiltonian. We truncate the onsite potential at fourth order in the local mode variable but keep isotropic terms to eighth order. Intersite interactions up to second order are included, since the constraints imposed by the sharing of Ge atoms by first and second neighbor local mode octahedra suggest the coupling is important. The lowest order terms involving long-wavelength strain fields are included explicitly, as discussed above.

Carrying out this construction, we obtain the following explicit form for H_{mod}. The expression for the onsite potential is:

$$\sum_i \{A|\vec{\xi}(\vec{R}_i)|^2 + u_0|\vec{\xi}(\vec{R}_i)|^4 + v_0\sum_\alpha \xi_\alpha(\vec{R}_i)^4 + D|\vec{\xi}(\vec{R}_i)|^6 + E|\vec{\xi}(\vec{R}_i)|^8\},$$

with the first neighbor intersite interactions:

$$-1/2\sum_i \{\xi_x(\vec{R}_i)\,[\,a_1\sum_{\vec{d}\in\{(\pm\hat{x}\pm\hat{y}),(\pm\hat{x}\pm\hat{z})\}}\xi_x(\vec{R}_i+a_0\vec{d}/2) + a_2\sum_{\vec{d}\in\{(\pm\hat{y}\pm\hat{z})\}}\xi_x(\vec{R}_i+a_0\vec{d}/2)$$

$$+ a_3\sum_{\vec{d}\in\{(\pm\hat{x}\pm\hat{y})\}}(\vec{d}\cdot\hat{x})\,(\vec{d}\cdot\hat{y})\,\xi_y(\vec{R}_i+a_0\vec{d}/2)$$

$$+ a_3\sum_{\vec{d}\in\{(\pm\hat{x}\pm\hat{z})\}}(\vec{d}\cdot\hat{x})\,(\vec{d}\cdot\hat{z})\,\xi_z(\vec{R}_i+a_0\vec{d}/2)\Big]+\text{cyc.perm.}\Big\},$$

and second neighbor intersite interactions

$$-1/2\sum_i\Big\{\xi_x(\vec{R}_i)\Big[b_1\sum_{\vec{d}\in\{\pm\hat{x}\}}\xi_x(\vec{R}_i+a_0\vec{d}) + b_2\sum_{\vec{d}\in\{\pm\hat{y},\pm\hat{z}\}}\xi_x(\vec{R}_i+a_0\vec{d})\Big]+\text{cyc.perm.}\Big\},$$

where $\vec{\xi}(\vec{R}_i)$ is the local mode variable at the fcc lattice site $\vec{R}_i$.

With the strain tensor $\overleftrightarrow{e}_{\alpha\beta}= (\delta u_\beta/\delta x_\alpha + \delta u_\alpha/\delta x_\beta)/2$, the lowest order terms which describe long wavelength strain deformations and their coupling to the order-parameter are:

$$(\Omega_0)^{-1}\int d^3r\,\Big[C_{11}\sum_\alpha e_{\alpha\alpha}^2(\vec{r})/2 + C_{12}\sum_{\alpha\neq\beta}e_{\alpha\alpha}(\vec{r})\,e_{\beta\beta}(\vec{r})/2 + C_{44}\sum_{\alpha\neq\beta}e_{\alpha\beta}^2(\vec{r})$$

$$-g_0\sum_\alpha e_{\alpha\alpha}(\vec{r})\,|\vec{\xi}_i|^2/3-g_1\sum_{\alpha<\beta}e_{\alpha\beta}(\vec{r})\,\xi_{i,\alpha}\xi_{i,\beta}- g_2\sum_\alpha e_{\alpha\alpha}(\vec{r})\,(\xi_{i,\alpha}^2-|\vec{\xi}_i|^2/3)\Big].$$

These expressions define the model Hamiltonian coefficients A, u_0, v_0, D, E, a_1, a_2, a_3, b_1+2b_2, C_{11}, C_{12}, C_{44}, g_0, g_1, and g_2 which will be calculated in the next section.

III. TOTAL ENERGY CALCULATIONS

The values of the coefficients for GeTe are obtained by fitting the model Hamiltonian to the energies of a variety of local mode configurations. For the zero-strain coefficients A, u_0, v_0, D, E, a_1, a_2, a_3, b_1+2b_2 we must consider configurations with the full fcc translational symmetry (Fig.3a) as well as configurations with two translationally inequivalent types of local mode variables on fcc lattice sites. For the fcc lattice, there are only two ways to divide the sites into two inequivalent classes, giving rise to an arrangement with a tetragonal unit cell (Fig.3b) and to one with a rhombohedral unit cell (Fig.3c). In each type of unit cell, we study two families of local mode configurations, specified by a fixed polarization vector at each inequivalent site and a varying amplitude τ. For each family, the energy as a function of τ determines one combination of coefficients at each order. Unfortunately, the second neighbor couplings b_1 and b_2 cannot be separately determined without using still larger unit cells.

To obtain the strain coefficients C_{11}, C_{12}, C_{44}, g_0, g_1, and g_2, it is sufficient to consider configurations in which the local mode is uniform and only the lattice

changes. We study three types of variation corresponding to pure volume change ($e_{xx}=e_{yy}=e_{zz}$), pure rhombohedral angle change at fixed volume ($e_{xx}=e_{yy}=e_{zz}$, $e_{xy}=e_{yz}=e_{xz}$), and uniaxial strain (e_{zz}). The coefficients C_{11}, C_{12}, C_{44} are obtained from configurations with $\tau = 0$, while for g_0, g_1, and g_2 a configuration with nonzero τ must be included at each e.

As discussed in Section II, the local mode configuration energy can be taken as the minimum over the energies of ionic configurations with the same translational and point symmetries. The types of zero-strain ionic configurations for which we must calculate the energy are specified in Table I and Fig.4. For families (a), (b), (e) and (f) the choice of τ and the symmetry requirement completely specify the ionic configuration, For families (c) and (d), the symmetry requirement is less restrictive, resulting in a one-dimensional space of ionic configurations, here labelled by σ, which must be searched for the energy minimum.

The necessary calculations of the energies of ionic configurations are performed using the self-consistent ab-initio pseudopotential total energy method[24,25]. We use

the spin-orbit averaged relativistic nonlocal atomic pseudopotentials for Ge and Te given by Bachelet, Hamann and Schluter[26]. Exchange and correlation are included through the local density approximation using the Ceperley- Alder- Perdew- Zunger parametrization[27]. Eigenfunctions are expanded in a plane wave basis with energy cutoff E_1 = 10.5 Ry, and Lowdin perturbation theory[28] is used to include the effect of plane waves up to E_2 = 16.5 Ry. Brillouin zone averages are performed using Monkhorst-Pack special $\vec{k}$-point sets[29]. The specific details of the k-point sets for each configuration are included in Table I. In previous work[4] we have seen that this gives extremely good basis set convergence, and the error is dominated by $\vec{k}$-point sampling. Computations were done on an IBM 370/4381 with 8-byte word length.

Details of the minimization procedure relating local mode configuration energies in families (c) and (d) to ionic configuration energies are shown fully in Figs.5 and 6. The results for the energies of all the zero-strain local mode configurations are shown in Fig.7. Energies of configurations including strain are shown in Fig.8. We include the results for smaller $\vec{k}$-point sets in Fig.7 to demonstrate the convergence. With the cutoffs used, energy curvatures are determined to about 10% accuracy.

The model Hamiltonian parameters were obtained through a two-step fitting process. First, the zero-strain coefficients were fit to the zero-strain local mode configuration energies, measured relative to the energies at τ=0. Then, the strain parameters were fit to the energies of strained configurations, holding the zero-strain coefficients fixed and letting the a_0 in the definition of $\vec{\xi}$ vary with $\overleftrightarrow{e}$. The quality of the fit can be seen from the solid lines in Figs.7 and 8. The resulting parameters are given in Table II.

IV. STATISTICAL MECHANICS

Given this microscopic Hamiltonian, the transition temperature and critical properties follow from the evaluation of the partition function. A systematic approach begins with a Hubbard-Stratonovich transformation on the partition function

$$Z = \int [\Pi d\vec{\xi}_i] \mathcal{D}\overleftrightarrow{e}(\vec{r}) \exp[-\beta H_{mod}(\{\vec{\xi}_i\}, \overleftrightarrow{e}(\vec{r}))]$$

to introduce a field $\vec{\phi}_i$ which couples linearly to the order parameter. The trace over $\vec{\xi}_i$ is expanded in $\vec{\phi}_i$ and $\overleftrightarrow{e}(\vec{r})$ to give a functional of the same form as the original Hamiltonian:

$$\beta H_{HS} = \int d^3r \{ (r_0(T-T_0)|\vec{\phi}(\vec{r})|^2 + |\vec{\nabla}\vec{\phi}(\vec{r})|^2)/2$$

$$+ (\sum_\alpha f(\partial_\alpha\phi_\alpha)^2 - \sum_{\alpha\neq\beta} h(\partial_\beta\phi_\alpha)(\partial_\alpha\phi_\beta))/2 + \bar{u}|\vec{\phi}(\vec{r})|^4 + \bar{v}\sum_\alpha \phi_\alpha(\vec{r})^4 + O(\phi^6)$$

$$+ (6\pi^2)^{-1} [\bar{z}_3\sum_\alpha e_{\alpha\alpha}(\vec{r})/3 + \bar{c}_{11}\sum_\alpha e_{\alpha\alpha}^2(\vec{r})/2 + \bar{c}_{12}\sum_{\alpha\neq\beta} e_{\alpha\alpha}(\vec{r})e_{\beta\beta}(\vec{r})/2$$

$$+ \bar{c}_{44}\sum_{\alpha\neq\beta} e_{\alpha\beta}^2(\vec{r}) - \bar{g}_0\sum_\alpha e_{\alpha\alpha}(\vec{r})|\vec{\phi}(\vec{r})|^2/3 - \bar{g}_1\sum_{\alpha<\beta} e_{\alpha\beta}(\vec{r})\phi_\alpha(\vec{r})\phi_\beta(\vec{r}) -$$

$$g_2\sum_\alpha e_{\alpha\alpha}(r)((\phi_\alpha(r)^2 - |\phi(r)|^2/3)] \} .$$

In anticipation of the RG analysis below, we have taken the continuum limit, defined the length scale so that the Brillouin zone is approximated by a sphere of radius 1 and normalized the $\vec{\phi}(\vec{r})$ so the $|\vec{\nabla}\phi(\vec{r})|^2$ term has coefficient 1/2. All the coefficients except r_0, f and h, which arise from the quadratic intersite coupling, are now functions of single-site traces (and thus of β) :

$$\langle p(\vec{\xi})\rangle = \frac{\int d^3\xi \exp(-\beta[A|\vec{\xi}|^2+u_0|\vec{\xi}|^4+v_0\sum_\alpha \xi_\alpha^4+D|\vec{\xi}|^6+E|\vec{\xi}|^8])p(\vec{\xi})}{\int d^3\xi \exp(-\beta[A|\vec{\xi}|^2+u_0|\vec{\xi}|^4+v_0\sum_\alpha \xi_\alpha^4+D|\vec{\xi}|^6+E|\vec{\xi}|^8])} .$$

Having manipulated the partition function into a standard functional integral form, we now proceed to evaluate it. The use of the stationary phase approximation

leads to a mean-field-theory transition temperature $T_{c,mf} = T_0 - 2\bar{g}_0\bar{Z}_3/(3r_0(\bar{C}_{11}+2\bar{C}_{12}))$. For GeTe, we find $T_c = 669$ K while the contribution from strain coupling contributes +4 K, giving $T_{c,mf} = 673$ K.

An estimate of the correction to the mean field value of T_c and information about the critical behavior can be obtained through the renormalization group in the ϵ-expansion. Since the critical temperature dependence is contained in the vanishing of $T - T_{c,mf}$, all other coefficients in βH_{HS} are evaluated at $T_{c,mf}$ and their temperature dependence is neglected in the following discussion. The resulting values of the coefficents in βH_{HS} are given in Table III. This type of compressible 3-component model with cubic anisotropy has been studied previously[30]. For the present discussion, we write the functional in the standard Landau- Ginzburg- Wilson form with n=3, d=3 and cubic symmetry, including the infinite-range intersite quartic couplings generated by integrating out the homogeneous strain. This leads to:

$$\beta H_{LGW} = \int d^3r \{ (r_0(T-T_{c,mf})|\vec{\phi}(\vec{r})|^2 + |\vec{\nabla}\vec{\phi}(\vec{r})|^2)/2 + u|\vec{\phi}(\vec{r})|^4 + v\sum_\alpha \phi_\alpha(\vec{r})^4 + O(\phi^6) + (f\sum_\alpha(\partial_\alpha\phi_\alpha)^2 - h\sum_{\alpha\neq\beta}(\partial_\beta\phi_\alpha)(\partial_\alpha\phi_\beta))/2 \}$$

$$+ \int d^3r \int d^3r' \{ w_0 \sum_{\alpha} \phi_\alpha(\vec{r})^2 \phi_\alpha(\vec{r}')^2 + w_1 \sum_{\alpha<\beta} \phi_\alpha(\vec{r})^2 \phi_\beta(\vec{r}')^2 + w_2 \sum_{\alpha<\beta} \phi_\alpha(\vec{r}) \phi_\beta(\vec{r}) \phi_\alpha(\vec{r}') \phi_\beta(\vec{r}') \}$$

In analyzing this model, we neglect the higher order anharmonicities and the anisotropic components of the gradient terms since these are marginal or irrelevant fields and will modify the flows significantly only in extreme cases. Thus, we consider the differential recursion relations to first order in $\varepsilon = 4-d$ in the six-dimensional parameter space $r=r_0(T-T_{c,mf})$, u, v, w_0, w_1 and w_2:

$$dr/dl = 2r + (8\pi^2)^{-1}(20u+12v+4w_0+4w_1)/(1+r)$$

$$du/dl = u - (8\pi^2)^{-1}u(44u+24v)/(1+r)^2$$

$$dv/dl = v - (8\pi^2)^{-1}v(36u+48v)/(1+r)^2.$$

$$dw_0/dl = w_0 - (8\pi^2)^{-1}(24w_0u+8w_1u+24w_0v+4w_0^2)/(1+r)^2.$$

$$dw_1/dl = w_1 - (8\pi^2)^{-1}(32w_1u+8w_0u+24w_1v+2w_1^2+4w_0w_1)/(1+r)^2$$

$$dw_2/dl = w_2 - (8\pi^2)^{-1}(8w_2u+2w_2^2)/(1+r)^2$$

By iterating the recursion relations numerically, we examine the changes in the flows as the system moves along the line in parameter space according to the physical temperature T, and find a shift in T_c of -16K, yielding T_c

= 657K.

An analogous treatment of the nearest neighbor Ising model on a face-centered-cubic lattice gives a shift in T_c of -14%, comparable to that of -18% obtained from numerical studies[31] in d=3. The smaller shift in the present case results from smaller ratios of the fourth order couplings to r_0, as determined by the several independent microscopic coupling constants. To lowest order, the strain-related fluctuation contribution to the shift in T_c can be estimated by mapping to an effective cubic-anisotropy model[31] $\tilde{r}=r+(2\pi^2)^{-1}(w_0+w_1)$, $\tilde{u}=u$, $\tilde{v}=v$, which shows that at this level, the shift of 0.35K is independent of w_2. In fact, in the present case higher order effects are also important since comparison of the full flows with those in which we set $w_i=0$ yields a slightly larger contribution of 3K.

This RG analysis can also be used to understand the observed first-order character of the transition. At the fixed points of the pure cubic-anisotropy model[32] ($w_i=0$), the w_i are relevant. There are new fixed points with $w_i^*>0$, but these are not accessible to flows starting in the $w_i<0$ region of parameter space, as in the present case where

$w_0=-2.71\times10^{-3}$, $w_1=-3.83\times10^{-4}$ and $w_2=-3.60\times10^{-2}$. The resulting runaway behavior of the strain-generated couplings is associated in principle with the occurrence of a first order transition. To see that this runaway, particularly in w_2, provides a plausible mechanism for the observed character of the transition, consider that within mean field theory, the effect of the strain coupling is to shift the effective values of (u,v) towards the mean-field phase boundary $u_{eff} + v_{eff}/3 = 0$, from (0.018,0.013) to $(-6.1\times10^{-4},0.028)$. This substantial shift suggests that though the transition within mean field theory is still second order, the strain effects could be large enough to produce an observable discontinuity within RG, and thus the transition is fluctuation-driven first-order.

V. DISCUSSION AND CONCLUDING REMARKS

Here we review the calculation to see where important approximations and calculational inaccuracies enter and to separate the features which are special to the GeTe transition from more widely applicable aspects.

We started by assuming that the transition could be described by a purely ionic Hamiltonian expanded about the prototype structure. Although models have been proposed in which the near-band-gap electronic states are the direct

source of the temperature dependence[33,34], it seems unlikely that this effect could be significant compared to the lattice anharmonicity in the case of GeTe. Defining a local mode variable, we formally obtained a model Hamiltonian that exactly reproduced the thermal behavior of the original. Then we approximated the model by a truncated expansion--local anharmonicity, no intersite interactions beyond second neighbor, lowest order local-mode-strain coupling-- with no temperature dependence in the coefficients. Because the definition of the local mode variable and truncation of the model Hamiltonian (which is important in determining the quantitative accuracy of the model) depends on the physics of the GeTe transition, the details of this part of the procedure would need to be rethought when applied to other systems. In particular, although the local mode approximation can be used to obtain model Hamiltonians for both displacive and order-disorder structural transitions[18], the large local anharmonicity in the latter case probably implies that nonlocal anharmonic terms must also be included for a good quantitative description. Therefore this approach is generally feasible only for transitions, like that in GeTe, which have displacive character.

In contrast, once we have obtained the numerical form of the model, the statistical mechanical analysis depends

mainly on the universality class of the transition. The dropping of terms from H_{LGW} and the validity of techniques such as the ϵ-expansion rely less on the physics of GeTe and are more subject to systematic improvement than the approximations in the form of H_{mod}. For example, the fluctuations could be described using the full Green's function instead of its gradient expansion, the analysis could be carried to higher order in ϵ, and the higher order anharmonicities, anisotropic fluctuations and the terms generated by the inhomogeneous strains could be included explicitly in the recursion relation analysis. In fact, to first order in ϵ the sixth order anharmonicities can be included in the analysis simply by introducing effective values of u and v^{35}. For the zero-strain coupling case, we find (u_{eff}, v_{eff}) shifts only slightly, from (0.018,0.013) to (0.013,0.011), so that this correction cannot account for the observed first order behavior.

The most important calculational errors enter via the total energy calculations. As discussed in section IV, $\vec{k}$-point convergence makes the largest contribution to errors at the level of ionic configuration energies, resulting in uncertainty in the quadratic coefficients in

H_{mod} of about 10%. Propagation through to T_c shows that the error in T_c is slightly sublinear in the uncertainty in the coefficents. At the level of H_{mod}, we also were unable to separate b_1 and b_2. Since we expect both of these to be positive, we introduce $\nu \in [0,1]$ with $b_1 = \nu(b_1+2b_2)$, $b_2 = (1-\nu)(b_1+2b_2)/2$. For the RG analysis, we chose $\nu = 0.37$ which is a reasonable value in view of the lack of strong anisotropy of the first neighbor interactions and has the additional advantage that f=0. If we had included f explicitly in the RG analysis, it would be possible to obtain quantitative bounds on $T_c(\nu)$. However, since $T_{c,mf}$ depends only on b_1+2b_2, T_c should be fairly insensitive to ν. With the above considerations, we make an estimate of the error in T_c to obtain a final answer of 657 +/- 100 K.

Aside from T_c and the character of the transition, a number of other properties derivable within this framework could be compared with experiment. Experimentally observable quantities related to the strain, include dT_c/dP, elastic constants and their discontinuity at the transition, and the discontinuity of the thermal expansion

coefficient at the transition. These provide information about the order-parameter strain couplings in the system and could be calculated using our approach, although a more refined treatment of the strain degrees of freedom would be required than that given here.

In summary, we have studied the phase transition of GeTe completely ab-initio, predicting T_c = 657K +/- 100K. This compares quite favorably with the range of experimental values of 625 - 700K. In addition, we find that the presence of the order-parameter strain coupling moves the system into the fluctuation-driven first-order region of the phase diagram, consistent with experimental indications of a discontinuous transition. This provides an encouraging prospect for future applications of the pseudopotential total energy method to the calculation of finite-temperature properties of solids.

References

1. J.Ihm, D.H.Lee, J.D.Joannopoulos and J.J.Xiong, Phys.Rev.Lett. 51,1872 (1983).

2. L.L.Boyer and J.R.Hardy, Phys.Rev.B 24,2577 (1981).

3. See, for example, references in Ref.4.

4. K.M.Rabe and J.D.Joannopoulos, Phys.Rev.B 32, 2302 (1985).

5. L.E.Shelimova, N.Kh.Abrikosov and V.V.Zhdanova, Russ. J. Inorg. Chem. 10, 650 (1965).

6. A.D.Bigava, A.A.Gabedava, E.D.Kunchuliya, S.S.Moiseenko and R.R.Shvangiradze, Neorg.Mater. 12, 835 (1976) [Inorg.Mater 12,708 (1976)].

7. N.Kh.Abrikosov, O.G.Karpinskii, L.E.Shelimova and M.A.Korzhuev, Neorg.Mater. 13, 2160 (1977) [Inorg.Mater. 13,1723 (1977)].

8. M.Iizumi, Y.Hamaguchi, K.F.Komatsubara and Y.Kato, J.Phys.Soc.Jpn 38, 443 (1975).

9. K.Schubert and H.Fricke, Z.Naturforschung 6a, 781 (1951); Str.Rep. 15, 72 (1951); Z.Metallkunde 44,457 (1953); Str.Rep. 17, 44 (1953).

10. J.N.Bierly, L.Muldawer and O.Beckman, Acta.Met. 11,447 (1963).

11. T.B.Zhukova and A.I.Zaslavskii, Kristallografiya 12,37 (1967). [Sov.Phys.--Crystallogr. 12, 28 (1967)].

12. N.Kh.Abrikosov, M.A.Korzhuev, L.A.Petrov, O.A.Teplov and G.K.Demenskii, Neorg.Mater. 19, 370 (1983) [Inorg.Mater.

19, 334 (1983)].

13. S.I.Novikova, L.E.Shelimova, N.Kh.Abrikosov, V.I.Galyutin and B.A.Evseev, Fiz.Tverd.Tel. 12, 3623 (1971) [Sov.Phys-- Sol.St. 12, 2945 (1971)].

14. S.I.Novikova, L.E.Shelimova, N.Kh.Abrikosov and B.A.Evseev, Fiz.Tverd.Tel. 13, 2764 (1972) [Sov.Phys-- Sol.St. 13, 2310 (1972)].

15. S.I.Novikova, L.E.Shelimova, N.Kh.Abrikosov and O.G.Karpinskii, Fiz.Tverd.Tel. 19, 1171 (1977) [Sov.Phys-- Sol.St. 19, 683 (1977)].

16. S.I.Novikova, L.E.Shelimova, E.S.Avilov and M.A.Korzhuev, Fiz.Tverd.Tel. 17, 2379 (1975) [Sov.Phys-- Sol.St. 17, 1570 (1975)].

17. N.Kh.Abrikosov, M.A.Korzhuev and L.E.Shelimova, Neorg.Mater. 13, 1757 (1977) [Inorg.Mater. 13, 1418 (1977)].

18. M.E.Lines and A.M.Glass, Principles and Applications of Ferroelectrics and Related Materials (Clarendon, Oxford,1977)

19. W.Cochran, Adv.Phys. 9,387 (1960).

20. P.W.Anderson, in Fizika Dielectrikov, edited by G.Skanavi (Moscow,Akad.Nauk,1960).

21. M.E.Lines, Phys.Rev. 177,797 (1969).

22. P.B.Littlewood, J.Phys.C 13,4855 (1980); 13,4875 (1980).

23. A.Bussmann-Holder, H.Bilz and P.Vogl, in Dynamical Properties of IV-VI Compounds, Vol.99 of Springer Tracts in

Modern Physics (Springer, New York, 1983).

24. M.T.Yin and M.L.Cohen, Phys.Rev.B 25, 7403 (1982).

25. D.Vanderbilt, Ph.D.thesis, Massachusetts Institute of Technology, 1981.

26. G.B.Bachelet, D.R.Hamann and M.Schluter, Phys.Rev.B 26, 4199 (1982).

27. D.M.Ceperley, Phys.Rev.B 18, 3126 (1978); D.M.Ceperley and B.J.Alder, Phys.Rev.Lett 45, 566 (1980); J.Perdew and A.Zunger, Phys.Rev.B 23, 5048 (1981).

28. P.O.Lowdin, J.Chem.Phys. 19, 1396 (1951).

29. H.J.Monkhorst and J.D.Pack, Phys.Rev.B 13, 5188 (1976).

30. T.Natterman, J.Phys.A 10,1757 (1977); K.K.Murata, Phys.Rev.B 15,4328 (1977); G.Bender, Z.Physik B 23, 285 (1976).

31. C.Domb and A.R.Miedema, in Progress in Low Temperature Physics IV, edited by C.J.Gorter (North-Holland, Amsterdam, 1964).

32. A.Aharony, Phys.Rev.B 8,4270 (1973); in Phase Transitions and Critical Phenomena, edited by C.Domb and M.S.Green (Academic, New York, 1976), Vol.6, p.357.

33. M.A.Korzhuev,L.I.Petrova,G.K.Demenskii and O.A.Teplov, Fiz.Tverd.Tel. 23, 3387 (1981) [Sov.Phys.--Sol.St. 23, 1966 (1981)] and references therein.

34. V.A.Volkov and Yu.V.Kopaev, Zh.Eksp.Teor.Fiz. 64, 2184 (1973) [Sov.Phys.--JETP 37, 1103 (1981)].

35. D.Blankschtein and A.Aharony, Phys.Rev.B 28, 386 (1983).

Table I. Specifications of the families of local mode configurations for which total energies were calculated, the combinations of quadratic parameters determined and the Monkhorst-Pack[29] k-point sets used. Open and filled circles are used to label translationally inequivalent lattice sites (see Fig.3).

Configuration	unit cell type	Local mode variables open circles	Local mode variables filled circles	quadratic parameters determined	k-point sets (number of points in full BZ)
(a)	fcc	$\tau(111)$	---	$A+4a_1+2a_2+b_1+2b_2$	125, 343
(b)	fcc	$\tau(010)$	---	$A+4a_1+2a_2+b_1+2b_2$	125, 343
(c)	tetragonal	$\tau(010)$	$-\tau(010)$	$A-4a_1+2a_2+b_1+2b_2$	48, 100
(d)	tetragonal	$\tau(101)$	$-\tau(101)$	$A-2a_2+b_1+2b_2$	48, 100
(e)	rhombohedral	$\tau(111)$	$-\tau(111)$	$A-4a_3-b_1-2b_2$	27, 125
(f)	rhombohedral	$\tau(112)$	$-\tau(112)$	$A+2a_3-b_1-2b_2$	27, 125

Table II: Model Hamiltonian parameters for GeTe (eV).

onsite		intersite		elastic		coupling	
A	59.3	a_1	6.08	C_{11}	29.7	g_0	167
u_0	8.73×10^3	a_2	10.5	C_{12}	0.12	g_1	420
v_0	4.12×10^3	a_3	4.38	C_{44}	5.75	g_2	134
D	-7.32×10^5	b_1+2b_2	42.0				
E	2.36×10^7						

Table III: Coefficients in the functional $\beta H_{HS}(\{\vec{\xi}_i\},\{e(\vec{r})\})$:

onsite		intersite		elastic		coupling	
r_0	$3.68(eV)^{-1}$	f	0.00	$\bar{C}_{11}$	1.03×10^3	$\bar{g}_0$	19.5
k_BT_0	669 K	h	0.10	$\bar{C}_{12}$	3.72	$\bar{g}_1$	57.5
$\bar{u}$	0.0175			$\bar{C}_{44}$	194.	$\bar{g}_2$	17.5
$\bar{v}$	0.0133			$\bar{Z}_3$	-5.75		

Figures

Fig.1 The low-temperature rhombohedral structure of GeTe is obtained by two independent distortions of the rocksalt structure: (a) relative displacement of the Ge and Te sublattices by $\tau\, a_0(111)$ and (b) shear along [111] which reduces the rhombohedral angle α from its fcc value of 60°.

Fig.2. The local mode variable is defined as $\vec{\xi}_i = a_0^{-1}(\vec{r}_{Te}{}^i - \sum_{n.n.j} \vec{r}_{Ge}{}^j/6)$. The sum runs over the six nearest neighbor Ge atoms, which in the rocksalt structure form an octahedron with the Te atom at the center.

Fig.3. The translational symmetries of the various local mode configurations studied are illustrated. An fcc lattice with all sites equivalent is shown in (a). The division of lattice sites into two inequivalent types, as indicated by filled and open circles, yields (b) a tetragonal unit cell with equivalent sites lying in (010) planes, and (c) a rhombohedral unit cell with equivalent sites lying in (111) planes.

Fig.4. For each family of zero-strain local mode configurations, labelled (a)-(f) as in Table I, the type of ionic configurations for which total energies are calculated is shown. These ionic configurations are constructed according to the symmetry of the corresponding local mode

configuration, as described in the text. Open and filled circles here represent Ge and Te ions, respectively. For (a), (b), (e) and (f) a fixed τ corresponds to a single ionic configuration. For (c) and (d), the requirements imposed by symmetry are less stringent and a one-dimensional space of ionic configurations, parametrized by σ, corresponds to fixed τ.

Fig.5. For each member of a family of local mode configurations, parametrized by τ, the space of corresponding ionic configurations of same translational and point symmetry, parametrized by σ, is searched for the minimum energy, which is assigned to the local mode configuration (inset). For the longitudinal tetragonal family shown here, the corresponding space is one-dimensional. Energies are given relative to the rocksalt structure minimum in meV per atom.

Fig.6. Same as Fig.5 for the transverse tetragonal family (d).

Fig.7. Calculated local mode configuration energies, given relative to the rocksalt structure minimum in meV per atom. Solid lines show fit using model Hamiltonian parameters given in Table II. The energies for six families of local mode configurations with zero strain are shown --

longitudinal and transverse: (a),(b)--fcc;
(c),(d)--tetragonal and (e),(f)-- rhombohedral. The crosses show the results of calculations with the smaller k-point sets given in Table I.

Fig.8. Same conventions as Fig.7. On the right, energies of configurations which include strain are shown: (a),(c) and (e) are pure strain distortions, while (b),(d) and (f) show $E(e,\tau=0.01) - E(e,\tau=0.00)$ which determines the order-parameter strain coupling. Note the differences in energy scale among (a),(c),(e); (b),(d),(f), and Fig.7.

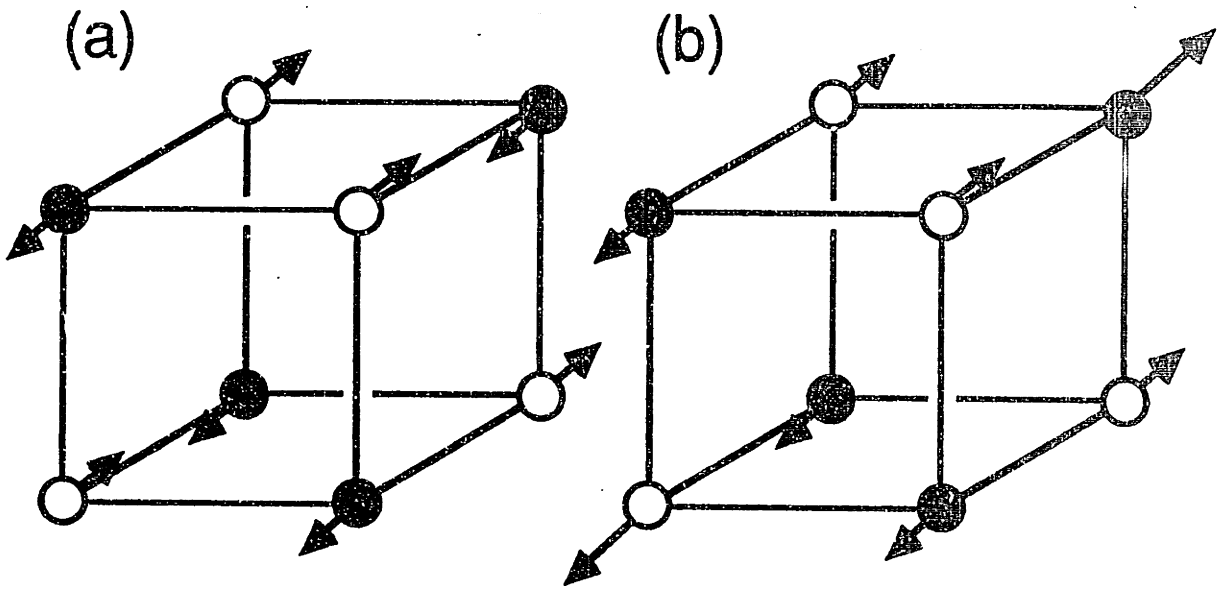

Fig. 1

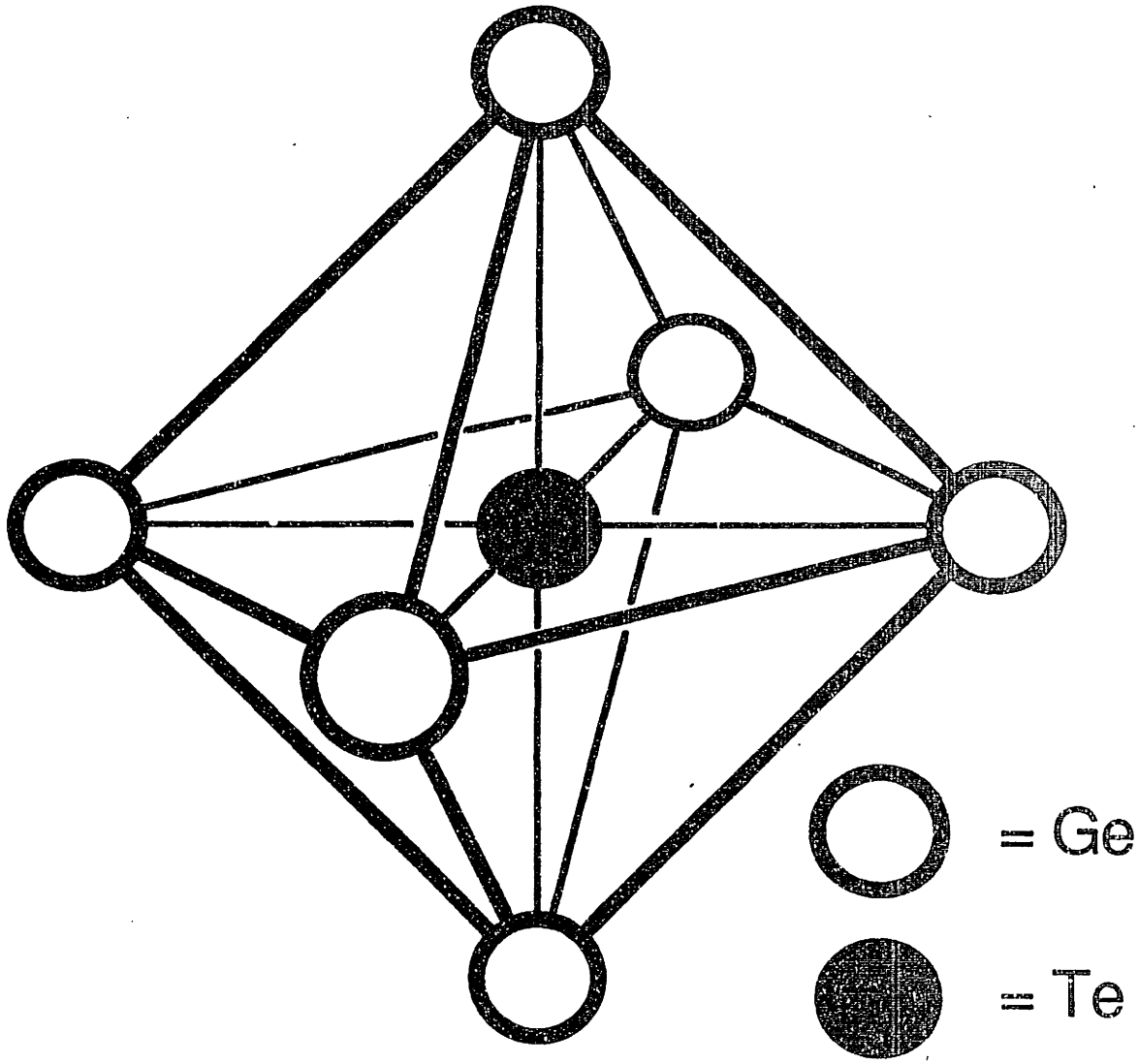

Fig. 2

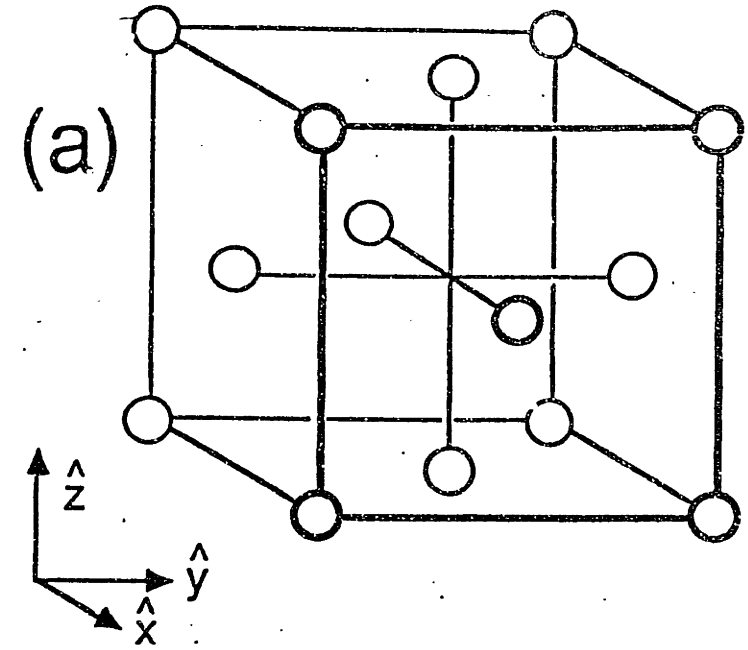

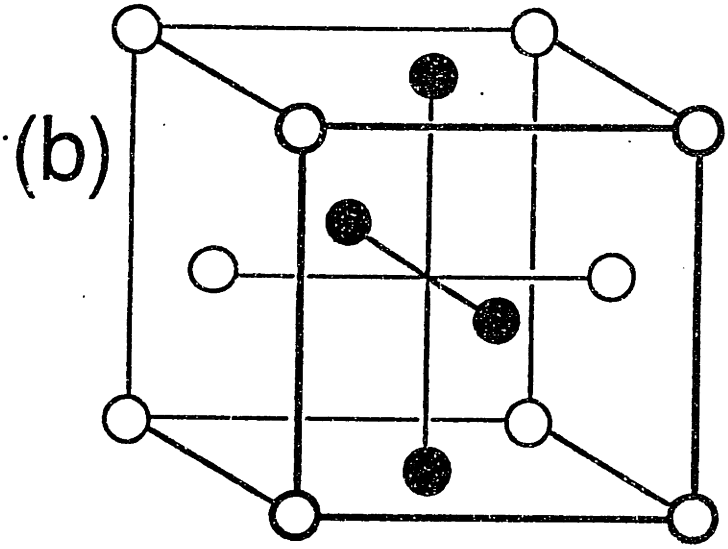

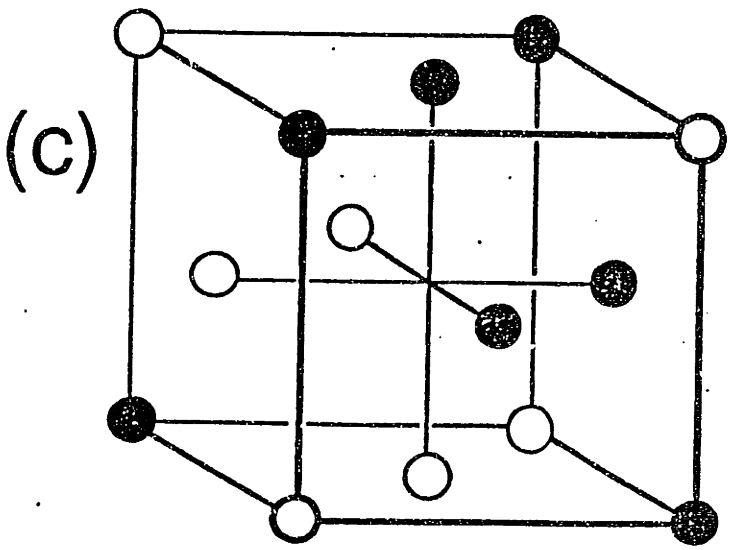

Fig. 3

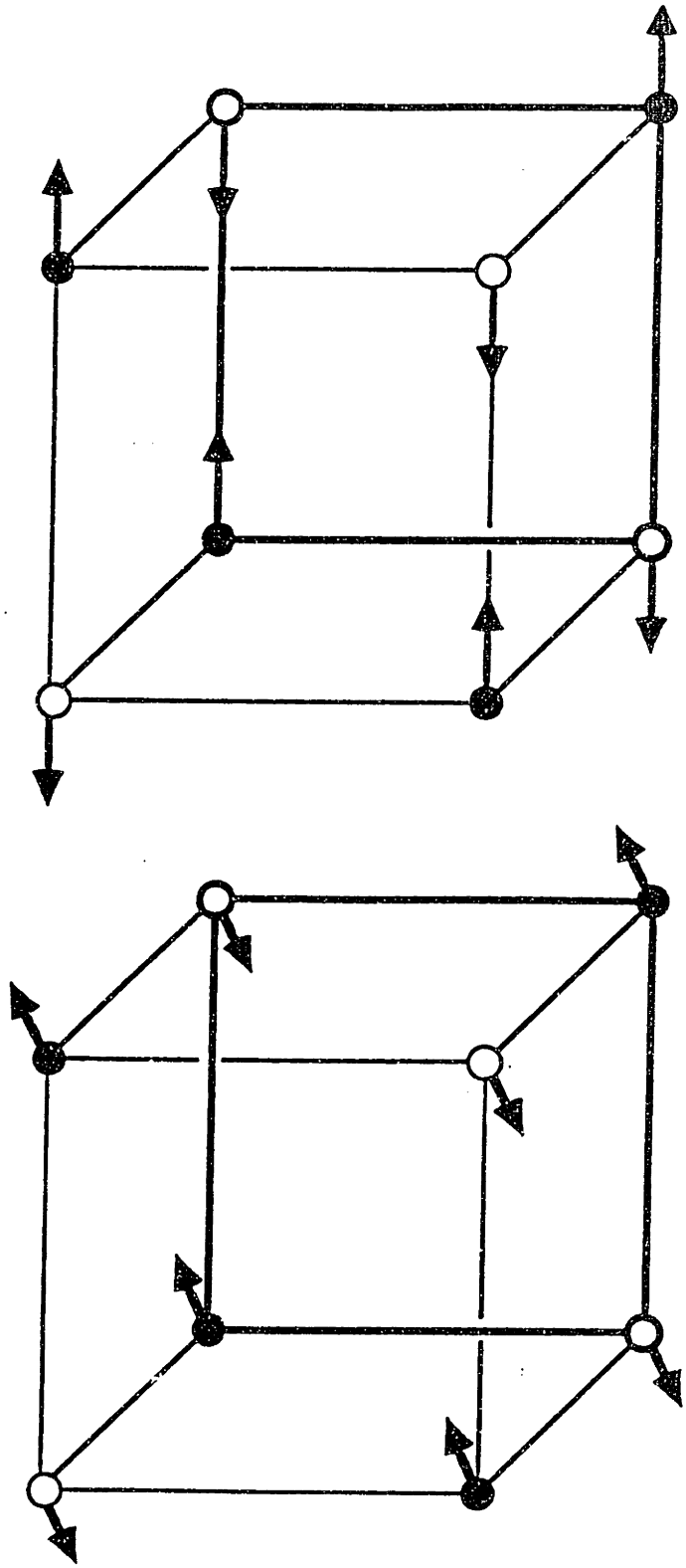

Fig. 4

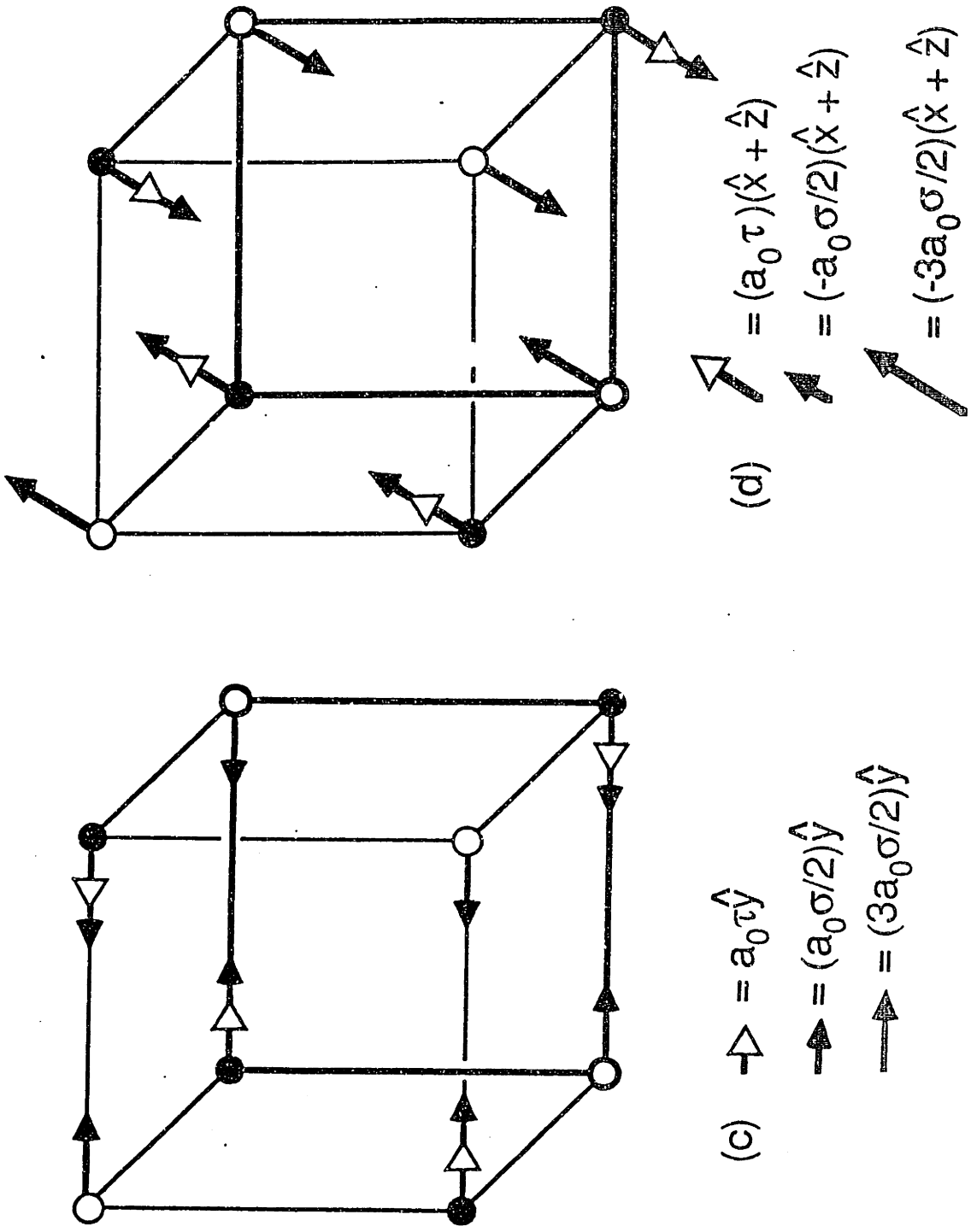
(d)
$= (a_0\tau)(\hat{x}+\hat{z})$
$= (-a_0\sigma/2)(\hat{x}+\hat{z})$
$= (-3a_0\sigma/2)(\hat{x}+\hat{z})$
(c)
$= a_0\tau\hat{y}$
$= (a_0\sigma/2)\hat{y}$
$= (3a_0\sigma/2)\hat{y}$

Fig. 4

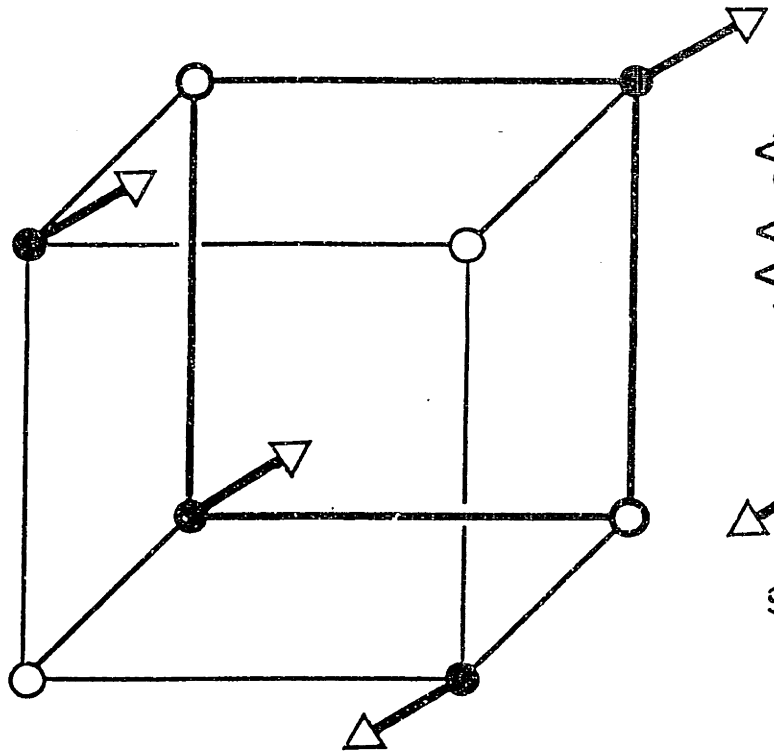

(f) $= a_0\tau(-\hat{x}-\hat{y}+2\hat{z})$

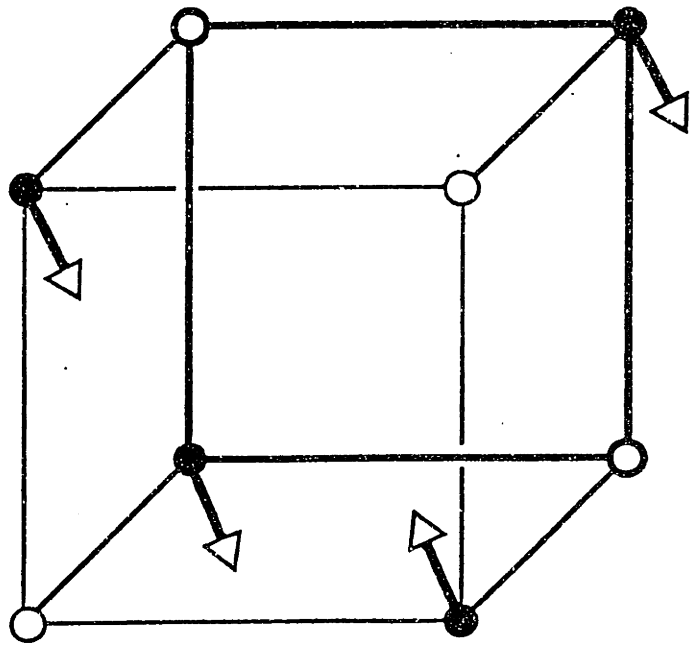

(e) $= a_0\tau(\hat{x}+\hat{y}+\hat{z})$

Fig. 4

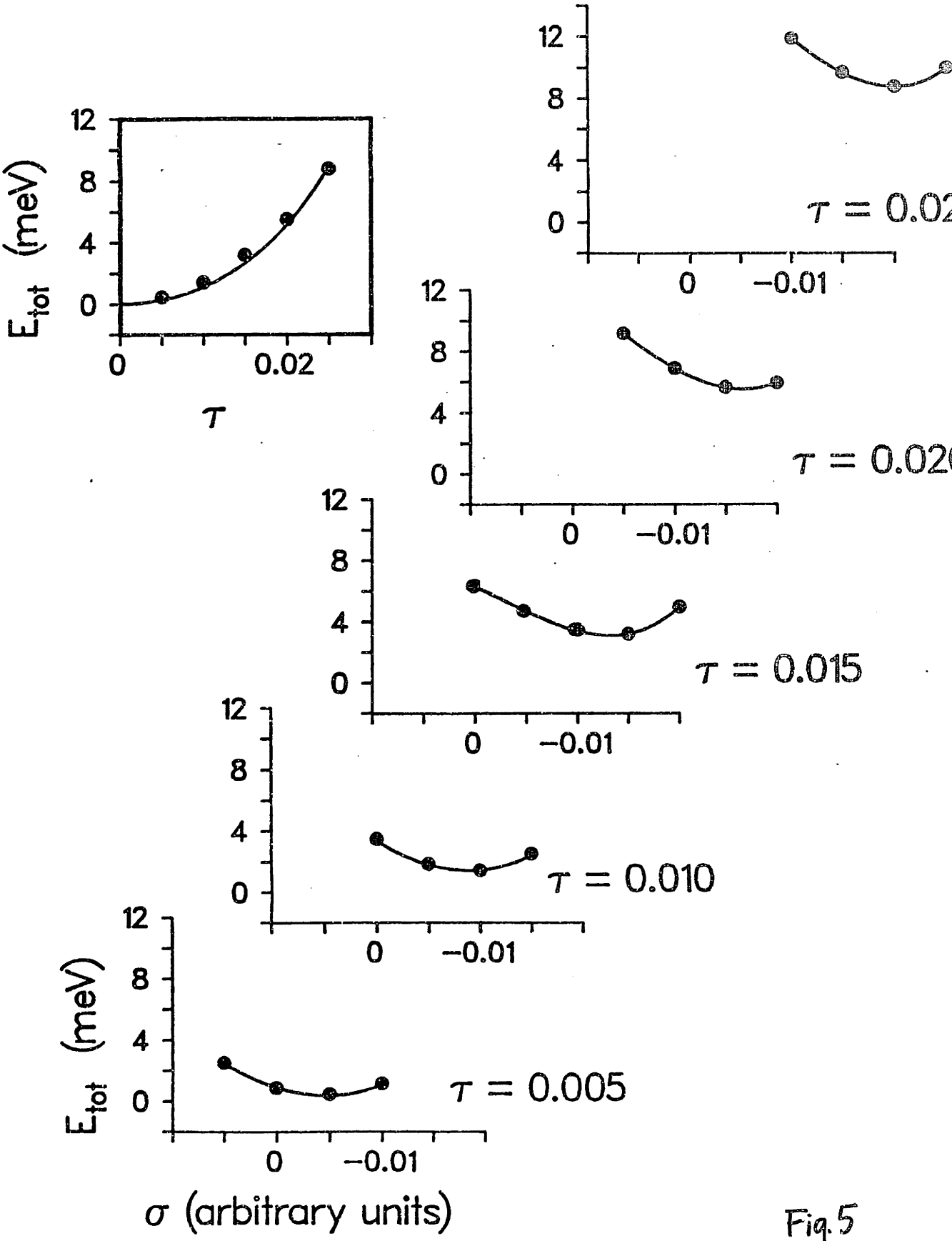
12
8
4
0
E_{tot} (meV)
0
0.02
τ
τ = 0.02
τ = 0.020
τ = 0.015
τ = 0.010
τ = 0.005
−0.01
σ (arbitrary units)

Fig. 5

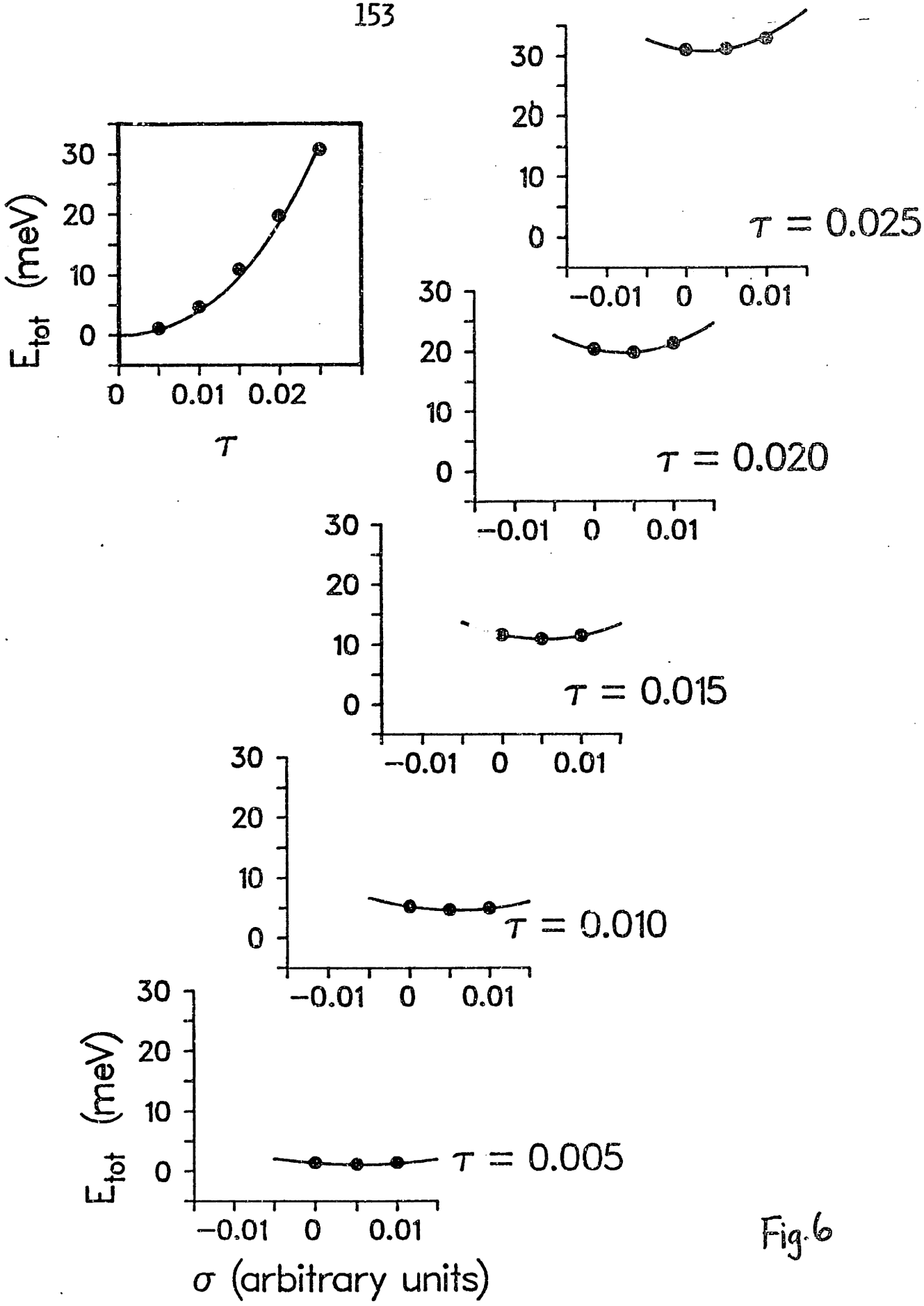
30
20
10
0
E_{tot} (meV)
0
0.01
0.02
τ
τ = 0.025
τ = 0.020
τ = 0.015
τ = 0.010
τ = 0.005
−0.01
0
0.01
σ (arbitrary units)

Fig. 6

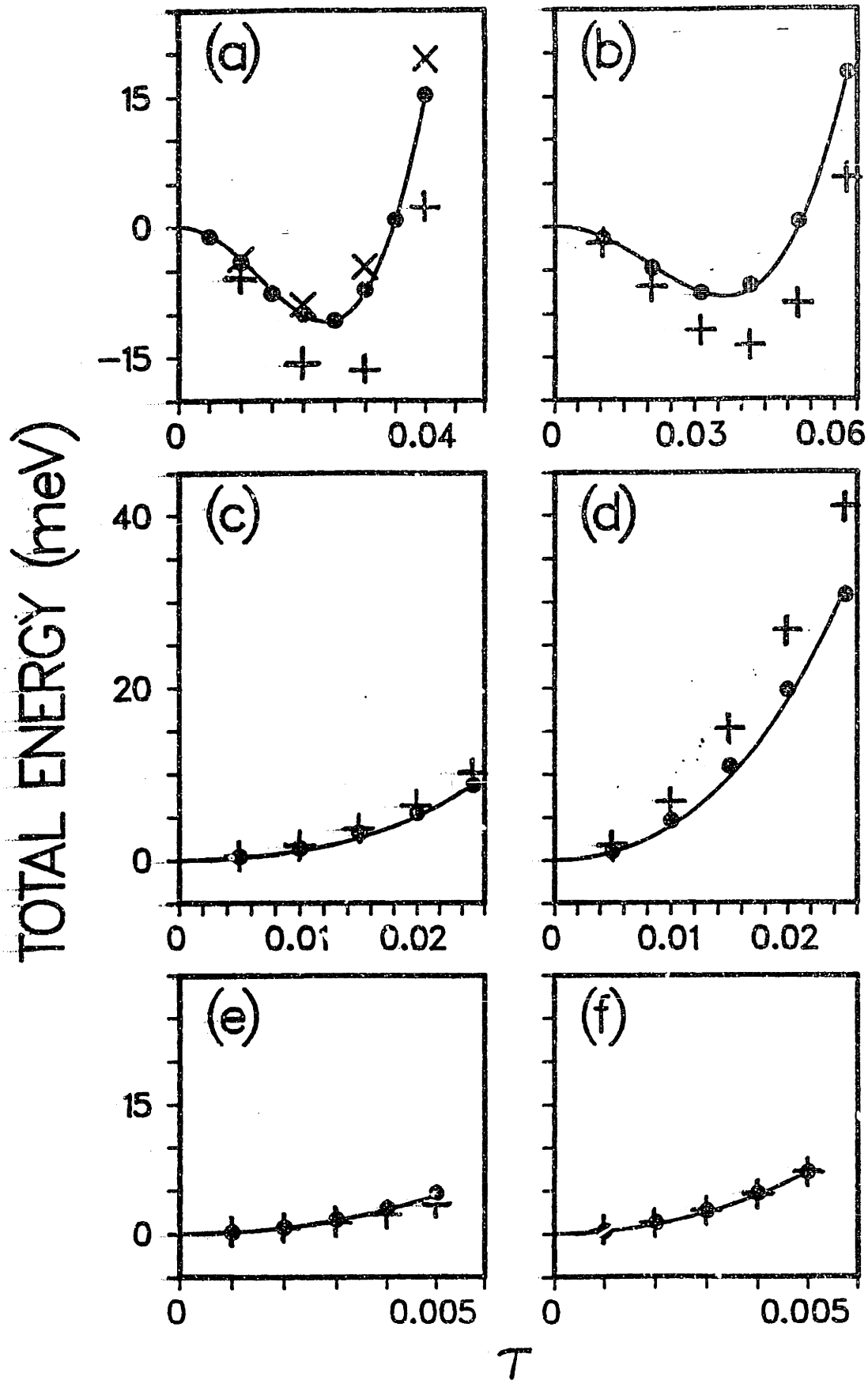
(a)
(b)
(c)
(d)
(e)
(f)
TOTAL ENERGY (meV)
T
15
0
−15
0
0.04
0.03
0.06
40
20
0.01
0.02
0.005

Fig. 7

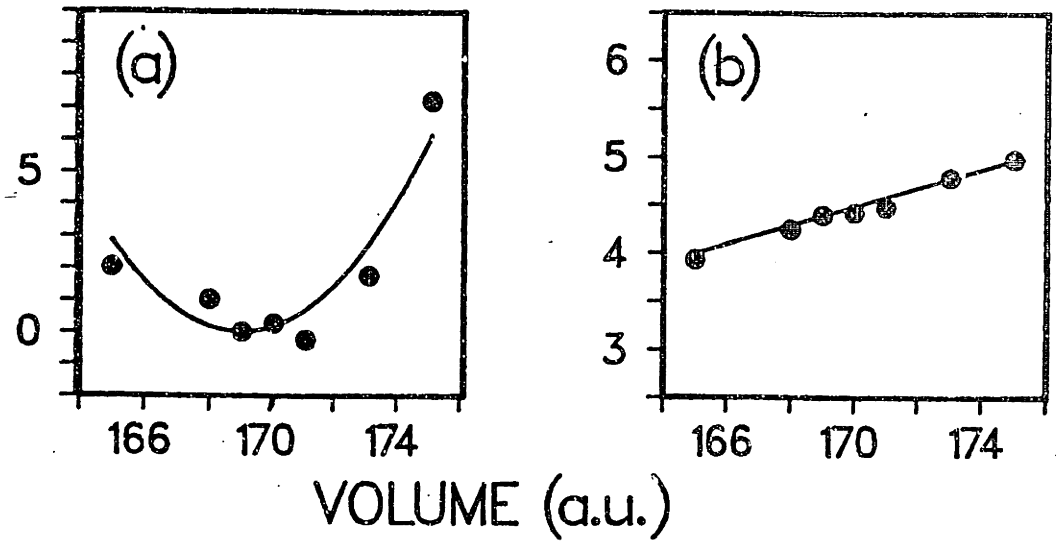

VOLUME (a.u.)

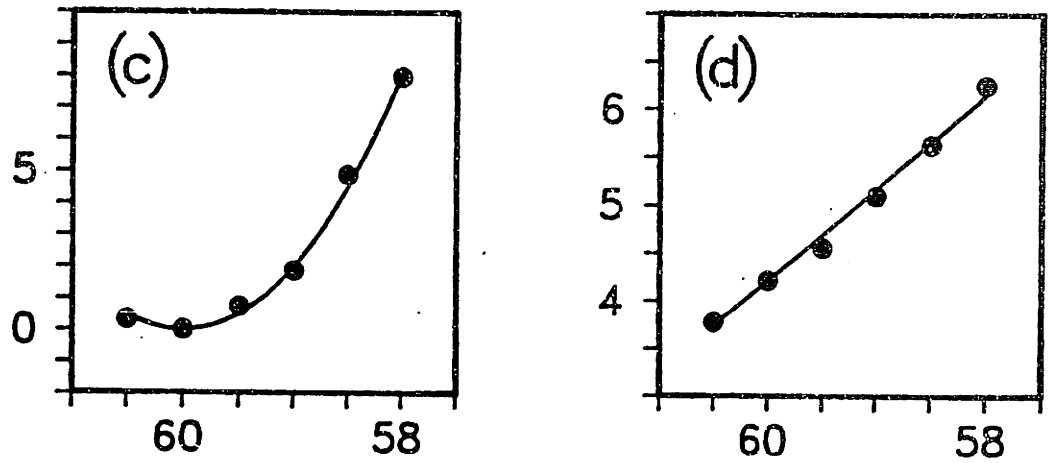

RHOMBOHEDRAL ANGLE α (deg)

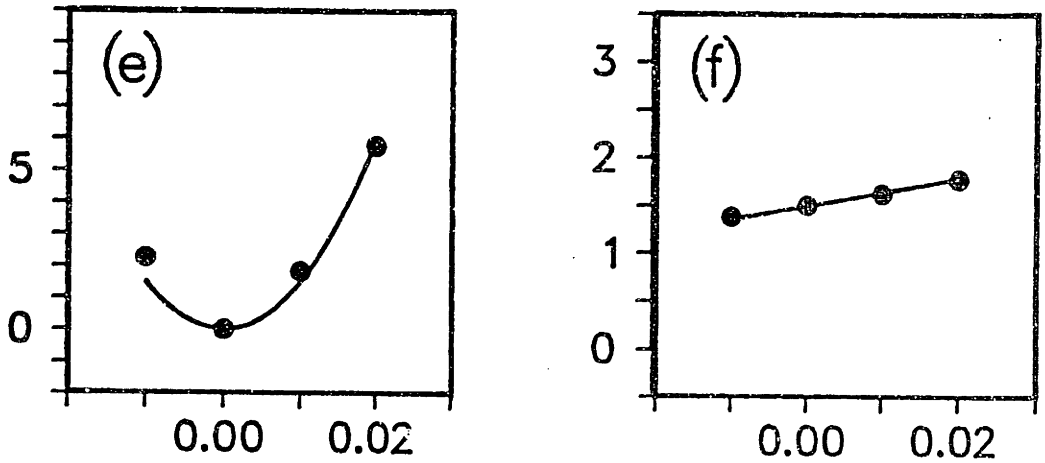

STRAIN e_{zz}

Fig.8

V. FUTURE PROSPECTS

Investigating a structural phase transition through an *ab initio* statistical mechanical approach involves combining results from two independent subfields of condensed matter physics. On the one hand, there has been a lot of interest in understanding the energetics of materials which undergo structural phase transitions. These studies focus on the microscopic origin in the character of the bonding that results in different structures being close in energy and also on the development of models that describe the energies of low lying configurations in a unified way. On the other hand, in a purely statistical mechanical context an ever-increasing number of systems with different types of order parameters and a large variety of interactions are being classified and studied. Multidimensional phase diagrams can be generated within mean field theory as well as with renormalization group approaches. The latter have also been used to study properties of fixed points and reveal the nature of the various phase boundaries. Thus, it is clear that a great deal of the groundwork for *ab initio* statistical mechanics studies already exists, and that the establishment of the final links through *ab initio* total energy calculations should potentially yield useful insights into structural phase transitions in a number of systems.

In three dimensional systems, the emphasis will be on understanding the microscopic physics of the transition, and predicting the sequence of phases and transition temperatures. Natural candidates for further studies are transitions in perovskite compounds, such as $SrTiO_3$, or, because of the complications involved in working with O potentials, fluorine based perovskites such as $RbCaF_3$. With applied stress, the critical behavior becomes more interesting-- for example, various multicritical points and 3-state Potts model behavior in $SrTiO_3$.[1]

The primary difficulty in the calculations for the perovskites is the accuracy of the *ab initio* method. This would be much less of a problem in studying ordering in semiconductor alloys, since there the pseudopotentials are so well behaved that accurate calculations can be performed for complex unit cells containing on the order of 100 atoms.[2] For this system, the main effort

would be in the development of an appropriate microscopic Hamiltonian, and in the selection of an interesting transition to study.

In general, systems in two dimensions exhibit a much richer variety of critical behavior. The (100) surfaces of Si and Ge apparently have a very stable dimerization reconstruction. As a function of temperature, the dimers can then tilt and order in a variety of ways, providing a natural mapping onto a two-dimensional Ising Hamiltonian[3]. The energy resolution needed for the differentiation of the various ordered structures is beyond that of the semi-empirical tightbinding method, and so *ab initio* calculations are required for further progress[4].

W(001) and Mo(001) are observed to have transitions from (1x1) to c(2x2) and an incommensurate structure, respectively, in what appears to be a charge density wave transition with short coherence length. The adsorption of H can modify the transitions considerably. For these transitions, the development of model Hamiltonians from microscopic Hamiltonians has been discussed in detail, but their quantitative derivation has not been carried out[5]. It was suggested that this should be done with the construction of a force constant model as an intermediate step, but based on the experience with GeTe, it seems likely that a direct fit of the model to configurational energies would give more accurate results.

The microscopic interactions in chemisorbed surface layers cannot be easily extracted from phenomenology as in the case of physisorbed layers of rare gas atoms. It has been suggested that the phase diagram of Se on Ni(100) contains a phase boundary with Ashkin-Teller character, which has nonuniversal continuously varying critical exponents[6]. An analysis of the structure of the underlying microscopic Hamiltonian shows the presence of terms which could destroy this behavior[7]. Through the combination of an ab-initio determination of the microscopic interactions with the real-space renormalization group phase diagrams[8], the controversial aspects of the complex phase diagram of this system could be clarified considerably.

Progress in the application of statistical mechanics methods to real systems should also stimulate interest in the generation of accurate phase diagrams for specific models using

numerical methods such as Monte Carlo. In the case of the model Hamiltonian for GeTe, such data would be a significant improvement on the results we obtained in d=4-ε. Also, development of *ab initio* total energy methods will presumably be accelerated with respect to solving the problems in materials of interest, both in improving numerical algorithms and increasing the accuracy of the physical approximations,

As discussed in Chap I(A), some progress has been made in developing methods which could permit studies of phase transitions in real materials other than the lattice-driven ones considered here. The capability of calculating electronic entropy contributions to the free energy could make possible the study of transitions where this is an important factor. In addition, there are a number of systems where there is an interesting interplay between structural and electronic phase transitions. For example, $KMnF_3$ undergoes a series of magnetic and structural phase transitions as a function of temperature[9]. In the layered perovskite $La_{2-x}Sr_xCuO_4$, there appears to be a signficant relationship between the superconducting and structural phase transitions that may provide some insight into the mechanism for the high-T_c superconductivity[10].

Unfortunately, even if the theoretical problems were solved, the last-mentioned investigations would involve such demanding computations as to be impossible in a practical sense at this point. However, as discussed above, there are many examples of systems where the necessary calculations do fall within the range of feasibility, and it seems likely that the *ab initio* approach to statistical mechanics will evolve and yield many interesting results.

REFERENCES

1. J.F.Fontanari and W.K.Theumann, Phys.Rev.B33,3530 (1986).

2. E.Kaxiras, Y.Bar-Yam, J.D.Joannopoulos and K.C.Pandey, Phys.Rev.B33, 4406 (1986).

3. J.Ihm, D.H.Lee, J.D.Joannopoulos and J.J.Xiong, Phys.Rev.Lett.51, 1872 (1983).

4. M.Needels, M.C.Payne and J.D.Joannopoulos, Phys.Rev.Lett.58, 1765 (1987).

5. S.C.Ying, in Dynamics of Surfaces and Interfaces, ed.by Willis, Nizzoli and Rieder (Springer-Verlag, Berlin, 1985).

6. P.Bak, P.Kleban, W.N.Unertl, J.Ochab, G.Akinci, N.C.Bartelt and T.L.Einstein, Phys.Rev.Lett.54, 1539 (1985).

7. A.N.Berker, R.G.Caflisch and A.Aharony, preprint (1987).

8. A.N.Berker and R.G.Caflisch, Phys.Rev.B29, 1279 (1984).

9. M.Hidaka, J.Phys.Soc.Japan 39, 103, 180 (1975); M.Hidaka, N.Ohama, A.Okazaki, H.Sakashita and S.Yamakawa, Solid State Commun. 16, 1121 (1975).

10. D.McK.Paul, G.Balakrishnan, N.R.Bernhoeft, W.I.F.David and W.T.A.Harrison, Phys.Rev.Lett.58, 1976 (1987).

ACKNOWLEDGEMENTS

I am very glad to have this opportunity to express my feelings of gratitude and affection for my advisor, John Joannopoulos. As a beginning student in his course, 'Theory of Solids,' I enjoyed his lucid and enthusiastic style in lectures and problem sets. In doing research, I find impressive his ability to identify interesting physics problems and to generate excitement in solving them. Lastly, most important for me as a student was his skill in guiding research and demanding work to a high standard while at the same time giving the freedom which permitted me to develop a sense of independence as a scientist and confidence in my work.

I would also like to extend my thanks to Nihat Berker, whose course in statistical mechanics greatly stimulated my interest in the field and provided me with a solid understanding of the important concepts and techniques. As a colleague, he played an significant role in the early stages of the work on structural phase transitions. As a friend, he has been an unfailing source of inspiration and support through my years at MIT.

I was supported through my entire graduate study by a GRPW fellowship from AT&T Bell Laboratories, in an excellent program which provided not only financial support but opportunities for frequent contact with physicists from Bell Labs. First and foremost among these was my mentor, Ron Pindak, with whom I had the pleasure to spend the summer of 1982 doing experimental research in liquid crystals, and who in the following years gave me much useful advice and feedback.

I would like to thank the students and post-docs who have been fellow members of the group: Alex Antonelli, Yaneer Bar-Yam, Guillermo Gomez-Santos, Thimios Kaxiras, Dung-Hai Lee, Mark Needels, Michael Payne, Doug Stone and Eugen Tarnow. In particular, I would like to thank Dung-Hai for the many hours he spent educating me about a broad spectrum of problems in condensed-matter and many-body physics. Also, I am grateful to my office-mate Thimios, both for countless interesting physics

discussions and for his steady cheerfulness and ability to put things in perspective.

On a more personal note, I would like to thank my mother and sister for their interest in my progress and my work. To Greg Moore, I owe thanks not only for shaping my approach to physics and mathematics from the very beginning of my studies, but mainly for helping me to find joy in a rich life of which physics is a vital part.